MINERALOGY, GEOCHEMISTRY, AND GEOCHRONOLOGY OF THE LITTLE NAHANNI PEGMATITE GROUP, LOGAN MOUNTAINS, SOUTHWESTERN NORTHWEST TERRITORIES

by

MARK H.F. MAUTHNER

B.A. (Modern Languages), University of Lethbridge, Lethbridge, 1986

B.Sc. (Geological Sciences), University of British Columbia, Vancouver, 1992

A THESIS SUBMITTED IN PARTIAL FULFILLMENT OF

THE REQUIREMENTS FOR THE DEGREE OF MASTER OF SCIENCE

in

THE FACULTY OF GRADUATE STUDIES

(Department of Geological Sciences)

We accept this thesis as conforming to the required standard

THE UNIVERSITY OF BRITISH COLUMBIA

December, 1995

In presenting this thesis in partial fulfilment of the requirements for an advanced degree at the University of British Columbia, I agree that the Library shall make it freely available for reference and study. I further agree that permission for extensive copying of this thesis for scholarly purposes may be granted by the head of my department or by his or her representatives. It is understood that copying or publication of this thesis for financial gain shall not be allowed without my written permission.

Department of Geological Sciences

The University of British Columbia
Vancouver, Canada

Date 1/19/96

ABSTRACT

While pegmatites of the Canadian shield have been extensively studied, Canadian Cordilleran pegmatites have not. A cooperative study of the regional geology of pegmatites in the Canadian Cordillera was begun in 1992, by workers from the University of British Columbia and the Canadian Museum of Nature.

Attention in this thesis has been focussed on the Little Nahanni Pegmatite Group, located in the Logan Mountains, about 47 km northwest of Tungsten, Northwest Territories. Fieldwork and laboratory studies were conducted in an attempt to classify, outline and map the extent of the pegmatite group, to describe the setting, mineralogy, geochemistry and internal evolution of the pegmatite dikes, to examine the interaction between the pegmatitic fluid and the host rocks, and to date the pegmatite intrusive event.

The group is hosted by deformed, upper greenschist to lower amphibolite facies metasedimentary rocks of the Upper Proterozoic Hyland Group. The dikes that make up the group are characteristic of the albite-spodumene type of rare-element class of granitic pegmatite. The dikes are up to only several metres wide (most are less than 1 m), yet can extend up to several kilometres along strike. Mineralogical and geochemical data show the group to belong to the LCT family as classified by Černý (1991a). Internal zonation consists of a fine-grained albite(Ab)-quartz(Qtz) (± tourmaline(Tur), ± apatite(Ap)) border zone, a medium- to coarse-grained Ab/Kfs-Qtz-muscovite(Ms) wall zone, a coarse-grained Ab and/or Ksp-spodumene(Spd) intermediate zone, and rarely, a coarse-grained quartz core. Late albitic units (Ab-Qz±Ms±lepidolite(Lpd)) comprise bands and irregular pods cutting all previously crystallized zones, and, in some cases, comprise entire dikes. Two notable expressions of rhythmic banding in the dikes are: 1) the alternation of pegmatitic, Spd-bearing bands and aplitic Fsp-Qtz bands, and 2), banded aplitic and pegmatitic Lpd-Ab-Qtz. No one mechanism seems to be responsible for both styles of banding. Accessory minerals include: columbite group minerals, cassiterite, apatite (commonly Mn-bearing), beryl, lithiophilite, triploidite,

montebrasite, rutile, uraninite, uranmicrolite, helvite, galena, sphalerite and zeolites. The dikes are strongly enriched in Li and F, moderately enriched in P, and weakly enriched in B, Mn, Be, Nb and Ta. Several phases show enrichment in Mn with respect to Fe, and in Ta with respect to Nb. Beryl crystals with Cs-rich rims are associated with late-stage features. The virtual absence of magmatic Fe-Mg allowed B to remain, for the most part, partitioned in a vapour phase throughout the crystallization of the pegmatites, at the end of which B left the system to form tourmaline exocontacts in the host rock.

Geochronological and Pb isotopic studies were carried out to constrain the petrogenesis, emplacement age(s) and relationships of the Little Nahanni pegmatite group to other granitoids in the region. A U-Pb age of 81.6 $\pm$ 0.5 Ma for columbite was obtained. K-Ar ages for micas were determined to be 65.4 ± 4.0 Ma for muscovite, and 65.8 ± 3.4 Ma and 65.4 ± 3.6 Ma for lepidolite. The U-Pb age is interpreted as the emplacement age for the pegmatites and the K-Ar ages are interpreted to be the timing of a thermal event responsible for resetting the K-Ar mica system. The U-Pb columbite age is 8 to 13 Ma younger than the average age of the plutons in the Selwyn plutonic suite and indicate that these pegmatites represent a magmatic event that has not been previously recognized. Likewise, the K-Ar ages point to a later thermal event not previously recognized in this area.

Fractionation trends in the pegmatite, Pb isotopic compositions of the feldspars, mineralogy and the general peraluminous nature of the pegmatites suggest that they are the product of moderate to high levels of fractionation of an upper-crustally derived granitic melt. This melt is likely to be the result of partial melting associated with tectonic movement during the Late Cretaceous formation of the Mackenzie fold and thrust belt.

TABLE OF CONTENTS

LIST OF TABLES

LIST OF FIGURES

ACKNOWLEDGEMENTS

Many thanks to: Lee Groat, for offering me this excellent project and his support, Scott Ercit, for his helpful conversations and Jim Mortenson, for his help with the geochronology chapter, which basically would not have existed without his aid. Many thanks go also to Mati Raudsepp and Bob Gault for their help with analyses and to my committee members, Greg Dipple, Mati Raudsepp and Kelly Russell.

I thank the staff at UBC Geology, especially Donna Anderson, Marc Baker, Bryon Cranston, Teresa Karchewski, Nancy Myrah, Doug Polson, Ray Rodway and Merilyn Staheli for making "daily life" at UBC that much easier.

For their part along this sometimes bumpy road, I heartily thank my friends and family, particularly, Joe Nagel, for his conversations and view on life, my parents, Hermann and Ursel, for their ever present support and, above all, my wife, Tanya, for her patience and understanding.

Field and laboratory work was made possible by funding provided by DIAND-Yellowknife, Yukon Geoscience Office, and NSERC.

1 INTRODUCTION

1.1 Location

The Little Nahanni Pegmatite Group is located in an unnamed range in the Logan Mountains about 47 kilometers northwest of Tungsten (62°12' N, 128°50'W, NTS 105I/2, Fig. 1.1). The easiest access to the area, at the time of writing, is by air: either by float plane from Watson Lake to Moose Lake or by helicopter from either Watson Lake or Ross River. Access is also possible on foot as a portion of the Range Road to Tungsten comes within 15 kilometres of the south end of the Little Nahanni Pegmatite Group. For exploration purposes, it would seem to be a simple matter to upgrade the Range Road, then push a new road from it to the Little Nahanni locality. The road to Howard's Pass, which leaves from the Range road further east than the point mentioned above, passes close to the north end of the pegmatite group.

1.2 Exploration History

D.C. Rotherham first recorded these pegmatites in 1961 during an exploration program run by the Canada Tunsgten Mining Corporation Ltd. In 1977, V. Ahlborn, then of Erex International Ltd. further explored the locality on behalf of Canadian Superior Exploration Ltd. and the latter staked the Cali claims that year. This activity was part of a larger exploration program targetting alternative energy resources (i.e. lithium and other rare elements) in the Northwest Territories and was supervised by R. Lasmanis, then of Canadian Superior. During the winter of 1978, Cominco staked the Lica claim blocks adjacent to the Cali claims. Cominco continued primarily geochemical exploration until August, 1980.

The pegmatites were the subject of company reports by Rotherham (1962), Beavon (1977), and Ahlborn (1977a, b), which include descriptions of the Cali/Lica claims.

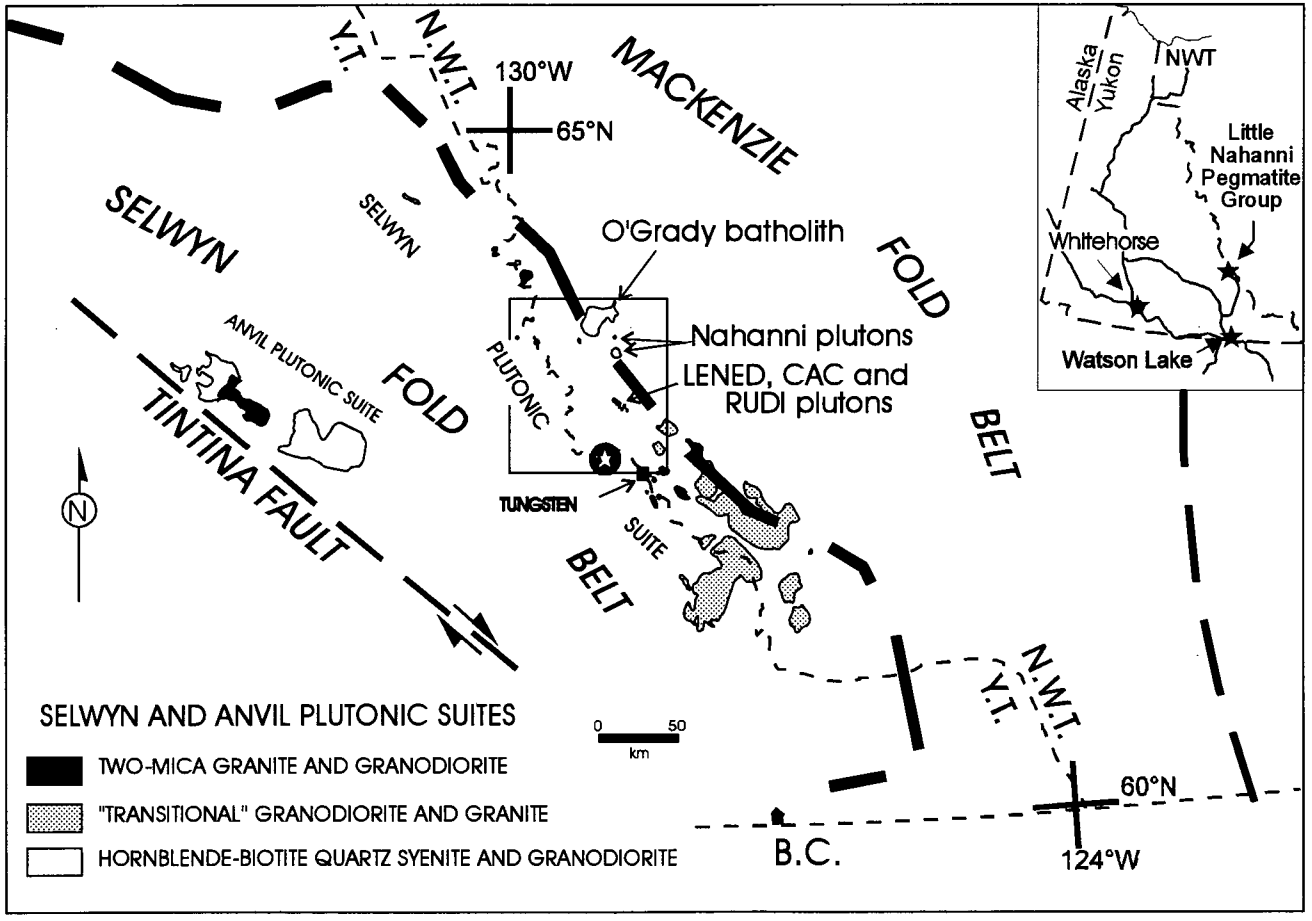

Figure 1.1 Location map showing Little Nahanni Pegmatite Group and surrounding plutons. Heavy dashed lines at right indicate eastern margin of tectonic deformation.

1.3 Proposed Study

The intent of this study is:

a. to classify, outline and map the extent of the pegmatite group,
b. to describe the setting, mineralogy, geochemistry and internal evolution of the pegmatite dikes,
c. to examine the interaction between the pegmatitic fluid and the host rocks,
d. to determine the age of the pegmatite group and its relationship to other intrusive rocks in the region.

1.4 Field Work and Sampling

A collaborative research project (between the University of British Columbia and the Canadian Museum of Nature) began in 1992 with a reconnaissance study of the Little Nahanni locality. This study showed the pegmatite group to be extensive in area, rich in rare elements and worthy of further investigations.

The author's involvement began in 1993. During that field season (three weeks in August), approximately 75% of the Little Nahanni Pegmatite Group was mapped and sampled. The same field party returned during the 1994 field season (five days) to complete the mapping (Fig. 1.2 - map in pocket) and sampling of the group (Groat *et al.* 1994, 1995).

Accessory minerals, feldspars and specimens exhibiting various textures were the primary focus for sampling and study. Dikes were labelled in the following format: XXX-#1-#2 (e.g. LMM-5-8), where the first letter represents the particular field season (C = 1992; L = 1993; N = 1994), the next two letters are the initials of the mapper, the first number indicates the cirque in which the dike is located, and the last number is the actual dike number within a cirque. In the example given above, the dike was the eighth mapped in cirque 5, by the author (Mark Mauthner) during the 1993 field season.

Samples collected on one of the plateau-like ridges between cirques, are given a "cirque" designation consisting of the two cirque numbers, ordered from north to south, separated by a

"hat" symbol (e.g. "1^2" = ridge between cirques 1 and 2). Samples collected in the talus were marked in one of two ways. If the sample could be associated with a particular dike with a reasonable degree of certainty (i.e. just below the dike, and the next dike being some distance away) a "t" was added to the dike number. If the source dike was unknown or ambiguous, the sample was given a "t" designation in place of a dike number, and a circled, sequential number where more than one of such a sample existed for a given cirque. All samples were recatalogued with sequential catalogue numbers on a multi-relational, specifically-designed database, using "Superbase™" software as a platform. A full list of samples (correlating sample numbers and sample locations) used for this thesis is given in Appendix A.

2. ALBITE-SPODUMENE PEGMATITES: Review and World Localities

The first reference to albite-spodumene pegmatites as a "type" is made by Solodov (1962; see also Solodov, 1969 and 1971). While describing the rare-element class of pegmatites in terms of its function as a source of tantalum, Černý (1989a) provides a comprehensive review of the characteristics of the albite-spodumene (and other) type of pegmatites. A more encompassing analysis of rare-element class pegmatites is given in Černý (1991a,b ;1992). This review is based, for the most part, on Černý (1989a, 1991a,b).

Černý (1991a) summarizes pegmatite classification at three levels: family, class and type. The LCT [Li, Rb, Cs, Be, Sn, Ga, Ta>Nb (B, P, F)], NYF (Nb>Ta,Ti,Y,Sc,REE,Zr,U,Th,F) and mixed families are characterised by bulk composition, typical trace element assemblages (geochemical signatures), and parental granite type. Abyssal, muscovite, rare-element, and miarolitic classes outline the the principal conditions of pegmatite formation in four crustal settings. Černý (1991a) also summarized a classification scheme for rare-element class pegmatite types and subtypes based on pegmatite bulk chemistry, geochemical signature of accessory minerals, internal structure and P-T conditions of crystallization. Not every type or subtype is completely different from all others. A type or subtype is distinguished when one or more of these criteria is significantly different from another.

Pegmatites of the albite-spodumene type belong to the rare-element class and to the LCT geochemical family of pegmatites. Geologic ages for pegmatites of the rare-element class are wide ranging, from late Archean to early Miocene. Conspicuous concentrations of these pegmatites are related to the Kenoran (2,500 Ma), Karelian-Nullaghinian (2,100 Ma), Hudsonian-Svecofennian (1,700 Ma), Hercynian (300 Ma) and Cimmerian plus Alpine (200-20 Ma) orogens. Rocks hosting rare-element pegmatites typically belong to the Abukuma-type facies series and are of uppermost-greenschist to lower-amphibolite grade (Černý, 1989a).

Albite-spodumene pegmatites are described as predominantly homogeneous in appearance except for subtle compositional and textural zoning along contacts, a common, layered aplitic

assemblage, and rare pods displaying randomly oriented blocky texture in their central parts (Černý, 1989a, 1991a). Solodov (1969) discussed two zones that make up albite-spodumene pegmatites: a marginal quartz-albite zone, and a central quartz-albite-spodumene zone. A more thorough description of the zoning is given by Černý (1989). Where developed, it typically begins with a fine-grained, thin quartz and albite wall zone along the contact. The next, and dominant, zone consists of medium-grained albite and quartz (± mica) with subparallel spodumene and (subordinate) K-feldspar megacrysts. A central zone of blocky K-feldspar (± quartz) is subordinate or entirely missing (Černý, 1989a). The zoning, consisting of those just described, is commonly asymmetric (Solodov, 1962, 1971). Fine-grained, massive lepidolite and/or saccharoidal albite replacement units are also commonly present (e.g. Kesler, 1961; Sundelius, 1963; Göd, 1989). Spodumene, quartz and K-feldspar are typically elongate and normal to host rock/pegmatite contacts (Černý, 1989a, *cf* references therein for classic examples; Černý, 1991a). Internal structural differences between the albite-spodumene type and the spodumene subtype of the complex type of pegmatite are the chief distinguishing characteristic; their mineralogies are similar (Černý, 1991a).

Albite-spodumene pegmatites are the most Li-rich of any pegmatite type. With rare-element pegmatites in general, increases in Li content are expressed first by Li enrichment in the micas, then by the appearance of ferromanganoan Li-phosphates, and finally by the crystallization of Li aluminosilicates. As well, oxide minerals, phosphates and silicates show decreasing Fe/Mn, Al/Ga, Zr/Hf and Nb/Ta, and increasing Rb and Cs in potassic minerals (i.e. micas and feldspars) (Černý, 1989a). Albite-spodumene pegmatites typically carry Be, Sn and/or Nb/Ta mineralization with beryl usually hosted in the central, K-feldspar-bearing parts of a dike, and cassiterite and columbite-group minerals dispersed in the albite+quartz matrix of the dominant spodumene-rich zone. The Sn- and (Nb,Ta)-bearing minerals are also commonly dominantly concentrated in the saccharoidal albite and muscovite-rich assemblages that partly replace K-feldspar bearing zones.

Albite-spodumene pegmatite dikes are typically tabular in shape, with very high aspect ratios (50 to 100), up to 3 km long, and extend up to 1 km down-dip. They are not usually associated with pegmatites of other types. Where they are associated with complex pegmatites, albite-spodumene pegmatites are a minority within the group, and farther from the parental granite than any other type. Commonly, subparallel swarms approximate the intrusive course of the parental granites or follow prominent regional joint or fault systems (Černý, 1989a).

Albite-spodumene type pegmatites have been recognized from a number of world localities. Characteristics of major localities are outlined in tables 2.1a-c.

Locality	Zoning	Banding	Dimensions	Reference(s)
Kings Mountain, North Carolina	1) border zone: thin Ab+Qz 2) intermediate zone: layered aplite and K-pegmatite +Sp+Ksp 3) core zone: Sp+Ksp+minor Ms in Ab+Qz matrix	Zone 2) is layered	up to 90 m thick and 1000 m long	Kesler, 1961; Černý, 1989a; Thomssen & Anthony, 1977
Preissac-Lacorne, Quebec	"massive or zoned" (Mulja, 1995) zoned: 1) border zone aplite 2) Ms+Ab+Qz+Brl ± Sp 3) Ksp+Qz+Brl±Sp 4) Ksp+Qz±Sp 5) Qz±Sp	none mentioned	up to 8 m thick and 200 m long	Mulja, 1995; (also Mulligan, 1965 and Rowe, 1953)
Weinebene, Austria	"unzoned" 1) aplitic 'seam' along both contacts 2) central zone: Sp+Qz+Ksp 3) aplitic 'schlieren', resemble 1), cutting 2)	none	up to 5.5 m thick and 1.5 km long	Göd, 1989
Volta Grande, Brazil	"unzoned to indistinctly zoned" 1) Fspar+Qz+Ms+Sp 2) Fsp+Qz+M 3) Fsp 4) Qz+Ms+minor Fsp locally 5) Qz core (in 1 dike)	"several horizons" of spodumene bands	up to 20 m thick and 1.2 km long	Heinrich, 1964
Peg Claims, Maine	1) narrow Qz+Ms border zone 2) narrow Ab+Qz+Ms wall zone 3) dom. Ab+Qz+Sp+Ksp core 4) crosscutting, fine-grained Qz+Ab+Sp+Ms lenses within cores	none mentioned	up to 25 m thick and 183 m long	Sundelius, 1963
Gods Lake, Manitoba	"characterized by textural and structural homogeneity"	none mentioned	3 to 10 m thick, 2 km long and at least 250 m deep	Chackowsky, 1987

Table 2.1a. Summary of structural features of some albite-spodumene pegmatites.

Locality	Host Rock(s)	Exomorphic Aureole	Parental Granite
Kings Mountain, North Carolina	dominantly amphibolite within micaschists mid-amphibolite facies	holmquistite, tourmaline, rare-alkali biotite, calcite, apatite	spatially related to the Cherryville quartz monzonite
Preissac-Lacorne, Quebec	granite and metavolcanic rocks (Lacorne dikes); biotite-staurolite schists (Bouvier dikes)	biotite, holmquistite	Lacorne and Lamotte batholiths: two-mica granodiorites
Weinebene, Austria	eclogitic amphibolites (AH), mica schists (MH)	holmquistite & tourmaline at AH dike contacts (also garnet and biotite)	"no granitic intrusion exposed in the area"
Volta Grande, Brazil	amphibolite	gray-green, randomly-oriented biotite	regional granitic basement complex, but no relationship established
Peg Claims, Maine	dominantly amphibolite-facies (sillimanite) Qz+Bi+Ms schist with amphibolite lenses	quartz, tourmaline, muscovite, apatite	Waldoboro and Clark Island granites crop out within several miles of the pegmatites; a relationship with the former is suggested (Sundelius, 1963)
Gods Lake, Manitoba	metabasalts	none mentioned	no relationship made

Table 2.1b. Summary of host-rock features of some albite-spodumene pegmatites.

Locality	Pegmatite Tourmaline	Phosphates	Other Minerals	Comments
Kings Mountain, North Carolina	none	apatite; Fe-Mn phos related to wallrock contacts; secondary phosphates in post-emplacement fractures	secondary Be and P minerals in cross-cutting fractures, sphalerite	↑ Li toward core from border; ↑ Fe, Mn, P toward border; secondary P & Be mineralization in cross-cutting, post-emplacement fractures
Preissac-Lacorne, Quebec	none	lithiophyllite	spessartine, bismuthinite, hematite, molybdenite	- Černý (1991a) mentions the presence of albite-spodumene pegmatites in the Preissac-Lacorne area - only the dikes referred to as "spodumene" or "spodumene-beryl" type in Mulja (1995) are considered possible "albite-spodumene" types
Weinebene, Austria	contact related	contact rel. apatite (AH); secondary phoshates (MH)	zircon, (graphite, sulphides - contact related)	mica schist-hosted pegs almost "gneissic"
Volta Grande, Brazil	none	none	ilmenite, magnetite, spessartine	deeply kaolinized, altered
Peg Claims, Maine	contact related: small amounts in border zone	apatite in border zone; Li-Fe-Mn phosphate alt'n product in one place	garnet	↓ Ab, Qz, Ms, and ↑ Sp, Ksp toward core from border; ↓ Na_2O and ↑ K_2O, Li_2O, Rb_2O and Cs_2O toward core from border
Gods Lake, Manitoba	none	none	none found	

Table 2.1c. Summary of mineralogical features of some albite-spodumene pegmatites.

Locality	Spodumene	Lepidolite	Sn, Be, Nb/Ta mineralization	Reference(s)
Kings Mountain, North Carolina	normal to wallrock contact	none	cassiterite, beryl, columbite-tantalite, niobian-rutile	Kesler, 1961; Cerny, 1989a; Thomssen & Anthony, 1977
Preissac-Lacorne, Quebec	normal to wallrock contact	yes	columbite-tantalite, microlite, phenakite	Mulja, 1995; Rowe, 1953; (Mulligan, 1965)
Weinebene, Austria	parallel to dike attitude	none	cassiterite, rare columbite	Göd, 1989
Volta Grande, Brazil	normal to wallrock contact, not always (criss-cross near footwall)	yes ("altered spodumene")	cassiterite, microlite tantalite	Heinrich, 1964
Peg Claims, Maine	normal to wallrock contact but not as well as Ksp laths	none	beryl in border zone	Sundelius, 1963
Gods Lake, Manitoba	normal to wallrock contact	purple, lithian muscovite as cross-cutting, late-stage stringers	heavy mineral separates attempted, no other accessory minerals found	Chackowsky, 1987

Table 2.1c. Summary of mineralogical features of some albite-spodumene pegmatites (cont'd).

3. GEOLOGY

3.1 Regional Geology

The general geology of the Selwyn Basin has most recently been described by Gordey and Anderson (1993), from which the following review of the regional geology is derived.

The field area is located within the Selwyn fold-and-thrust belt which forms the inner, southwest part of the arcuate MacKenzie fold-and-thrust belt (Fig. 1.1). Folds trend northwest-southeast, and plunge to the northwest. Major structural features in the field area are the Fork Anticline, Summit Syncline and the March Fault. The area is underlain by weakly metamorphosed late Proterozoic metasediments of the Hyland Group, which is subdivided into the Yusezyu and Narchilla formations.

3.1.1. Yusezyu Formation

The oldest strata known within the Selwyn basin belong to the Yusezyu Formation, which consists of a thick succession of interbedded sandstones and shales. A minor, discontinuous limestone member denotes the top of this formation. It consists of fine crystalline, light to dark grey limestone of variable thickness, from 0 to 15 metres. The uppermost parts of the formation are variably calcareous, and abrupt and irregular changes from carbonate to silica cement occur. The uppermost Yusezyu sandstone is highly calcareous where the limestone member is absent. Mineralogically, the sandstone generally consists of quartz, less than 4% each of plagioclase and K-feldspar, and traces of lithic fragments. Detrital zircon and tourmaline also occur as small anhedral grains in trace amounts.

With the exception of the far northeastern corner (cirque -1 and part of cirque 0) the entire pegmatite group outcrops within the Yusezyu Formation.

3.1.2 Narchilla Formation

The Narchilla Formation consists of a several hundred-metre thick accumulation of dark grey or maroon shales which overlie the coarse clastic rock and limestone of the Yusezyu formation. Gordey and Anderson (1993) describe a fine grained quartzose sandstone in the middle part of the formation along the Fork Anticline and parts of the Steel Syncline. Like the sandstones in the Yusezyu Formation, the Narchilla sandstone member contains quartz, minor feldspar, rare detrital muscovite and chlorite, and traces of tourmaline, zircon, and opaque material.

3.1.3 Selwyn Plutonic Suite

The plutonic rocks of the region belong to the mid-Cretaceous, calc-alkaline Selwyn suite. The suite consists of radiogenic, metaluminous to peraluminous granitoid rocks. Gordey and Anderson (1993) subdivide the plutonic suite into three groupings: (1) hornblende-bearing plutons, (2) two-mica plutons, and (3) transitional plutons with attributes intermediate to those of (1) and (2). Contact aureoles about plutonic rocks are typically andalusite- and biotite-bearing; the first appearance of andalusite occurs within one-half kilometer of intrusive contacts. Gordey and Anderson (1993) suggest an epizonal to mesozonal depth of emplacement for granitoid plutons in the region. Granitic pegmatites are associated with some of the plutons of the suite, both with hornblende-bearing (metaluminous) and hornblende-free (peraluminous) plutonic rocks.

3.1.3.1 Hornblende-bearing plutons

Gordey and Anderson (1993) describe two varieties of hornblende-bearing plutons: (1) alkali feldspar-rich quartz syenite and granodiorite, and (2) homogeneous granodiorite which lacks titanite and opaque minerals.

The O'Grady batholith is the local type locality for the alkali feldspar-rich composite intrusions. From the core outward, the batholith grades from a massive, medium to coarse-grained,

crowded megacrystic hornblende quartz syenite to a foliated transitional (biotite-) hornblende quartz syenite to an equigranular medium-grained hornblende-biotite granodiorite. Tourmaline-bearing aplite and pegmatite segregations and dikes are common along the western margin of the batholith. Also typical of the alkali-feldspar-rich quartz syenite and granodiorite variety are the Emerald Lake pluton and parts of the Keele Peak pluton (Gordey and Anderson, 1993 and references therein).

The Northern and Central Nahanni plutons typify the homogeneous massive, equigranular or seriate, medium-grained hornblende-biotite granodiorite variety; the Central Nahanni pluton is the type locality (Gordey and Anderson, 1993). This granodiorite is similar to the granodiorite phases in the alkali feldspar-rich plutons (i.e. O'Grady Batholith).

3.1.3.2 Two-mica plutons

Small areal extent, composite nature, a paucity of porphyritic mafic dikes (but common peraluminous dikes), and the presence of muscovite and common large feldspar megacrysts are all diagnostic features of the two mica plutons. Two compositionally similar, but texturally different granite or granodiorite phases make up these plutons. An alkali feldspar megacrystic phase grades outward to an equigranular, peraluminous granite along the margin of the pluton (Gordey and Anderson, 1993).

The only essential mafic mineral is biotite. Accessory minerals, including muscovite, garnet, andalusite and/or tourmaline, are concentrated in the equigranular granite along a margin or in satellitic dikes. This type of pluton hosts abundant irregular aplite and pegmatite intrusions within and along the pluton's margin (Gordey and Anderson, 1993).

The MacTung pluton is the local type locality for the peraluminous, two-mica plutons (Gordey and Anderson, 1993) which represent the most evolved members of the suite. Other examples include the Clea, Lened, Cac, Rudi, Nar, Mount Wilson and Pelly River plutons (Gordey and Anderson, 1993).

3.1.3.3 Transitional plutons

In the Southern Nahanni pluton, the best example of transitional type plutons, a core of seriate or equigranular hornblende-biotite grades outward to a coarsely megacrystic biotite granite along the margin. The latter lithologically resembles the two-mica plutons and the core resembles the more leucocratic phases of the hornblende-bearing plutons.

As with many of the other types, aplite and pegmatite dikes occur with these plutons.

3.2 Local Geology

The granitic pegmatites are located in an unnamed mountain range bounded to the northeast by the March Fault and to the southwest by an erosional surface denoted by Steel Creek. The pegmatites are localized in the northeast limb to axial sections of the Fork Anticline. In general, they strike northwest; i.e., subparallel to the axial planes of the fold system. They are dominantly hosted by calcareous metasediments of the upper Yusezyu Formation. Only three dikes (LMM-¯1-1, LMM-¯1-2 and LSE-0-1) were were found to be hosted by the Narchilla Formation, the rest occur in the Yusezyu Formation. This was determined by overlaying the pegmatite dike location map on the geological map produced by Gordey and Anderson (1993). No attempt was made to remap the actual contact between the Narchilla and Yusezyu formations in the field.

There do not appear to be any exposures of granitic plutons in the vicinity of the pegmatite group. However, scattered occurrences of andalusite porphyroblasts, which are locally coarser in areas to the north of the group, suggest the existance of a pluton at shallow levels below the present-day erosional surface.

3.3 Pegmatite Dikes

The pegmatite bodies range from tabular to lenticular in shape and have high aspect ratios (Fig. 3.1). Typical of albite-spodumene pegmatites, single dikes in the Little Nahanni Pegmatite Group are a maximum of about seven meters in width, yet can extend for hundreds of meters

along strike. The dikes commonly occur in subparallel swarms consisting of aproximately 5 to 25 bodies. These features, plus the fact that the general attitude of the pegmatite group seems to be structurally controlled, are consistent with the description of the albite-spodumene pegmatite type by Černý (1989a). Contacts are typically sharp (Fig. 3.2) and locally irregular depending upon the type of host rock. Pegmatites emplaced in calcareous metasedimentary rocks show evidence of low degrees of assimilation as evidenced by calcite-lined fractures and late calcium-rich mineral assemblages (very commonly including apatite). Pegmatites emplaced in pelitic metasedimentary rocks have up to 10 cm wide exomorphic aureoles rich in coarse silvery mica or narrow (several mm) bands of black tourmaline.

The dikes show no obvious signs of regional zonation. Dikes generally have the same appearance throughout the group, given some minor variation with respect to internal zonation. One exception is a dike in the very south end of the group (ridge 10^11) which contains a late-stage, replacement lepidolite-albite-beryl unit, which was not observed in any other part of the group (see Fig. 5.25).

A minor fault cutting a dike in the NMM-1N-18 swarm, and observable and measurable displacement on several dikes, especially NMM-1N-9 and 10 (see Fig. 3.21) were found in cirque 1N, and pinching and swelling features, possibly interpretable as boudinaging, were also found in cirques 1N, 9 and 10 (Figs. 3.22, 3.23 and 3.25). The dikes that exhibiting the pinching and swelling features do not exhibit corresponding internal deformation.

Only one clearly cross-cutting pair of dikes (LMM-10-7 and LMM-10-6) was observed in cirque 10 (Figs. 3.24 and 3.26). Two other dike pairs also possibly had cross-cutting relationships (NMM-1N-18s (2) and LMM-5-1A and -1B). These, however, may well have been single dikes splitting into two of varying textures and/or mineralogy as both pairs were buried by talus from the "fork" downward.

Figure 3.1: Dike LMM-0-1, showing the tabular nature typical of Little Nahanni Pegmatite Group dikes. The dike is about 80 cm wide.

Figure 3.2: Dike LMM-5-1. Pegmatite/host schist contact showing muscovite-rich and muscovite absent wall zones in pegmatite. Scale is in inches.

3.3.1 Internal Structure

Internal zoning of the pegmatites is variable. Generally, the outward to inward succession of zones consists of a number, or all, of the following: a quartz-plagioclase (± apatite) border zone, a quartz-muscovite-plagioclase wall zone which can sometimes be divided into outer and inner wall zones, a spodumene-K-feldspar-quartz intermediate zone, and rarely a quartz core. Fine-grained, massive lepidolite and saccharoidal or clevelanditic albite replacement units also occur. Aplitic material occurs as layers between pegmatitic bands, parallel to the pegmatite/host rock contact and as irregular pods and stringers cutting pegmatite zones. The zones are discussed in further detail in chapter 6.

Directional crystal growth is strongly expressed by (1) banding in the aplitic layers, which is typically parallel to dike contacts (Fig. 3.12), by (2) elongate K-feldspar and spodumene crystals in the pegmatitic layers, which are perpendicular to dike contacts (Fig. 3.3), and by (3) the "fanning" inwards (toward the centre of the dike) of the muscovite and lepidolite and similarly, the inward broadening of elongate spodumene and K-feldspar crystals. Monomineralic quartz cores are rare and occupy central portions of the dikes (Fig. 3.4).

Many dikes contain late-stage fractures perpendicular to the pegmatite dike contacts. These fractures host smoky and colourless quartz, muscovite, clevelanditic albite, K-feldspars, apatite and beryl, and most, but not all, are filled by calcite. Where the fracture meets the contact between the dike and the host rock, the host rock commonly curves in towards the dike.

Figure 3.5 shows another cross-cutting feature observed in some dikes. Internal quartz veins, up to 10 cm+ thick, locally cut across a dike, but abruptly end at the pegmatite/wall rock contacts (i.e. they do not extend into the wall rock).

Open-space pockets also occur, albeit rarely. Examples of assemblages observed in filled and open-space pockets and fractures are listed in Table 3.1.

Figure 3.3: Photograph of boulder on the 1^2 ridge (Cali claims). The spodumene and K-feldspar crystals have grown perpendicular to the pegmatite/host rock contact and exhibit a broadening towards the centre of the dike. Note also the aplite stringers that cut the feldspar and spodumene.

Figure 3.4: Dike LLG-10-1. Note the quartz core in the centre. A tourmalinized raft of wall rock is also visible near the upper edge of the photograph. Dike width is about 60 cm.

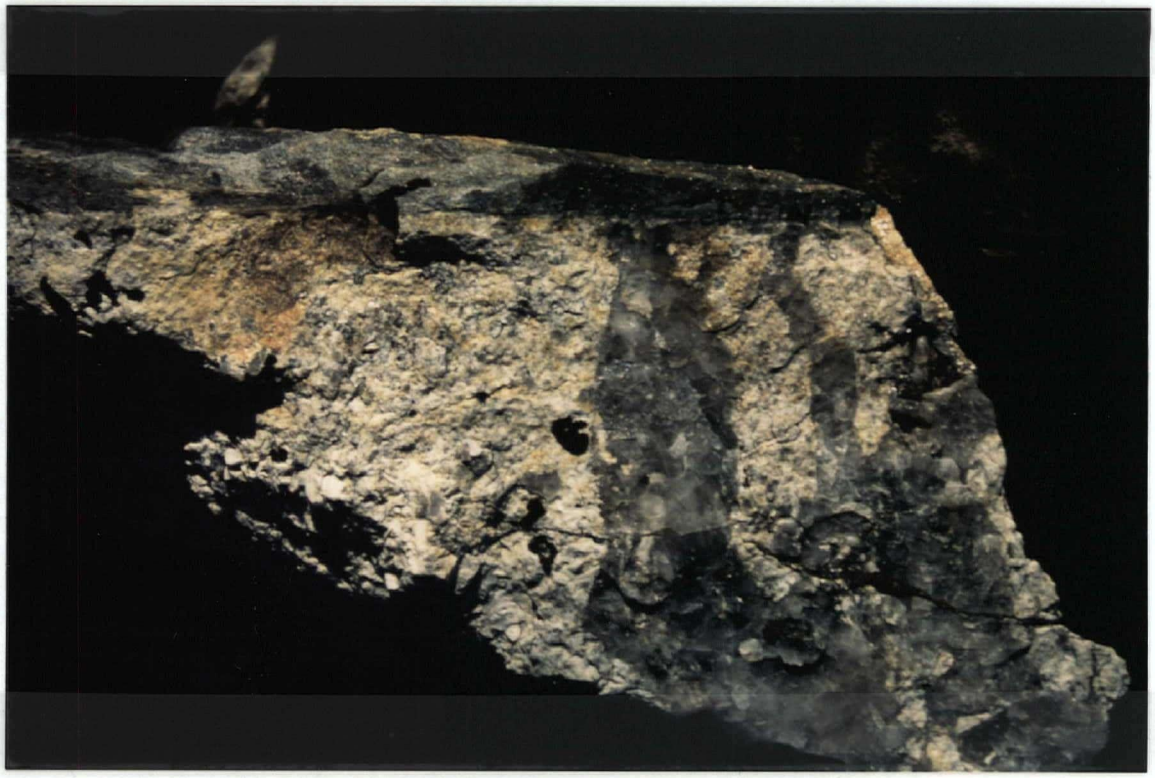

Figure 3.5: LMM-10-talus. Note the quartz body that cuts across the pegmatite dike and does not continue into the host rock. The right side of the boulder is approximately 90 cm thick.

Table 3.1: Examples and descriptions of filled and open-space fractures and pockets.

Sample Location	Filled or open-space?	Fracture or pocket?	Mineral assemblage & Paragenetic sequence	Remarks
NSE-1N-4s	calcite-filled	pocket	K-feldspar/quartz/beryl/apatite → albite/helvite → chabazite → calcite	K-feldspar heavily corroded; helvite on 'skeletal' remains of K-feldspar; yellowish to white massive calcite filling
LMM-5-talus	calcite-filled	fracture	K-feldspar/quartz → albite/muscovite/apatite	green, fluorescent, massive apatite at contact; platy to tabular purple apatite in vug; flaky, white calcite filling
LMM-5-talus	calcite-filled	fracture	tourmaline/quartz/albite → laumontite calcite	tourmaline included in quartz;
NSE-1N-3t	open-space	pocket	K-feldspar/muscovite → (albite/purple apatite)	
NMM-1N-27t	open-space	pocket	lepidolite	"popcorn"-like lepidolite occupies cavities between very coarse-grained cleavelandite blades
LMM-5-talus	open-space	fracture	K-feldspar/quartz → albite/muscovite/apatite → pink mica	partially infilled by spongy, pink mica
LMM-6-talus	calcite-filled	fracture (?)	muscovite → quartz/beryl → calcite	tabular, "goschenite" beryl

3.3.2 Rhythmic Banding

Rhythmic banding occurs in several different styles, which seems suggests that no one mechanism is responsible for these textures. The banding is defined by variations in mineralogy, grain size or both (see Figs. 3.6 to 3.19). With respect to banding, dikes in the Little Nahanni Pegmatite Group may be broadly classified in two groups depending on the presence or absence of aplitic material. Each group can be further subdivided into those dikes that show banding and those that do not (see also Table 3.2).

Type A dikes are unbanded and appear quite homogeneous, especially those of aplitic texture. Some unbanded pegmatite dikes show internal zoning, but this is not to be confused with rhythmic banding (Fig. 3.6 and 3.7). Unbanded aplitic dikes appear homogeneous in all respects.

Figures 3.8 and 3.9 show example of type B banding in pegmatitic dikes. Dikes with this type of banding are banded with respect to the spodumene crystals only. Individual spodumene crystals within the bands have grown perpendicular to the contact and no aplitic material separates these bands of spodumene. In hand sample, there appears to be no difference in the mineralogy of the "matrix" between the bands and between the individual crystals of spodumene. The spodumene bands are commonly densest along the outside edges of the intermediate zone. Figure 3.8 is a drawing of a dike that shows this feature. Spodumene crystals between the bands, toward the centre of the dike, have the same orientation as those within the bands but are not as aligned parallel to the dike/host rock contact. More typical of this type of banding are multiple spodumene bands separated by coarse feldspar bands (± elongate, blebby quartz). In the case shown in figure 3.9, large blocky K-feldspars transect the spodumene bands. With the exception of the elongate quartz 'cores', quartz content within the spodumene bands is generally greater than between the bands.

Table 3.2: Types of dikes with respect to banding.

Type	Aplitic material present	Banding	Remarks
A	No	Unbanded	Except for subtle zonation, apparently homogeneous pegmatite dike.
B	No	Yes	Spodumene occurs in bands.
C	No	Yes	Subtle banding with respect to feldspar and quartz; spodumene not banded.
D	Yes	Unbanded	Homogeneous appearing aplitic dike.
E	Yes	Yes	Alternating bands of aplitic material and quartz-feldspar (i.e. non-spodumene-bearing) pegmatitic layers. Pegmatitic feldspars may show directional growth.
F	Yes	Yes	Alternating bands of pegmatitic (spodumene-bearing) material and aplitic material.

Type C banded pegmatite is in some ways similar to the type just described except that the spodumene crystals do not form in bands. Banding is expressed by non-continuous, but alternating layers of quartz and feldspar (see Figs. 3.10 and 3.11).

Some of the most visually striking banding occurs when pegmatitic and aplitic layers alternate. Type E banding involves the alternation of aplitic bands with pegmatitic quartz + feldspar ± mica bands; spodumene is entirely absent from these bands (Figs. 3.12 and 3.13). Colloform textures and strong directional growth are prominent features of this banding type (Figs. 3.14 and 3.15; see also appendix D).

Perhaps the most common type of banding is that shown in figures 3.16 to 3.19. In type F banding, bands of spodumene + quartz + feldspar alternate with bands of aplitic material. The spodumene-rich bands may vary in grain size or width but the mineralogy is essentially the same. Individual bands in this type (F), rarely extend along strike for more than a few metres. For example, the photographs in figures 3.16 and 3.17 are of the same dike, taken at locations about four metres apart. The type of banding is the same, though the dike sections appear dissimilar upon first glance. Figure 3.19 shows a dike in the OMM-3-4 swarm exhibiting type F banding that includes lepidolite in the spodumene bands. In fact, the lepidolite seems to be banded within the wider spodumene bands. Figure 3.20 is a photograph of a boulder from the 1^2 ridge (the Cali claims). Clearly visible are two bands of spodumene + K-feldspar + quartz separated by an aplitic layer. However, the crystals comprising the inner spodumene-bearing band are much larger than those of the outer band. The quartz content of the inner band is also considerably less than that of the outer band; less than ten percent in the former *versus* about thirty-five percent in the latter. Whether this represents "banding" or "zonation" (i.e. inner and outer intermediate zones) is debatable. Here they are considered bands of essentially equivalent, spodumene-bearing bands within a single zone.

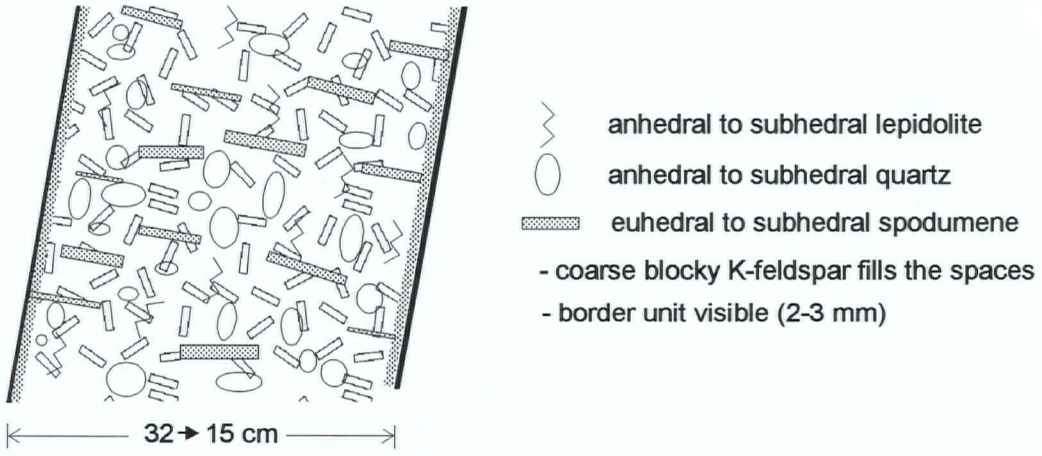

Figure 3.6: An apparently homogenous dike. Only border unit and intermediate unit are present (drawing of dike NMM-1N-3).

Figure 3.7: Photograph of a sample from dike LMM-4-1. This is an example of an unbanded (type A) dike as depicted in figure 3.6. Scale in centimetres.

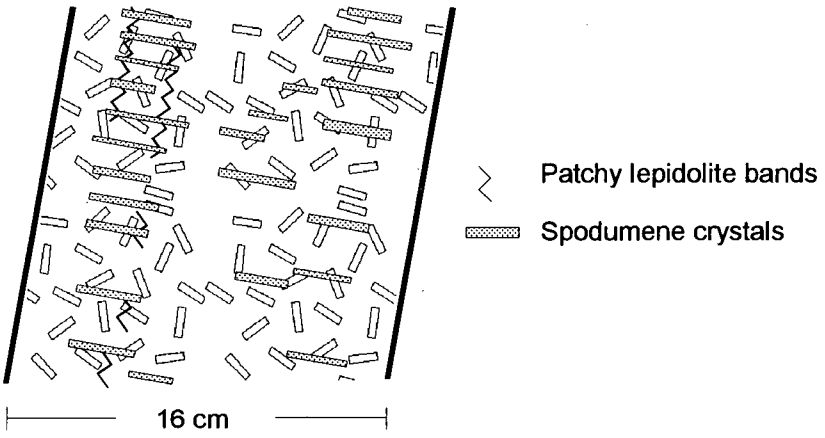

Figure 3.8: Rhythmic banding, type B (NMM-1N^1S-24). There is no textural difference from contact to contact with respect to the "matrix" feldspar (dominant) and quartz (minor). The border unit is less than 1 mm thick if present at all. The spodumene banding is noticeable, but not sharp. Note that this example may also be considered as type A. See text.

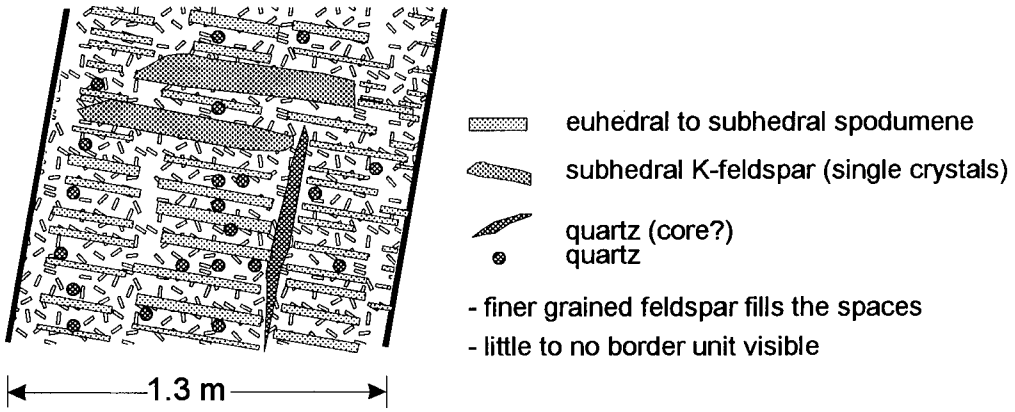

Figure 3.9: Another example of type B banding. This portion of a dike, found in a large talus boulder below NMM-1N-7s, shows very coarse spodumene banding with large feldspars appearing to cut across the bands.

Figure 3.10: Photograph of dike NMM-1N-13. Note the elongate quartz bodies parallel to the dike contact. The rusty-coloured crystals to the left of the lens cap are spodumene. The lens cap is 52 mm in diameter.

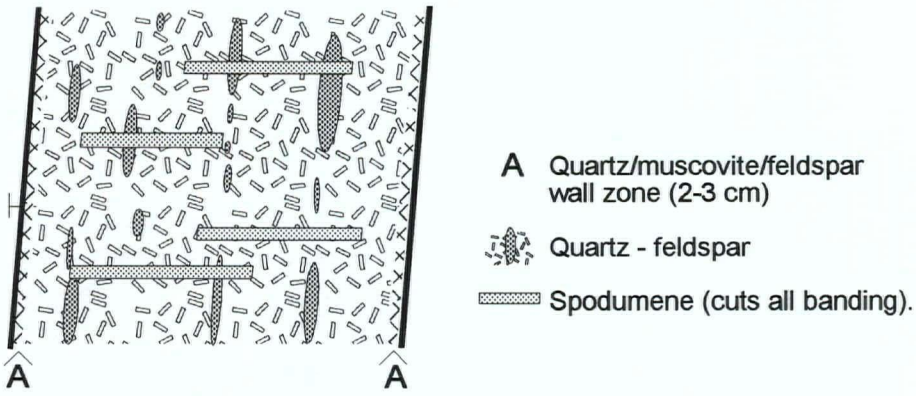

Figure 3.11: Type C banding in dike NMM-1N-13. The spodumene crystals are parallel to one another, but randomly distributed across the dike. It is the elongate quartz bodies that give the banded appearrance to this dike.

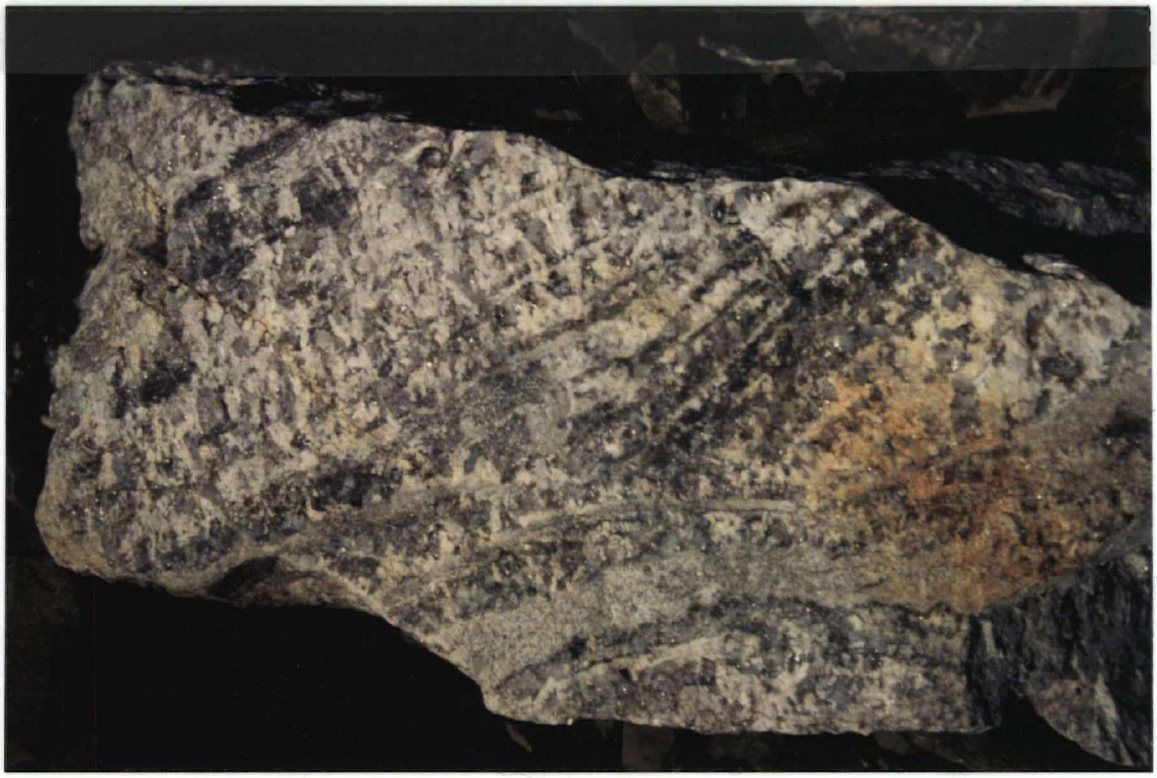

Figure 3.12: A boulder from LMM-6-1 exhibiting type E banding. Note the directional growth expressed by the feldspar crystals. The boulder is approximately 50 cm across.

Figure 3.13: Cross-section of a boulder in cirque 6 showing type E banding. The photo is approximately to scale.

Figure 3.14: Photograph of sample 455 showing colloform banding (type E). Cm scale on right.

Figure 3.15: Photograph of sample 360 showing directional crystal growth in type E banding. Cm scale.

Figure 3.16: Type F banding in dike NMM-1N-9. Note the density of the spodumene crystals in the bands. Boot size is men's 9.5...approximately 10 cm wide.

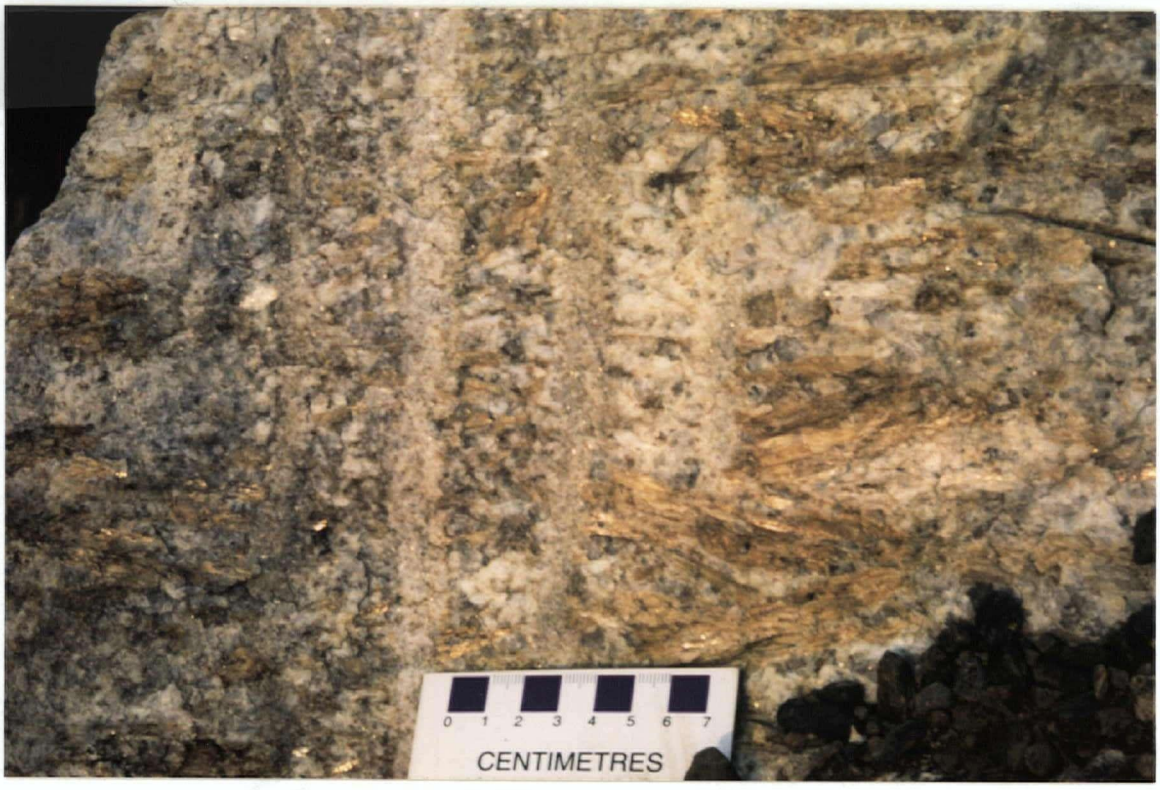

Figure 3.17: Type F banding in dike NMM-1N-9. Note the cutting relationships between the aplitic bands and the spodumene crystals. The aplite transects some spodumene crystals and not others.

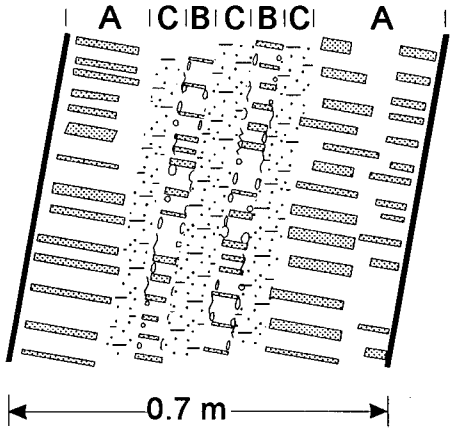

A = Coarse-grained spodumene, quartz and feldspar.

B = Finer-grained spodumene, quartz and feldspar bands with quartz/muscovite selvages.

C = Fine-grained (<2-3mm) feldspar + muscovite.

- sharp contacts between A & C and B & C

Figure 3.18: Type F banding. This drawing was made of a section of dike NMM-1N-9 a few metres away from where the photographs in figures 3.16 and 3.17 were taken. Note that not all the spodumene bands are divided by an aplite layer.

Figure 3.19: Type F banding in dike OMM-3-4. Note the multiple lepidolite bands within the spodumene bands, especially in the right hand portion of the dike.

Figure 3.20: Type F banding in a boulder on the Cali claims. Note the much large spodumene and K-feldspar crystals in the inner pegmatitic band (the bottom of the photograph corresponds to the pegmatite/host rock contact).

Figure 3.21: Dike NMM-1N-9. The upper block of this dike has been displaced by several metres to the right (down-slope). The creek flows along the surface of the slippage plane.

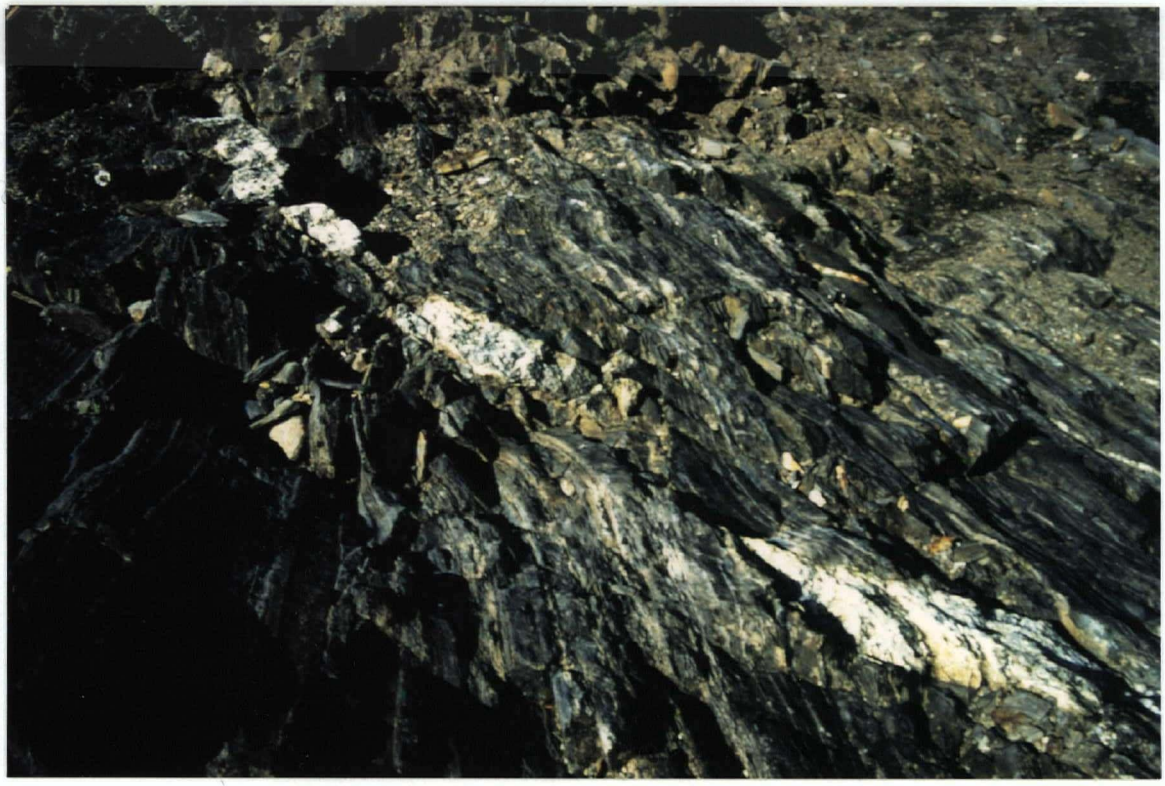

Figure 3.22: A dike in cirque 9 exhibiting either a pinch and swell feature or boudinaging.

Figure 3.23: Dike NMM-1N-10. This pinch feature may be the result of shrinkage in the dike or post-emplacement pinching (boudinaging). The dike is about 1 m wide.

Figure 3.24: Photograph of the north side of cirque 10. The cross-cutting dikes, LMM-10-6 and 7, can be seen near the centre of the photograph.

Figure 3.25: A spectacular example of boudinage in a dike in the LMM-10-12 swarm. The dike two metres to the east of this one is likewise boudinaged.

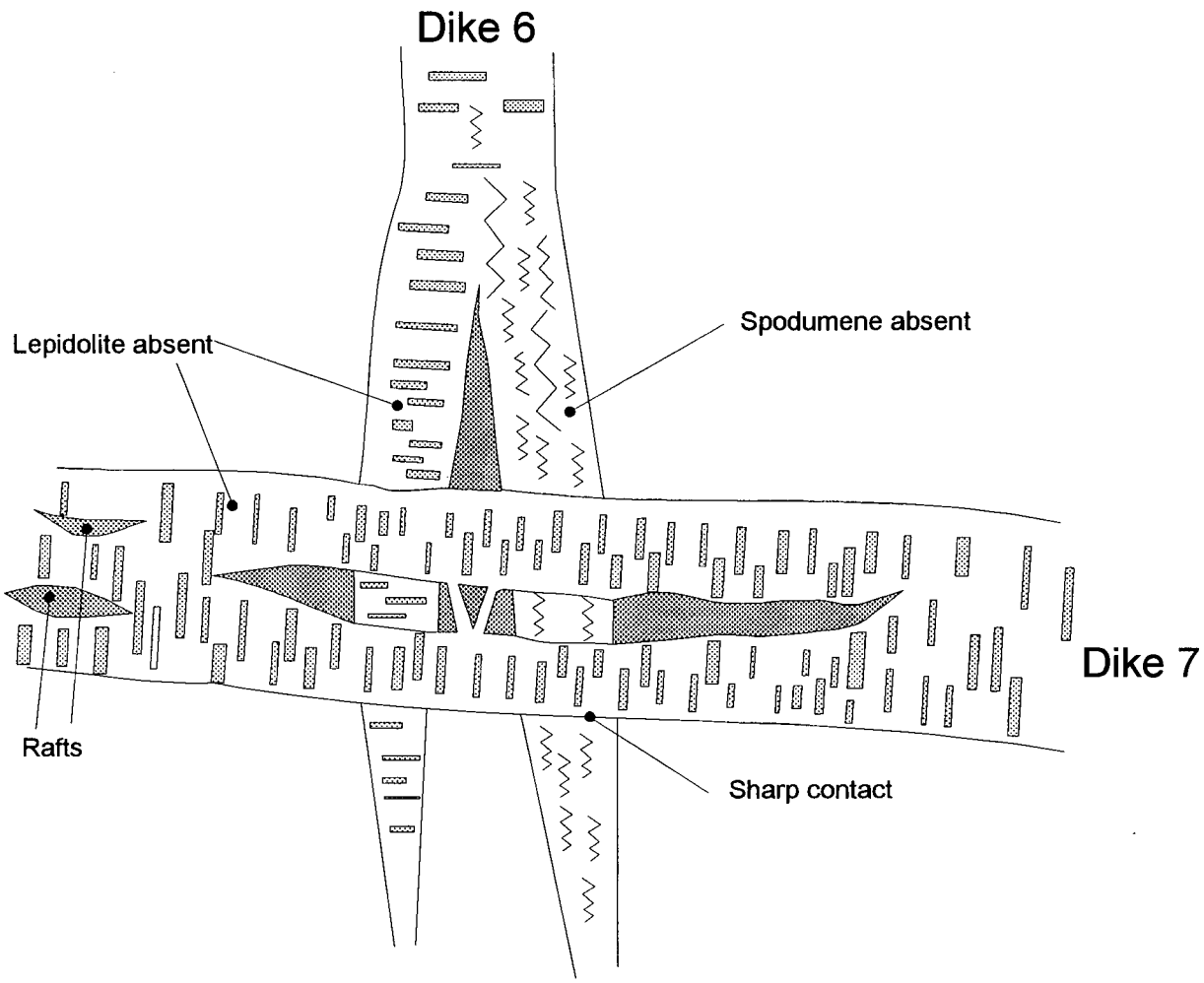

Figure 3.26: These dikes (LMM-10-6 and 7) represent the only pair of confirmed cross-cutting relationship in the Little Nahanni Pegmatite Group.

4 EXPERIMENTAL METHODS

4.1 X-ray Diffraction

Structural states of plagioclase and potassium-feldspars were determined following the procedures outlined by Wright and Stewart (1968) and Bambauer *et al.* (1967). X-ray diffraction work was done on a Siemens D5000 diffractometer at 30 mA and 40 kV using monochromated Cu$K\alpha_1$ radiation of 1.5406 angstroms. Annealed CaF_2 standard (a = 5.4635(2): against NBS Si (batch 640b) using Cu $K\alpha_1$ = 1.5406) was added to correct measured 2Θ values for potassium feldspars and BaF_2 standard (a = 6.1978(3): against NBS Si (batch 640b) using Cu $K\alpha_1$ = 1.5406) was used for plagioclase. Samples were run between 12 and 55 2Θ in 0.01 steps counting for 2 seconds per step.

The structural states of columbite group minerals were also determined using the same diffractometer. The same CaF_2 standard was used to correct peak positions. Samples were run between 10 and 70 2Θ in 0.01 steps with a counting time of 2 seconds.

A version of the CELREF program of Appleman and Evans (1973) was used to index and refine unit-cell parameters.

4.2 Geochronology

Mica concentrates for K-Ar dating were prepared from hand specimens using conventional crushing, grinding, heavy liquid and magnetic separation methods. K concentrations were determined using conventional atomic absorption flame photometry, and Ar isotopic compositions were measured on a modified MS-10 mass spectrometer.

Columbite and feldspar separates for U-Pb dating and Pb isotopic analysis, respectively, were picked from hand specimens. A single columbite crystal was selected from each of the four pegmatite samples, and broken into several smaller fragments. Two to three fragments of fracture- and (visually) inclusion-free material, each of which comprised a single fraction, were

selected for U-Pb analyses, based mainly on variations in colour. The remaining fragments from these crystals were mounted for SEM studies.

The columbite grains were washed in warm 3N HNO_3, and were leached for ~10 minutes in a mixture of concentrated HF and HCl to remove surface contaminants and possible U-bearing phases such as apatite. The columbites were dissolved in the presence of a ^{205}Pb-$^{233-235}U$ tracer on a 120 °C hot-plate in sealed 7 ml Savillex beakers in ~1 ml of concentrated HF with several drops of 16N HNO_3. Complete dissolution typically occurred in 1 to 3 hours. Fluoride precipitates that remained after drying down the solution were redissolved in ~1.5 ml 1 N HBr. After 48 hr on a ~80 °C hot plate, a small amount of white aggregates of insoluble fluoride precipitates remained in each beaker. The solutions were again dried down and 6 N HCl was added in an unsuccessful attempt to convert the remaining precipitates to chlorides. A second 24-hour dissolution on the hot-plate in 1N HBr following an ultrasonic bath to disaggregate the fluoride precipitates was successful. The sample solutions were loaded onto 0.25 ml capacity anion exchange columns for separation of U and Pb using conventional HNO_3-HBr chromatography (e.g., Parrish *et al.*, 1992).

Feldspar samples for Pb isotopic analyses were prepared from the same specimens from which the columbites had been separated. Clean, unaltered, inclusion-free feldspar grains were hand-picked under a microscope, then ground using an agate mortar and sieved to obtain a 74 to 149 μm sample. This material was again examined under a binocular microscope and grains containing visible inclusions or impurities were removed. After strong leaching in a mixture of concentrated HF and HCl, the sample was dissolved in sealed 7 ml Savillex beakers on a hot plate. Pb was separated and purified on 1 ml anion exchange columns using a 1N HBr medium.

U and Pb isotopic compositions were measured on a VG-54R mass spectrometer equipped with a Daly detector. Raw mass spectrometer data were corrected for mass fractionation effects, based on replicate analysis of the NBS-981 Pb standard and the isotopic compositions

recommended by Todt *et al.*, (1984). Errors associated with the ages were calculated using the numerical error propagation method of Roddick (1987), and are given at a 2σ level.

4.3 Electron Microprobe

Electron-microprobe analyses (wavelength dispersion spectroscopy) for all minerals (except most phosphates) were made using a JEOL 733 electron microprobe with Tracor-Northern 5500 and 5600 automation. Operating conditions were 15 *kV* accelarating voltage, 20 *nA* beam current, point focus to 10 μm beam diameter. Before analysis, chemical heterogeneities were determined using backscattered electron imaging. Data for standards were collected for 50 seconds or 0.25% precision (4σ level), whichever was attained first; data for samples were collected for 25 seconds or 0.50% precision. Exceptions to this were feldspar trace elements (Ba, Sr, Rb, Cs and Pb) and beryl trace elements (Mn, Sc,V, Cr and Cs) which were counted for 100 and 200 seconds, respectively, to improve detectability. An element was considered observed only if it was significant at the 4σ (meas.) level. Data reduction was done with a conventional ZAF routine in the Tracor-Northern TASK series of programs. The standards used are listed in Appendix B-1.

Phosphates other than (most) apatites were analysed on a CAMECA SX-50 microprobe, in the wavelength-dispersion mode with the following operating conditions: accelerating voltage, 15 *kV*; beam current, 20 nA; and at least a 10 μm beam diameter.

4.4 Wet Chemical

Wet chemical analyses were performed by Chemex Labs in North Vancouver, British Columbia. Preparation and method for the various elements analyzed are summarized in appendix C-1; results are tabulated in appendix C-2.

4.5 Scanning Electron Microscope

A Phillips XL-30 scanning electron microscope was used to make preliminary examinations of probe mounts and to produce backscattered electron images of probe mounts. The SEM was

also used to obtain qualitative chemical data (energy dispersive spectroscopy) for preliminary mineral identification.

4.6 Fluorescence/Irradiation

To help identify phases and features not readily distinguishable in normal light and to determine fluorescent properties, all samples were subjected to shortwave and longwave ultraviolet light.

Several specimens (apatite and spodumene) were irradiated to determine the effects of radiation on colour. All samples were subjected to 2.5 megarads of gamma radiation from a cobalt 60 source. Irradiation experiments were conducted at the University Hospital by Craig Smith, Radiation Protection Officer.

5 MINERALOGY/GEOCHEMISTRY

5.1 Feldspars

5.1.1 K-feldspar

Abundant K-feldspar is most easily recognized in the intermediate zones as relatively large (2 to 70 cm long), blocky to elongate anhedral to (rarely) euhedral, crystals exhibiting perfect cleavage. These crystals are white, to grey, to a mottled brown in colour. Elongate K-feldspar crystals are usually oriented perpendicular to the pegmatite/wall rock contact, as are associated spodumene laths (Fig. 5.1). Blocky, euhedral K-feldspar also commonly surrounds quartz cores (Fig. 5.2)

K-feldspar is commonly microperthitic to perthitic, although visually homogenous crystals also occur. Perthite types range from strings and rods to interpenetrating (Deer *et al.*, 1966). The cores of some large, blocky K-feldspars are heavily quartz-included; enough to obliterate the cleavage. K-feldspar also occurs as finer-grained, anhedral grains in the wall zone of many dikes. K-feldspar occurs as euhedral crystals in calcite-filled fractures and "pockets". Sample 341 exhibits a large K-feldspar crystal through which a late-stage fracture has cut, and upon which a subsequent overgrowth of gemmier K-feldspar has occurred. However, more commonly, "pocket" K-feldspar crystals are heavily etched.

Nineteen K-feldspar samples were analyzed for Al and Si as well as Na, K, Ca, Rb, Cs, Mn, Sr, Ba, Fe and P using electron microprobe techniques. Seven of these samples were analyzed for Li, Sr, Rb, Ba, Pb and F using wet chemical methods. The samples with their locality information are listed in Appendix A. Microprobe data are provided in Appendix B-2 (diskette). Wet chemical data are provided in Appendix C. Table 5.1 summarizes average compositions for the nineteen samples analyzed by electron microprobe.

Figure 5.1: Elongate K-feldspar and spodumene crystals in a large boulder on the Cali claim. The top and bottom edges of this photograph are parallel to the contacts of this dike.

Figure 5.2: Dike cross-section (sample 132). Note quartz core with euhedral feldspars. Scale in cm.

The K-feldspar compositions range from Or_{90} to Or_{98}. The nineteen samples analyzed show high levels of fractionation with respect to their Li and Rb contents and K/Rb ratios. Lithium contents, measured by wet chemical methods, range from 76 to 440 ppm. Samples analyzed by microprobe contained between 0.003 and 0.032 Rb atoms per formula unit and have K/Rb ratios from 317.67 to 28.32 (Fig. 5.3). Little Cs was detected in the K-feldspars. The highest analysis gave 0.007 wt % Cs_2O in sample 344, which is still close to the detection limit of the electron microprobe. No Cs was detected by wet chemical methods. The reverse is true for Pb: wet chemical analyses showed 22 to 122 ppm Pb, whereas no Pb was detected at all by microprobe analysis. SEM and microprobe analysis did, however, reveal inclusions of galena in some K-feldspars which may account for the Pb values obtained by wet chemistry.

XRD analyses of seven K-feldspar samples show them to be orthoclase. Three of the samples also contained enough albite to cause peak overlaps, making those analyses undesirable for further structural study. The 2Θ values of 060 are plotted against the 2Θ values of $\bar{2}04$ for the remaining four, relatively homogeous K-feldspar samples, as well as five albite samples, in figure 5.4. They are compared to values plotted by Wright (1968). Another common plot (e.g. Černý *et al.* 1984; Chackowsky, 1987) for indicating the general structural state of alkali feldspars is the *b-c* plot of Wright and Stewart (1968), or later versions of it (*cf* Stewart and Wright, 1974; Stewart, 1975; Kroll and Ribbe, 1983). This plot is shown in figure 5.5.

Some replacement textures, as shown in the section dealing with perthites by Deer *et al.* (1966), can be observed in samples from the Little Nahanni Pegmatite Group. In particular, some samples of blocky, greyish K-feldspar have rims around and/or penetrating "fingers" or patches of albite in them (e.g. sample 153). K-feldspar crystals in some calcite-filled "pockets" are heavily etched where only skeletal frameworks are all that remain (e.g. sample 330). Cleavelanditic albite and zeolites have commonly grown on these "boxwork" remains.

Most samples of blocky K-feldspar fluoresced white under short-wave ultraviolet light. K-feldspars with many inclusions or a lack of obvious cleavage (i.e. fine-grained) did not fluoresce as well or at all. For example, sample 167(B) exhibits a "granular" interior (due to fine-grained quartz inclusions) that neither shows a cleavage nor does it fluoresce. However, the outer rim of this crystal is shows a continuous cleavage plane and a white fluorescence under ultraviolet light. Ultraviolet light is also useful for looking at the alteration of blocky K-feldspar. Remnant, unaltered K-feldspar 'eyes' fluoresce white while albitized rims and stringers fluoresce red.

Table 5.1: Average electron probe microanalyses of K-feldspar samples.

Sample	161	186	113	167	154	251
# of analyses	8	11	4	5	9	6
SiO_2	64.49(45)	64.91(29)	63.39(48)	63.85(21)	64.05(31)	63.83(35)
Al_2O_3	18.40(17)	18.68(6)	18.12(14)	18.64(10)	18.65(12)	18.55(8)
Fe_2O_3	nd	0.01(2)	0.04(1)	nd	0.01(2)	nd
K_2O	15.65(61)	15.14(19)	15.70(15)	14.93(27)	15.22(15)	15.41(25)
Na_2O	0.41(18)	0.74(14)	0.33(8)	1.12(12)	0.82(13)	0.76(15)
CaO	nd	nd	0.01(1)	nd	nd	nd
Rb_2O	0.45(6)	0.45(6)	0.28(5)	0.49(3)	0.58(5)	0.36(2)
Cs_2O	nd	nd	0.01(1)	0.01(2)	nd	0.01(2)
MnO	nd	nd	nd	nd	nd	nd
SrO	0.10(2)	0.10(1)	0.13(4)	0.09(1)	0.10(1)	0.09(1)
BaO	nd	nd	0.02(2)	nd	nd	nd
P_2O_5	0.15(20)	0.31(4)	0.06(7)	0.43(4)	0.37(4)	0.34(5)
Total	99.65	100.34	98.09	99.56	99.80	99.35
Si^{4+}	2.992	2.983	2.992	2.963	2.968	2.970
Al^{3+}	1.006	1.012	1.008	1.020	1.019	1.017
Fe^{3+}	nd	nd	0.001	nd	nd	nd
K^+	0.926	0.888	0.945	0.884	0.900	0.915
Na^+	0.037	0.066	0.030	0.101	0.074	0.069
Ca^{2+}	nd	nd	0.001	nd	nd	nd
Rb^+	0.013	0.013	0.008	0.015	0.017	0.011
Cs^+	nd	nd	nd	nd	nd	nd
Mn^{2+}	nd	nd	nd	nd	nd	nd
Sr^{2+}	0.003	0.003	0.004	0.002	0.003	0.002
Ba^{2+}	nd	nd	nd	nd	nd	nd
P^{5+}	0.006	0.012	0.002	0.017	0.015	0.013
Mole% Or[a]	0.96	0.93	0.97	0.90	0.92	0.93
Mole% Ab[a]	0.04	0.07	0.03	0.10	0.08	0.07
Mole% An[a]	0.00	0.00	0.00	0.00	0.00	0.00
K/Rb	71.23	68.31	118.13	58.93	52.94	83.18

a Calculations based on relative molar abundance of K, Na, and Ca, respectively.
nd Not detected.
() Standard deviation.

Table 5.1: (continued).

Sample	220	226	186	218	160	341
# of analyses	8	11	7	8	5	16
SiO_2	64.10(19)	63.67(29)	64.05(39)	63.69(26)	63.01(44)	64.32(45)
Al_2O_3	18.57(8)	18.73(14)	18.73(20)	18.63(9)	18.49(25)	18.60(14)
Fe_2O_3	0.01(2)	0.01(2)	0.01(3)	nd	0.05(1)	0.02(3)
K_2O	15.16(20)	15.04(25)	15.40(27)	15.25(19)	15.58(19)	15.24(47)
Na_2O	0.87(15)	1.11(15)	0.76(16)	0.82(12)	0.55(14)	0.72(28)
CaO	nd	nd	nd	nd	nd	nd
Rb_2O	0.40(4)	0.39(3)	0.46(6)	0.61(9)	0.28(7)	0.85(12)
Cs_2O	nd	nd	nd	0.01(1)	0.01(1)	0.01(2)
MnO	nd	nd	nd	nd	nd	nd
SrO	0.10(1)	0.10(1)	0.10(1)	0.10(1)	0.12(1)	0.09(2)
BaO	nd	nd	nd	nd	0.02(3)	nd
P_2O_5	0.23(3)	0.5(3)	0.38(6)	0.33(7)	0.27(24)	0.24(11)
Total	99.44	99.55	99.89	99.44	98.38	100.09
Si^{4+}	2.977	2.955	2.965	2.966	2.966	2.978
Al^{3+}	1.017	1.024	1.022	1.022	1.026	1.015
Fe^{3+}	nd	nd	nd	nd	0.002	0.001
K^+	0.898	0.890	0.910	0.906	0.935	0.900
Na^+	0.078	0.100	0.068	0.074	0.050	0.065
Ca^{2+}	nd	nd	nd	nd	nd	nd
Rb^+	0.012	0.012	0.014	0.018	0.008	0.025
Cs^+	nd	nd	nd	nd	nd	nd
Mn^{2+}	nd	nd	nd	nd	nd	nd
Sr^{2+}	0.003	0.003	0.003	0.003	0.003	0.002
Ba^{2+}	nd	nd	nd	nd	nd	nd
P^{5+}	0.009	0.020	0.015	0.013	0.011	0.009
Mole% Or[a]	0.92	0.90	0.93	0.92	0.95	0.93
Mole% Ab[a]	0.08	0.10	0.07	0.08	0.05	0.07
Mole% An[a]	0.00	0.00	0.00	0.00	0.00	0.00
K/Rb	74.83	74.17	65.00	50.33	116.88	36.00

[a] Calculations based on relative molar abundance of K, Na, and Ca, respectively.
nd Not detected.
() Standard deviation.

Table 5.1: (continued).

Sample	344	340	167	153	246
# of analyses	11	14	4	4	8
SiO_2	63.78(54)	63.72(51)	64.74(8)	64.83(22)	63.82(32)
Al_2O_3	18.36(13)	18.89(12)	18.32(10	18.32(14)	18.25(11)
Fe_2O_3	0.01(2)	nd	0.05(1)	0.05(2)	0.03(1)
K_2O	15.42(34)	15.11(35)	15.86(27)	16.06(5)	16.17(12)
Na_2O	0.74(23)	0.84(20)	0.46(17)	0.26(3)	0.24(4)
CaO	0.01(2)	nd	0.02(1)	nd	nd
Rb_2O	0.62(4)	0.51(4)	0.36(1)	0.32(7)	0.19(7)
Cs_2O	0.02(3)	nd	0.01(0)	0.01(1)	0.01(1)
MnO	nd	nd	0.01(1)	0.01(1)	0.01(1)
SrO	0.11(1)	0.10(2)	0.12(1)	0.11(1)	0.11(1)
BaO	nd	nd	0.01(2)	0.02(2)	0.01(1)
P_2O_5	0.25(15)	0.77(19)	nd	0.02(1)	0.03(3)
Total	99.32	99.94	99.96	100.01	98.87
Si^{4+}	2.977	2.944	2.999	3.001	2.991
Al^{3+}	1.010	1.029	1.000	1.000	1.008
Fe^{3+}	nd	nd	0.002	0.002	0.001
K^+	0.918	0.891	0.937	0.948	0.967
Na^+	0.067	0.075	0.041	0.023	0.022
Ca^{2+}	0.001	nd	0.001	nd	nd
Rb^+	0.019	0.015	0.011	0.010	0.006
Cs^+	nd	nd	nd	nd	nd
Mn^{2+}	nd	nd	nd	nd	nd
Sr^{2+}	0.003	0.003	0.003	0.003	0.003
Ba^{2+}	nd	nd	nd	nd	nd
P^{5+}	0.010	0.030	nd	0.001	0.001
Mole% Or[a]	0.93	0.92	0.96	0.98	0.98
Mole% Ab[a]	0.07	0.08	0.04	0.02	0.02
Mole% An[a]	0.00	0.00	0.00	0.00	0.00
K/Rb	48.32	59.40	85.18	94.80	161.17

[a] Calculations based on relative molar abundance of K, Na, and Ca, respectively.
nd Not detected.
() Standard deviation.

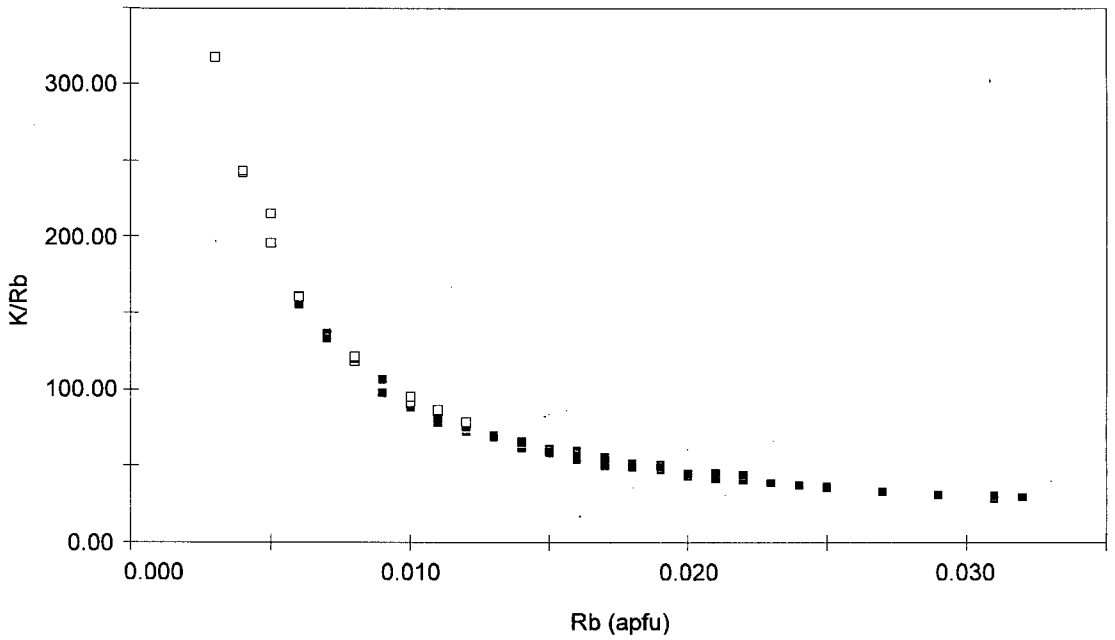

Figure 5.3: K-feldspar K/Rb plotted versus Rb. Solid squares represent sample in which the K-feldspar is a major constituent and open squares represent minor K-feldspar.

Table 5.2: Unit cell dimensions of blocky orthoclase crystals.

Sample	Locality	*a*	*b*	*c*	β	Volume
167	C - 4 - 1B	8.599(4)	12.978(5)	7.207(2)	166.03(4)	722.7(4)
220	LLG - 9 - 2	8.601(8)	12.971(5)	7.208(2)	116.03(6)	722.5(7)
226	C - 5 - 5B	8.591(3)	12.990(4)	7.206 1)	116.07(3)	722.4(3)
251	LSE - 2 - 1	8.616(13)	12.973(11)	7.209(4)	116.03(10)	724.1(11)

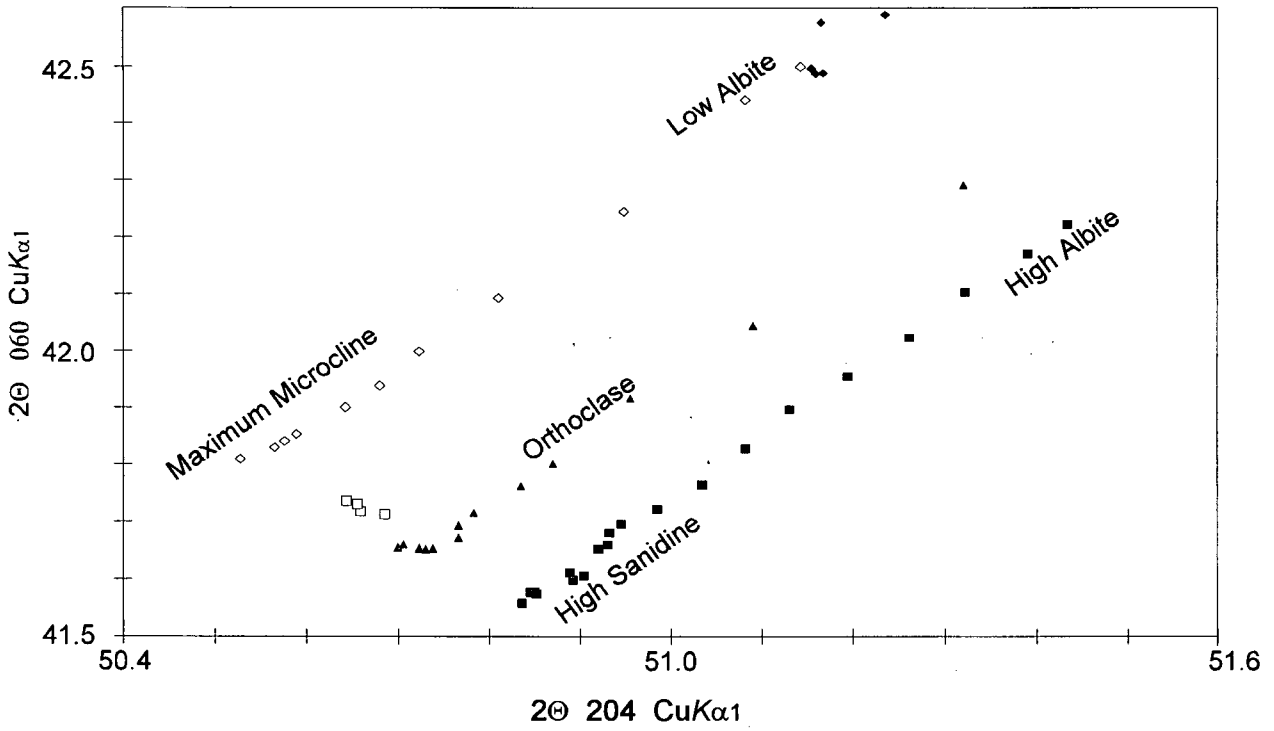

Figure 5.4: The observed 2Θ values of 060 are plotted against 2Θ values of $\bar{2}04$ for alkali feldspars of the Little Nahanni Pegmatite Group (open squares: orthoclase; solid diamonds: low albite), which are compared to similarly plotted values summarized by Wright (1968). The values for the maximum - low albite series and the high sanidine - high albite series are from Orville (1967), and the P50-56 orthoclase series values are from Wright and Stewart (1968) (modified after Wright, 1968).

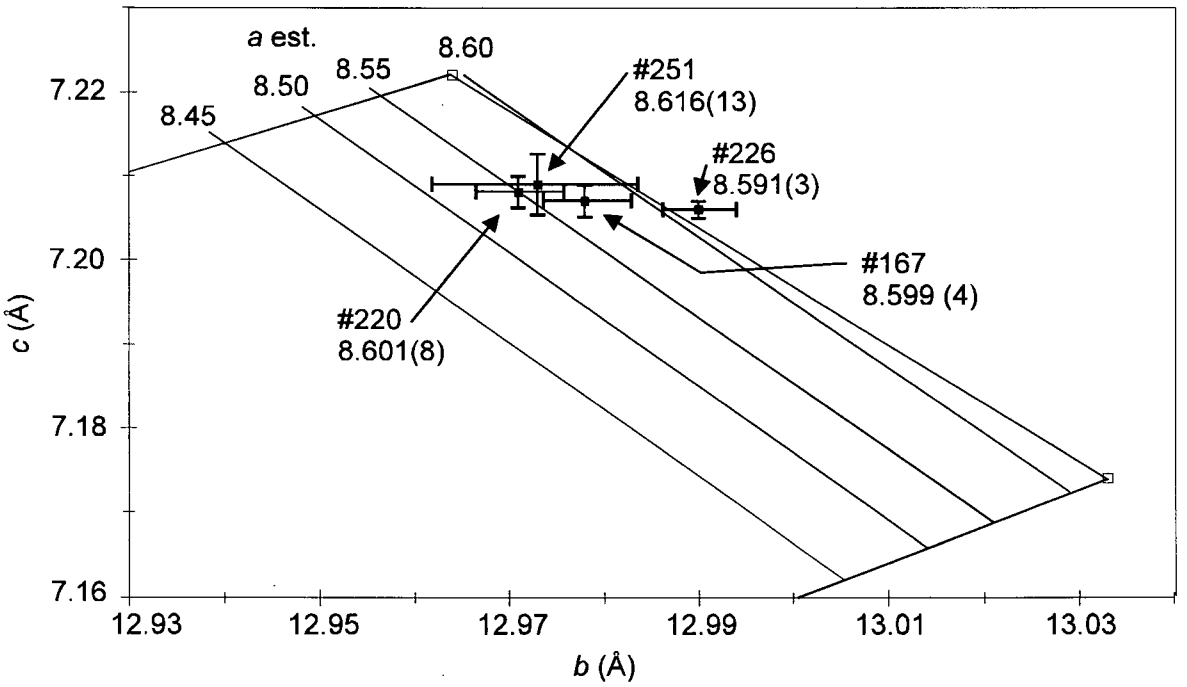

Figure 5.5: A *b* - *c* plot of the blocky K-feldspars, including measured *a* in Å, listed in table 5.2. Error bars are 1σ. (modified after Stewart, 1975)

5.1.2 Plagioclase

Albite appears to be the most dominant mineral in the Little Nahanni pegmatite group, and occurs in many forms. Volumetrically, three types are the most significant. First, white to cream-coloured, coarse-grained (0.5 to 5 cm) cleavelandite, associated with quartz plus or minus mica, is commonly the dominant bulk contituent in coarse-grained, especially non-spodumene-bearing, dikes. The second type is a very fine-grained (~0.1 to 0.5 mm), white to slightly greyish, saccharoidal albite, which also occurs associated with equally fine-grained lepidolite, and quartz. The third type of albite is brownish-grey ("dirty-looking"), and fine to medium-grained (1 to 5 mm). This albite, combined with more or less equal amounts of similarly grain-sized quartz, plus or minus muscovite, comprises the "aplitic" layers, pods, and even entire dikes throughout the pegmatite group.

Euhedral cleavelandite predominantly comprises the crystallization in calcite-filled, cross-cutting fractures.

As mentioned previously in the "K-feldspar" section, albite is found in blocky K-feldspars as strings and rods (as defined in Deer *et al.*, 1966). As well, albite seems to replace some large blocky potassium feldspars of the intermediate zone. Another example of this is seen in sample 235 where large, greyish orthoclase "eyes" are surrounded by whiter, cleavelanditic albite. The contact between the two is diffuse, but distinguishable by the grey colour and more prominent cleavage in the orthoclase and by the different colours of fluorescence.

Samples 384 is an example that contains spheroidal "bursts" of radiating, coarse-grained cleavelandite in blocky K-feldspar-quartz pegmatite similar to those shown in Cameron *et al.* (1949, p. 86).

Twenty two albite samples were analyzed for Al and Si as well as Na, K, Ca, Rb, Cs, Mn, Sr, Ba, Fe and P using electron microprobe techniques. Eight of these samples were analyzed for B, and five of this subset were analyzed for Sr, using wet chemical methods. The samples with their locality information are listed in Appendix A. Microprobe data are provided in Appendix B-2. Wet chemical data are provided in Appendix C. Table 5.3 summarizes average compositions for the twenty two samples analyzed by electron microprobe.

Averaged analyses show Little Nahanni Pegmatite Group plagioclase to range from An_2 Ab_{98} to Ab_{95} Or_5. All samples contained Sr; up to 0.11 % (sample 174). Only two samples showed the presence of Mn (0.02 and 0.01 % MnO for samples 197 and 167, respectively). Sample 197 was also the only to contain Cs (0.01 % Cs_2O). Sample 197 comprises fine-grained, saccharoidal, white albite associated with Cs-bearing beryls, and fine-grained lepidolite and quartz. Phosphorus contents range from 0.11 to 0.68 % P_2O_5.

The peaks 060, $\bar{2}04$, 131, and $1\bar{3}1$ were measured by powder XRD for five albite samples. 2Θ values for these peaks are summarized in table 5.4. All the samples plot as "low albite" on the $060/\bar{2}04$ plot (Fig. 5.3). $\Delta 131$ *versus* mole % An is plotted for four of these samples in figure 5.6. All four samples plot below the peristerite gap and represent almost fully ordered low albite.

Table 5.3: Average electron probe microanalyses of albite samples.

Sample	197	235	167	153	246	377	363	323
# of analyses	8 (m)	7 (m)	7 (m)	7 (m)	8 (m)	7 (m)	9 (m)	4 (m)
SiO_2	67.64(29	68.05(53	68.17(23	68.25(61	68.26(35	67.52(29	68.03(43	67.84(88)
Al_2O_3	19.49(38	19.88(8)	19.74(14	19.56(17	19.43(19	19.51(15	19.57(19	19.05(58)
Na_2O	11.66(21	11.56(11	11.63(8)	11.71(7)	11.59(12	11.44(6)	11.53(8)	10.78(26)
K_2O	0.06(2)	0.11(2)	0.11(3)	0.10(3)	0.14(10	0.11(2)	0.14(5)	0.81(8)
CaO	0.36(2)	0.30(3)	0.15(7)	0.04(3)	0.06(5)	0.23(10	0.04(4)	0.04(5)
Cs_2O	0.01(1)	nd	nd	nd	nd	nd	nd	nd
MnO	0.02(5)	nd	0.01(1)	nd	nd	nd	nd	nd
SrO	0.05(1)	0.06(1)	0.04(1)	0.05(2)	0.06(2)	0.03(3)	0.04(3)	0.07(3)
BaO	0.01(1)	0.01(1)	nd	nd	nd	nd	nd	nd
Fe_2O_3	0.03(2)	0.03(1)	0.05(2)	0.04(1)	0.03(1)	nd	0.10(2)	nd
P_2O_5	0.50(9)	0.26(12	0.14(12	0.16(20	0.06(9)	0.13(10	0.12(8)	0.02(5)
Total	99.81	100.26	100.04	99.92	99.62	98.98	99.48	98.61
			Formula contents based on 8 anions (O).					
Si^{4+}	2.963	2.967	2.979	2.984	2.993	2.981	2.984	3.008
Al^{3+}	1.006	1.022	1.015	1.008	1.004	1.015	1.012	0.995
Na^{+}	0.990	0.977	0.985	0.993	0.985	0.979	0.981	0.927
K^{+}	0.003	0.006	0.006	0.006	0.008	0.006	0.008	0.046
Ca^{2+}	0.017	0.014	0.007	0.002	0.003	0.011	0.002	0.002
Cs^{+}	nd	nd	nd	nd	nd	nd	nd	nd
Mn^{2+}	0.001	nd	nd	nd	nd	nd	nd	nd
Sr^{2+}	0.001	0.002	0.001	0.001	0.002	0.001	0.001	0.002
Ba^{2+}	nd	0.001	nd	nd	nd	nd	nd	nd
Fe^{3+}	0.001	0.001	0.002	0.001	0.001	nd	0.003	nd
P^{5+}	0.019	0.010	0.005	0.006	0.002	0.005	0.004	0.001
Mole% An	0.02	0.01	0.01	0.00	0.00	0.01	0.00	0.00
Mole% Ab	0.98	0.98	0.99	0.99	0.99	0.98	0.99	0.95
Mole% Or	0.00	0.01	0.01	0.01	0.01	0.01	0.01	0.05

Note: Rb and Pb sought but not detected
(m) = major constituent in probe mount
(i) = inclusion in K-feldspar
nd = not detected

Table 5.3: (continued).

Sample # of analyses	354 4 (m)	161 5 (i)	186 4 (i)	167 4 (i)	154 7 (i)	251 2 (i)	220 5 (i)	226 6 (i)
SiO_2	68.20(26	68.24(63	68.94(28	68.11(36	68.07(20	68.12(52	68.00(24)	67.68(49
Al_2O_3	19.57(5)	19.51(19	19.59(12	19.44(12	19.48(15	19.38(18	19.51(6)	19.74(9)
Na_2O	11.57(3)	11.70(3)	11.81(2)	11.68(8)	11.74(11	11.64(23	11.69(16)	11.75(10
K_2O	0.13(2)	0.12(8)	0.16(2)	0.13(3)	0.10(2)	0.14(2)	0.17(4)	0.14(3)
CaO	0.05(4)	nd	nd	nd	0.01(2)	0.06(1)	nd	0.05(5)
Cs_2O	nd	nd	nd	nd	nd	nd	nd	nd
MnO	nd	nd	nd	nd	nd	nd	nd	nd
SrO	0.03(3)	0.05(1)	0.03(3)	0.04(3)	0.05(2)	0.05(0)	0.05(1)	0.04(2)
BaO	nd	nd	nd	nd	nd	nd	nd	nd
Fe_2O_3	nd	nd	nd	nd	nd	nd	nd	nd
P_2O_5	0.16(4)	0.28(18	0.12(14	0.21(11	0.17(18	0.08(11	0.11(6)	0.34(10
Total	99.70	99.89	100.63	99.60	99.61	99.46	99.53	99.74
			Formula contents based on 8 anions (O).					
Si^{4+}	2.986	2.983	2.992	2.986	2.985	2.992	2.986	2.966
Al^{3+}	1.010	1.005	1.002	1.005	1.007	1.003	1.010	1.020
Na^{+}	0.982	0.992	0.994	0.993	0.998	0.991	0.995	0.998
K^{+}	0.007	0.007	0.009	0.007	0.006	0.008	0.010	0.008
Ca^{2+}	0.002	nd	nd	nd	nd	0.003	nd	0.002
Cs^{+}	nd	nd	nd	nd	nd	nd	nd	nd
Mn^{2+}	nd	nd	nd	nd	nd	nd	nd	nd
Sr^{2+}	0.001	0.001	0.001	0.001	0.001	0.001	0.001	0.001
Ba^{2+}	nd	nd	nd	nd	nd	nd	nd	nd
Fe^{3+}	nd	nd	nd	nd	nd	nd	nd	nd
P^{5+}	0.006	0.010	0.004	0.008	0.006	0.003	0.004	0.013
Mole% An	0.00	0.00	0.00	0.00	0.00	0.00	0.00	0.00
Mole% Ab	0.99	0.99	0.99	0.99	0.99	0.99	0.99	0.99
Mole% Or	0.01	0.01	0.01	0.01	0.01	0.01	0.01	0.01

Note: Rb and Pb sought but not detected
(m) = major constituent in probe mount
(i) = inclusion in K-feldspar
nd = not detected

Table 5.3: (continued).

Sample	186	218	160	341	344	340
# of analyses	3 (i)	6 (i)	4 (i)	3 (i)	3 (i)	3 (i)
SiO_2	67.74(27	67.92(37	67.62(56	68.28(59	67.73(31	67.53(30
Al_2O_3	19.74(4)	19.52(9)	19.42(18	19.57(2)	19.35(18	19.90(27
Na_2O	11.82(4)	11.80(10	11.50(10	11.66(13	11.39(12	11.59(8)
K_2O	0.14(5)	0.14(3)	0.13(3)	0.14(1)	0.18(4)	0.14(1)
CaO	0.01(2)	nd	0.05(2)	nd	0.03(5)	nd
Cs_2O	nd	nd	nd	nd	nd	nd
MnO	nd	nd	nd	nd	nd	nd
SrO	0.05(1)	0.05(1)	0.04(2)	0.05(1)	0.06(1)	0.01(2)
BaO	nd	nd	nd	nd	nd	nd
Fe_2O_3	nd	nd	0.02(3)	0.04(4)	nd	nd
P_2O_5	0.24(3)	0.13(11)	0.16(8)	0.20(10)	0.20(0)	0.68(16)
Total	99.70	99.56	98.93	99.94	98.93	99.85
			Formula contents based on 8 anions (O).			
Si^{4+}	2.970	2.983	2.985	2.984	2.988	2.952
Al^{3+}	1.020	1.010	1.010	1.008	1.006	1.025
Na^{+}	1.005	1.005	0.984	0.988	0.974	0.982
K^{+}	0.008	0.008	0.007	0.008	0.010	0.008
Ca^{2+}	nd	nd	0.002	nd	0.001	nd
Cs^{+}	nd	nd	nd	nd	nd	nd
Mn^{2+}	nd	nd	nd	nd	nd	nd
Sr^{2+}	0.001	0.001	0.001	0.001	0.002	nd
Ba^{2+}	nd	nd	nd	nd	nd	nd
Fe^{3+}	nd	nd	0.001	0.001	nd	nd
P^{5+}	0.009	0.005	0.006	0.007	0.007	0.025
Mole% An	0.00	0.00	0.00	0.00	0.00	0.00
Mole% Ab	0.99	0.99	0.99	0.99	0.99	0.99
Mole% Or	0.01	0.01	0.01	0.01	0.01	0.01

Note: Rb and Pb sought but not detected
(m) = major constituent in probe mount
(i) = inclusion in K-feldspar
nd = not detected

Table 5.4: Structural data for albites (including 060/$\bar{2}$04 peaks for orthoclase samples used in Fig. 5.3)

Cat #	Species	Locality	An (mole %)	°2Θ 131	°2Θ 1$\bar{3}$1	Δ 131	°2Θ 060	°2Θ $\bar{2}$04
167	Albite	C-4-1B	1	31.230	30.131	1.10	42.590	51.235
197	Albite	LMM-10^11-t	2	31.366	30.319	1.05	42.576	51.165
235	Albite	C-6-2	1	31.314	30.194	1.12	42.497	51.154
246	Albite	LMM-5-t	0	31.293	30.141	1.15	42.487	51.159
277	Albite	LMM-$\bar{1}$-1					42.489	51.167
167	Orthoclase	C-4-1B					41.718	50.659
220	Orthoclase	LLG-9-2					41.736	50.643
226	Orthoclase	C-5-5B					41.713	50.685
251	Orthoclase	LSE-2-1					41.731	50.655

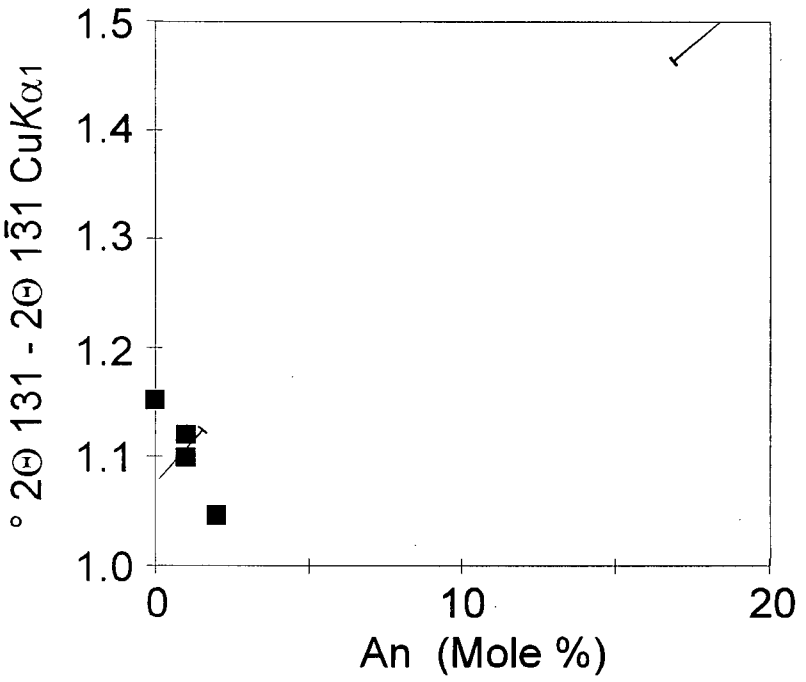

Figure 5.6: Structural states of four albites. The break in the line represents the peristerite gap, and is, including the gap length, as shown in Bambauer *et al.*, 1967.

5.2 Oxides

Oxides are not dealt with in detail in this thesis as they are the subject of another, concurrent research project by T.S. Ercit, L.A. Groat and others. However, as this thesis is predominantly an overview, at least a cursory glance at some of the pertinent details regarding the occurrence and chemistry of accessory oxide minerals is appropriate. Analyses used in this thesis are gratefully acknowledged as coming from work by T.S. Ercit and R.A. Gault.

5.2.1 Columbite Group

Columbite-group minerals (manganocolumbite, ferrocolumbite, manganotantalite and ferrotantalite) occur throughout the Little Nahanni pegmatite group. The columbites are generally euhedral, tabular to blocky crystals, and range from less than 1 mm to 5 cm in size. They are invariably associated with one or more types of albite, as described in section 5.1.2., in the inner wall and intermediate zones, and in the aplitic units. This association is consistent with the description of the occurrence of tantalum mineralization in albite-spodumene type pegmatites in Černý (1989a).

Thirty samples were analyzed by electron microprobe for Nb, Ta, Fe, Mn, Mg, Ti, Sc, Zr, Sn, and W. Investigations in BSE mode showed some samples to be highly oscillatorily zoned, especially with respect to Ta/Nb ratios. Late-stage magmatic replacement textures are also exhibited by some samples (Fig. 5.7). Columbite group minerals are dominantly manganocolumbite (see figure 5.8) though all four species (manganocolumbite, [ferro]columbite, ferrotantalite and manganotantalite) have been identified: Mn/Mn+Fe ratios range from 0.40 to 1.00 and Ta/Ta+Nb ratios vary from 0.09 to 0.79. One sample from cirque 2 (215) contained all four species. Samples from cirque 2 had the highest Fe contents and seem to follow a trend (Fig. 5.9) that is not consistent with most trends given for Mn-Fe and Ta-

Nb fractionation in rare-element pegmatites (e.g Černý *et al.*, 1985). Some similar examples in Černý (1985) are noted though.

Structural states of eight columbite group samples were determined (by M. Raudsepp and T.S. Ercit) using powder XRD methods. The unit cell parameters of the eight samples are summarized in Table 5.5. Figure 5.10 is an *a-c* diagram which represents the columbite group structural states of the Little Nahanni samples.

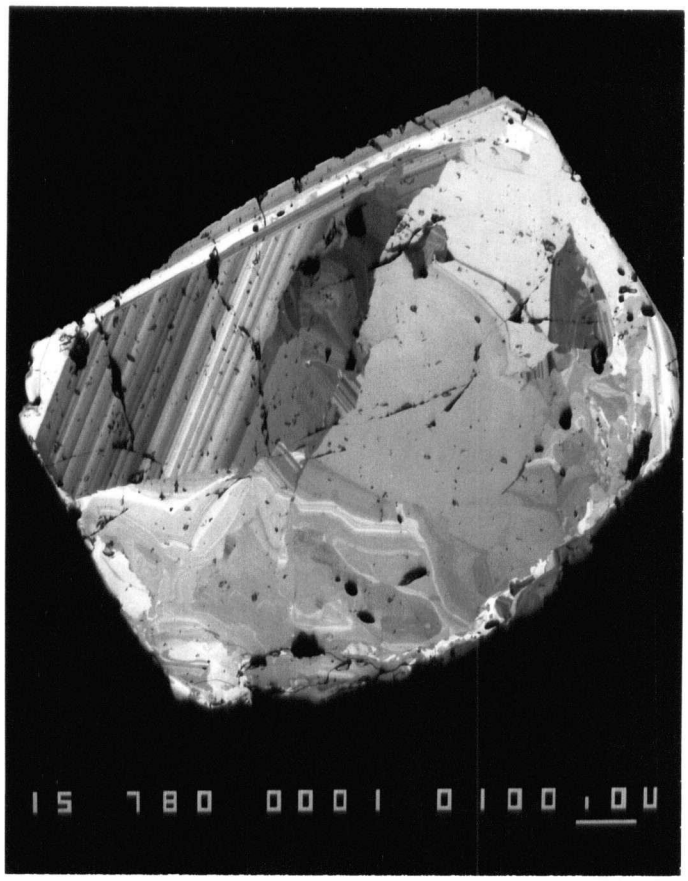

Figure 5.7: Photograph of manganocolumbite (sample 373; mount 127) taken in back-scattered electron imaging mode. Note the late-stage magmatic replacement textures cutting across the straight-lined oscillatory zoning.

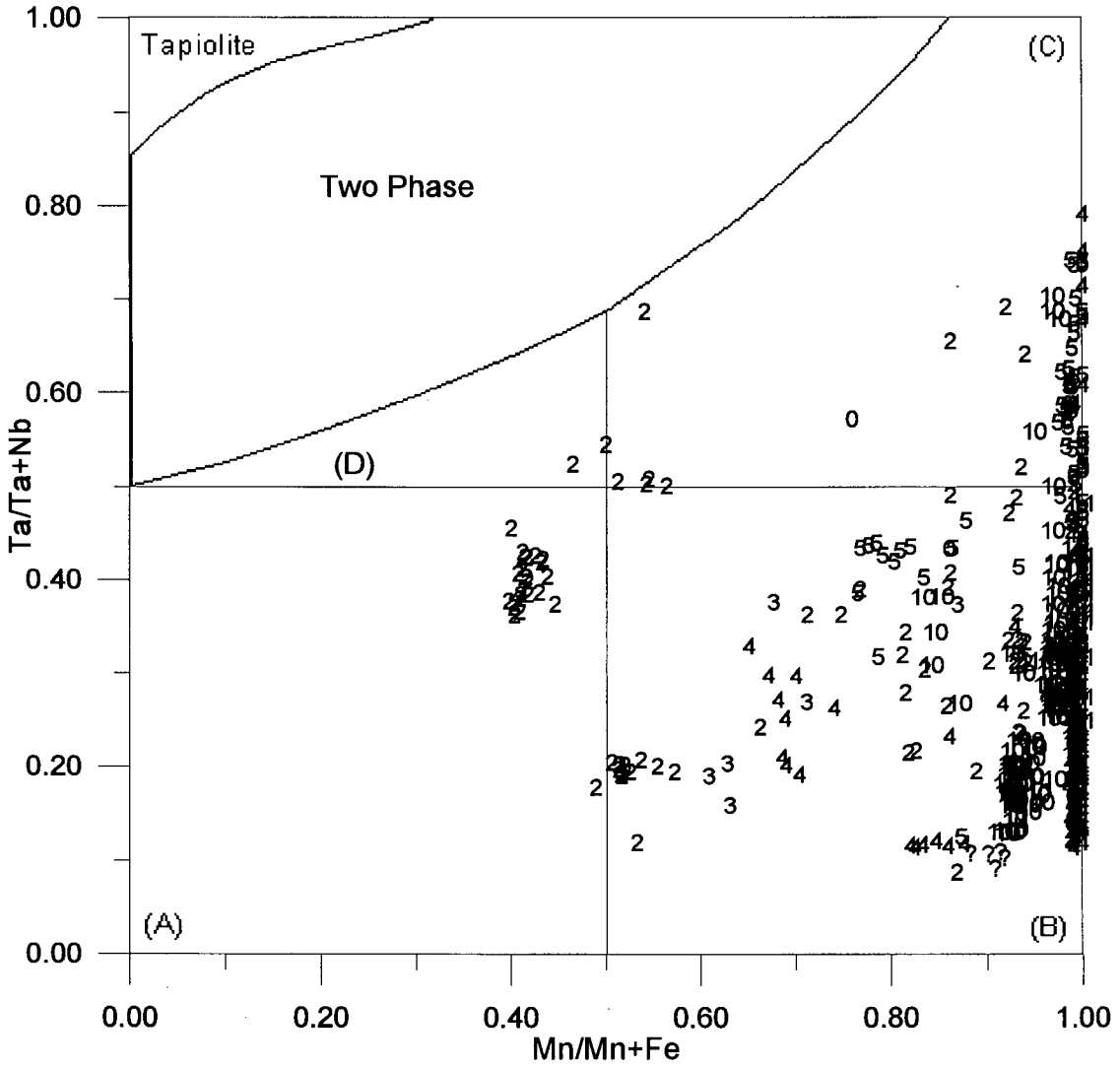

Figure 5.8: The Ta/Ta+Mn *versus* Mn/Mn+Fe ratios (apfu) for Little Nahanni columbite group minerals. Data point numbers represent the cirque from which the samples came ("0" is the northernmost cirque represented and "11", the southernmost). End-members are: (A) = ferrocolumbite; (B) = manganocolumbite; (C) = manganotantalite; and (D) = ferrotantalite.

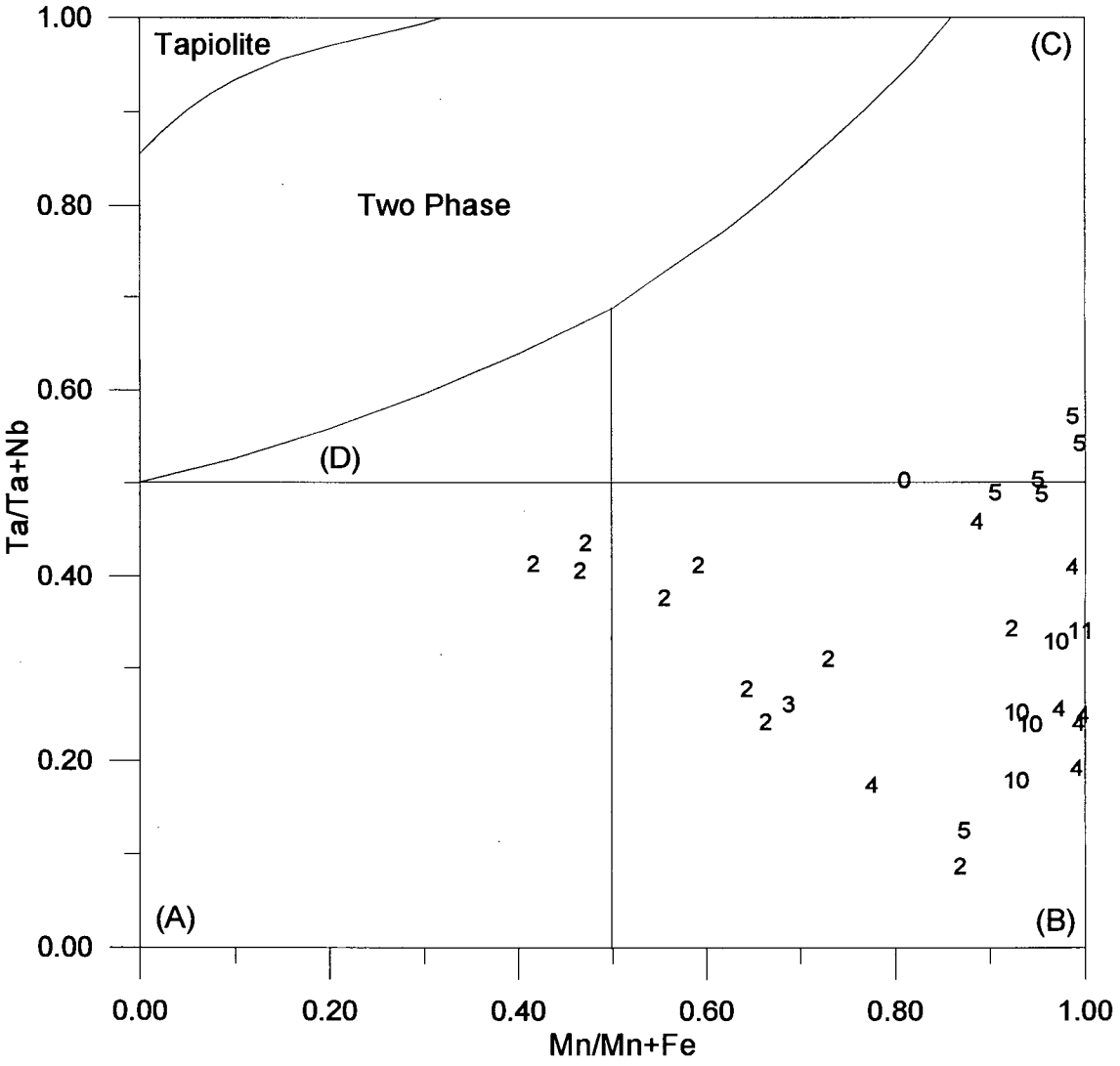

Figure 5.9: The Ta/Ta+Mn versus Mn/Mn+Fe ratios (apfu) for Little Nahanni columbite group minerals. Each data point represents an average analysis for every sample. Data point numbers and end-members are the same as in figure 5.7.

Table 5.5: Unit cell dimensions of columbite group minerals.

Sample	Locality	*a*	*b*	*c*
301	C - 4 - 1C	14.419(3)	5.7628(9)	5.0953(11)
?	C - 4 - 1B	14.425(2)	5.7622(9)	5.0959(13)
233	LBW - 10	14.422(2)	5.7605(7)	5.0944(7)
164	LSE - 10 - 1	14.425(1)	5.7622(7)	5.0917(6)
164	LSE - 10 - 1	14.420(2)	5.7611(8)	5.0880(8)
164	LSE - 10 - 2	14.402(2)	5.7580(10)	5.0950(10)
?	OSE - 4W - 1	14.390(4)	5.7504(9)	5.1162(12)
?	NMM - 1N	14.407(2)	5.7559(7)	5.1035(8)

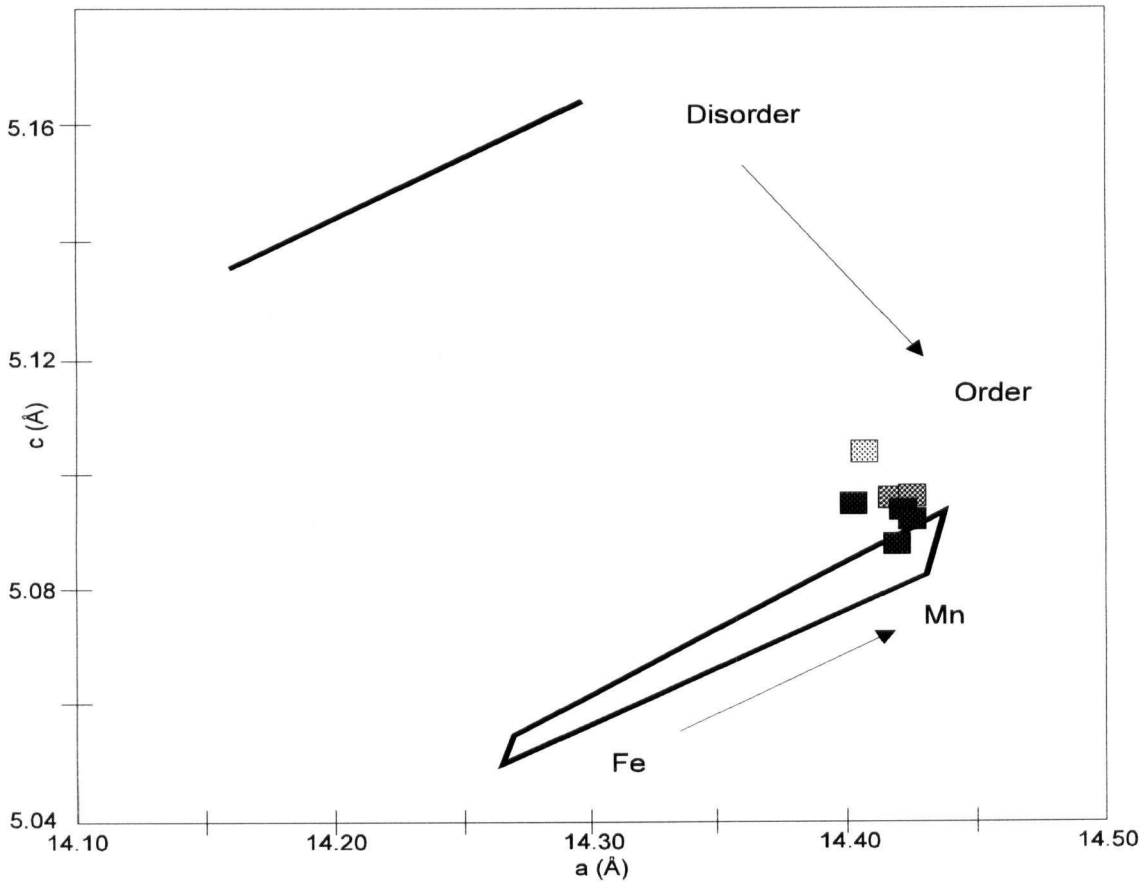

Figure 5.10: Structural states of columbite group minerals. In order from darkest to lightest, the squares represent samples from the following cirques: 10 (4), 4W (1), 4 (2), and 1N (1).

5.2.2 Cassiterite

Cassiterite is found in the wall and intermediate zones, generally associated with massive quartz and mica (lepidolite or muscovite). Both the quartz and mica occur fine- to coarse-grained: cassiterite grains range from microscopic inclusions to 1.5 cm crystals and are commonly euhedral. Cassiterite is also found as sharp, lustrous, wedge-shaped crystals in calcite-filled "pockets". Uncommonly, cassiterite forms as bands (series of crystals). Figure 5.11 is a photograph of sample 234, which exhibits such banding.

Six cassiterite samples were analyzed by electron probe for Ta, Mg, Mn, Fe, Sn, Nb, and Ti. Cassiterite chemistry does not vary much throughout the field area and no fractionation trends are evident.

5.2.3 Other Oxide Minerals

A wodginite-like Fe-Ti Nb oxide was found in a sample from cirque 2. It is intergrown with columbite. Further (structural) work is planned to determine whether or not these samples represent either a new mineral or ixiolite.

Columbite group samples used for geochronology were checked in BSE mode for inclusions. One to five micron-size uranium oxide inclusions, believed to be uraninite, occur in some samples (e.g. 227 and 233), especially in Ta-rich zones. Tantalian rutile occurs as inclusions in columbite from cirque 2. Uranmicrolite was identified by EDS as an inclusion in apatite (sample 246) and in beryl (sample 309).

Figure 5.11: Photograph of cassiterite band (sample 234). Note the aplitic (or wall zone) Qtz-Lpd-Cass assemblage to the left of the band, and the pegmatitic Ab-Qtz-Lpd (no cassiterite) assemblage to the right. Scale in cm.

5.3 Phosphate Minerals

5.3.1 Apatite

Apatite is widespread in the Little Nahanni pegmatite group and occurs in four distinct ways. The most commonly and easily observed occurrence of apatite is as euhedral crystals with many habits in late-stage, cross-cutting fractures which are generally (i.e. not always) infilled with calcite (Fig. 5.12). Their colour varies from purple to green to colourless, and the crystals are commonly zoned with a green core and a purple rim. "Vug" apatite also occurs as acicular aggregates of mostly blue, subhedral crystals frozen in the intermediate and/or wall zones. The second type of apatite occurs as anhedral, blue-green blebs and patches in the wall zone near the wall rock contact, in zones of clevelanditic albite, and/or near crosscutting fractures. Less obvious, but readily visible under ultraviolet light, apatite from the aplitic and wall zone sections and along the wallrock contact fluoresces orange. The purple-coloured crystals found in the late-stage fractures do not fluoresce at all. The third occurrence of apatite is as inclusions in feldspar, which are possible exsolution features. The fourth type of apatite is an alteration product of lithiophilite and occurs as irregular grains and veinlets within the host lithiophilite.

Nine apatite samples were analyzed for Ca and P as well as Na, Ca, Sr, Mn, Fe, Mg, Ce, Nd, Si, V, Cl and F using electron microprobe techniques. The samples with their locality information are listed in Appendix A. Microprobe data are provided in Appendix B (diskette). Table 5.6a summarizes average compositions for the nine samples analyzed by electron microprobe. Table 5.6b lists selected electron probe microanalyses of apatite associated with the alteration of lithiophilite and montebrasite.

Compositions of Little Nahanni Pegmatite Group apatite range from fluorapatite to hydroxyapatite (average F/(F+OH) from 0.32 to 0.91). SrO contents range from 0.00 to 3.83 wt %. Mn contents vary from 0.00 to 13.04 wt % MnO. Grains of hydroxylapatite associated with (as alteration products of) type 2 lithiophilite have some of the highest MnO contents measured in the pegmatite group (from 4 to 13 wt %).

5.3.2 Lithiophilite and Associated Species

Two types of lithiophilite can be distinguished on the basis of occurrence, habit, chemistry and alteration products. Type 1 lithiophilite occurs in the (inner) wall zones as orange to salmon-coloured, irregular masses up to 20 cm in diameter and is associated with quartz and albite. It is essentially clear and colourless when viewed under magnification; the orange colour is imparted by alteration products intimately associated with the lithiophilite. Type 2 lithiophilite occurs as dark brown to black, subhedral to euhedral crystals up to 3 cm long, or veinlets (or series of anhedral crystals -- see Fig. 5.13) parallel to the dike contact in the wall zones. Some lithiophilite of this type occurs in the late-stage, aplitic albite units.

Electron-probe microanalyses of type 1 lithiophilite (e.g. table 5.7, sample 195) show its composition to be near end-member, with Mn/(Mn+Fe) between 0.95-0.97. Type 2 lithiophilite (e.g. table 5.7, samples 13, 244 and 339) is relatively Fe-rich with Mn/(Mn+Fe) between 0.75-0.84.

Irregular masses of light red triploidite, yellow to pale orange unknown Ca-Mn phosphate and hydroxylapatite surround and embay relatively unaltered "eyes" of type 1 lithiophilite. Like type 1 lithiophilite, the triploidite associated with it is near end-member in composition with Mn/(Mn+Fe) = 0.97 (Table 5.8). The unknown phosphate comprises much of the inter-grain material and is fairfield-like in character ($Ca_{1.1}Mn_{1.8}Fe_{0.1}(PO_4)_2 \cdot 2H_2O$; Raudsepp *et al.*, 1995 and personal communication), but this remains to be confirmed (Table 5.9). Triploidite associated with type 2 lithiophilite is relatively rare and occurs as small, isolated grains and veins. The "unknown Ca-Mn phosphate" is likewise rare and occurs as minor veins with triploidite. Several generations of apatite, with highly variable Mn contents (see also section 5.3.1), are present. Table 5.6b lists selected analyses of apatite associated with type 2 lithiophilite (samples 244 and 13). Grain boundaries between quartz and both types of lithiophilite are heavily altered to Mn- and Fe-oxides.

Figure 5.12: The greyish-green band along the left side of the photograph is apatite. Where this band meets, and within the fracture, apatites are purple. Other fracture minerals include cleavelandite, muscovite, quartz and in the lower central part of the photograph, cookeite. The field of view is about 4 cm wide.

Figure 5.13: Band of altered lithiophilite crystals in a boulder at the Cali claim.

Table 5.6a: Average electron probe microanalyses of apatite.

Sample	391-1	397	98	391-2	341	340	91	394	398
# of analyses	8	9	9	3	4	8	5	4	5
Na_2O	--	--	--	--	0.10	0.02	0.04	--	0.09
CaO	55.47(78	55.60(65	54.79(75	56.27(99	51.30(116	54.81(89	56.22(73)	55.31(84	54.71(80
SrO	0.26(25	0.34(20	1.45(12	0.58(35	0.54(16)	0.90(27	0.85(88)	1.14(73	0.44(21
MnO	0.27(23	1.63(44	0.89(42	0.35(40	3.75(111	1.71(59	0.45(19)	0.30(11	1.10(23
FeO	0.03(4)	--	0.01(3)	0.04(4)	0.08(6)	0.04(4)	--	--	0.01(3)
P_2O_5	42.19(33	42.14(24	41.47(41	42.11(31	41.24(44)	42.06(30	41.51(16	42.31(24	41.61(54
F	2.41(24	2.02(16	1.85(10	1.70(22	2.68(60)	2.00(18	1.58(25)	1.66(17	2.01(10
H_2O [a]	0.65(12	0.85(8)	0.90(5)	0.99(11	0.48(28)	0.85(8)	1.04(16)	1.01(8)	0.82(47
Total	100.26	101.72	100.58	101.33	99.04	101.55	101.02	101.03	99.95
				Number of cations based on 13 anions (O, F, OH)					
Na^+	0.000	0.000	0.000	0.000	0.017	0.003	0.007	0.000	0.015
Ca^{2+}	4.982	4.953	4.955	5.021	4.709	4.901	5.053	4.947	4.952
Sr^{2+}	0.013	0.016	0.071	0.028	0.027	0.044	0.041	0.055	0.022
Mn^{2+}	0.019	0.115	0.064	0.025	0.272	0.121	0.032	0.021	0.079
Fe^{2+}	0.002	0.000	0.001	0.003	0.006	0.003	0.000	0.000	0.001
P^{5+}	2.994	2.966	2.964	2.969	2.991	2.972	2.948	2.990	2.976
F^-	0.639	0.531	0.494	0.448	0.726	0.528	0.419	0.438	0.537
OH^-	0.361	0.469	0.506	0.552	0.274	0.472	0.581	0.562	0.463

Note: MgO, Ce_2O_3, Nd_2O_3, SiO_2, V_2O_5 and Cl sought, but not detected
a determined by stoichiometry
() Standard deviation on averages.

Table 5.6b: Selected electron-probe microanalyses of apatite.

Sample	244(2)	244(10)	244(4)	13(11)	8(4)
P_2O_5	39.43	40.37	40.99	39.15	42.21
SO_3	0.22	0.01	0.08	0.04	0.00
SiO_2	0.02	0.02	0.00	0.17	0.00
FeO	0.07	0.21	0.06	0.73	0.00
MnO	11.51	7.44	4.13	13.04	4.71
CaO	44.36	48.90	51.94	42.25	50.80
Na_2O	0.00	0.03	0.06	0.08	0.00
F	1.32	1.68	3.45	1.08	3.79
H_2O [a]	1.06	0.94	0.11	1.17	0.00
O≡F	-0.56	-0.71	-1.45	-0.45	-1.60
Total	97.43	98.89	99.37	97.26	99.91
	Number of cations based on 26 anions (O, F, OH)				
P^{5+}	5.90	5.92	5.93	5.90	6.05
S	0.03	0.00	0.01	0.00	0.00
Si	0.00	0.00	0.00	0.03	0.00
Fe^{2+}	0.01	0.03	0.00	0.11	0.00
Mn^{2+}	1.72	1.09	0.60	1.97	0.68
Ca^{2+}	8.41	9.07	9.52	8.06	9.21
Na^{2+}	0.00	0.01	0.02	0.03	0.00
F	0.74	0.92	1.87	0.61	2.00
OH^-	1.26	1.08	0.13	1.39	0.00

Note: analyses made by M. Raudsepp
[a] Determined by stoichiometry.

5.3.3 Montebrasite

Montebrasite rarely occurs as anhedral grains associated with albite and lepidolite (samples 230 and 197). Electron-probe microanalyses show that elements other than Li, Al, P, and F are found only in trace-levels in the montebrasite and that F:OH ratios are about 0.25:0.75 (Raudsepp *et al.*, 1995). Montebrasite appears to be extensively altered to Mn-bearing fluorapatite (see sample 8, Table 5.6).

Table 5.7: Selected electron-probe microanalyses of lithiophilite.

Sample(Point)	230(10)	195(7)	244(1)	13(1)	339(3)
P_2O_5	45.27	45.38	46.38	46.01	45.61
FeO	1.73	1.55	11.07	11.77	6.90
MnO	43.58	43.01	34.46	33.60	38.08
MgO	0.01	0.01	0.04	0.11	0.00
CaO	0.15	0.06	0.13	0.03	0.08
Li_2O [a]	9.55	9.51	9.72	9.63	9.56
Total	100.29	99.52	101.80	101.15	100.23
		Formula contents based on 4 anions (O).			
P^{5+}	1.00	1.00	1.00	1.00	1.00
Fe^{2+}	0.04	0.03	0.24	0.25	0.15
Mn^{2+}	0.96	0.95	0.75	0.73	0.84
Mg^{2+}	0.00	0.00	0.00	0.00	0.00
Ca^{2+}	0.00	0.00	0.00	0.00	0.00
Li^+	1.00	1.00	1.00	1.00	1.00

Note: analyses made by M. Raudsepp

a Determined by stoichiometry.

Table 5.8: Selected electron-probe microanalyses of triploidite.

Sample(Point)	230(9)	230(12)	230(11)
P_2O_5	32.48	32.06	31.79
FeO	0.78	1.90	0.95
MnO	57.76	61.10	60.71
MgO	0.00	0.01	0.00
CaO	3.82	0.09	1.45
F	0.52	0.50	0.57
H_2O [a]	3.83	3.81	3.76
Total	98.99	99.26	99.04
Formula contents based on 5 anions (O, OH, F).			
P^{5+}	1.01	1.01	1.00
Fe^{2+}	0.02	0.06	0.03
Mn^{2+}	1.80	1.92	1.91
Mg^{2+}	0.00	0.00	0.00
Ca^{2+}	0.15	0.00	0.06
F^-	0.06	0.06	0.07
OH^-	0.94	0.94	0.93

Note: analyses made by M. Raudsepp
[a] Determined by stoichiometry.

Table 5.9: Selected electron-probe microanalyses of unknown Ca-Mn phosphate.

Sample(Point)	195(1)	195(3)	195(5)	195(6)
P_2O_5	38.80	38.58	38.84	38.75
FeO	1.54	1.64	1.64	1.39
MnO	35.06	34.26	34.78	34.95
MgO	0.00	0.00	0.00	0.00
CaO	16.76	17.51	17.00	16.71
H_2O [a]	9.85	9.79	9.86	9.84
Total	102.01	101.78	102.12	101.64
	Formula contents based on $2P^{5+}$ and $2H_2O$.			
P^{5+}	2.00	2.00	2.00	2.00
Fe^{2+}	0.08	0.08	0.08	0.07
Mn^{2+}	1.81	1.78	1.79	1.81
Mg^{2+}	0.00	0.00	0.00	0.00
Ca^{2+}	1.09	1.15	1.11	1.09
H^+	4.00	4.00	4.00	4.00
O^{2-}	9.98	10.01	9.98	9.97

Note: analyses made by M. Raudsepp
[a] Determined by stoichiometry.

5.4 Spodumene

Spodumene in the Little Nahanni pegmatite group occurs as colourless to lightly pinkish blades generally 10 to 15 cm, but occasionally up to 0.5 m, in length. It may be broadly subdivided into three groupings according to the degree of alteration the crystals have been subjected to. Within these groupings, one may consider associations to further subdivide types of spodumene occurrence (see table 5.10). Unaltered, sub- to euhedral crystals occur associated with either blocky K-feldspar and quartz, or massive, cream-coloured to white albite ± quartz and ± mica, or a mixture of both. Euhedral, well-terminated crystals have only been found in a massive quartz matrix. This observation was also made by Kesler (1961) in the Kings Mountain pegmatites. Moderately altered spodumene crystals predominantly occur associated with aplitic albite units. The spodumene appears splintery or fragmented, and partially resorbed. The original crescumulate texture of the crystals is commonly intact and the remains of large, blocky K-spars may be evident. Highly altered spodumene occurs only as relict fragments within some pseudomorph of an alteration product after spodumene and always in albite. These will be discussed further in chapter 8. One sample (281) of green, gemmy, anhedral spodumene was found directly in contact with quartz-muscovite schist wallrock.

As with most albite-spodumene type pegmatites (Černý, 1989a; Černý, 1991a and references therein), spodumene crystals show a preferred parallel orientation perpendicular to the pegmatite dike attitude (see figures 3.7, 3.16 and 3.17). However, spodumene crystals almost perfectly parallel to the pegmatite contact as well as randomly-oriented crystals are also seen in some dikes (see Fig. 5.14). Figure 5.15 shows a cross-sectional view of a spodumene band in which the crystals are parallel with respect to their elongate dimension. However, the spodumene crystals are randomly orientation with respect to the *a* or *b* axes. Numerous

Figure 5.14: This dike in cirque 5 shows spodumene crystals (dark grey, elongate crystals neighbouring two orange lichen patches near centre of photograph) perpendicular and parallel to the pegmatite/wall rock contact.

Figure 5.15: A cross-sectional view of a spodumene band. Note that the spodumene crystal are randomly oriented in this view. Specimen is approximately 20 cm across.

Table 5.10: Types of spodumene occurrence.

Alteration	Matrix	Examples	Comments
unaltered	blocky K-feldspar (50%), quartz (25%), spodumene (25%)	113	"ideal" intermediate zone crystallization
unaltered	massive quartz		well-terminated crystals
little alteration	quartz (40 to 60%), feldspar (40 to 20%), spodumene (20%)	121, 247	
little to moderate alteration	remnant, interstitial coarse quartz + feldspar partially or entirely invaded by "aplitic" (albite 45%, quartz 45%, mica 10%) material	151, 146, 159	spodumene appears partially resorbed, broken and/or splintery; large, blocky "phenocrysts" of remnant Kspar may also occur
little to moderate alteration	"clean", white, cleavelanditic albite (35%), lepidolite (25%), quartz (20%), spodumene (20%)	137	anhedral to subhedral; matrix very coarse grained
highly altered	cleavelandite, coarse mica (lep. or musc.), no quartz	150	mostly pseudomorphs of clay minerals after spodumene, only relict spodumene present
highly altered	albitized K-feldspar with slightly to heavily rounded relict K-feldspar	163, 118	as above; with vugs containing micas, zeolites and/or calcite
unaltered	in contact with host rock (schist)	281	anhedral, green spodumene

spodumene crystals also show evidence of having been broken and reset in a "bent" form (Fig. 5.16).

Spodumene is a lithium pyroxene with an ideal formula of $LiAlSi_2O_6$. Spodumene does not tend to vary much from this end-member composition. The most significant possible substitution is that of Li by Na. Small amounts of Fe^{3+} may replace Al. (Deer *et al.*, 1966)

Seven samples were analyzed for Al and Si as well as Na, K, Cs, Ca, Mg, Mn, Fe and Cr using electron microprobe techniques. Three of these samples plus two others were analyzed for B using wet-chemical methods. The samples with their locality information are listed in Appendix A. Microprobe data are provided in Appendix B-2 (diskette). Wet chemical data are provided in Appendix C. Table 5.11 summarizes average compositions for the seven spodumene samples analyzed by electron microprobe.

All samples analyzed contain Na, up to 0.15 wt % Na_2O, and those contents are fairly even throughout the pegmatite group. None of the samples analyzed contained any chromium. Fe and Mn contents were generally even throughout a given crystal though values may vary by up to 0.2 weight % across the crystal. Only sample 357 showed signs of zonation: an Fe-bearing core and Fe-free rim. Mn is dominant over Fe in 17 of 18 analyses in sample 357. The mount was checked under ultraviolet light to determine whether or not such zonation existed in the fluorescence. The rim of the spodumene crystal, where in contact with coexisting quartz, did appear more fluorescent than the central portions of the crystal, where the fluorescence was somewhat patchier. Sample 281 contains five times more Fe (up to 1.28 wt%) than all other samples analyzed. It is singular also in that is the only Mg-bearing and Mn-free sample. No Cs, Ca or K was detected in any of the samples analyzed except in one analysis of sample 161, which showed a minor presence of Ca and K. This point was near a section that appeared very altered and the analysis may have picked up some part of the neighbouring alteration/replacement products.

The five samples analyzed for B using wet chemical methods showed B contents between 20 and 65 ppm. Shearer and Papike (1986) found concentrations of up to 600 ppm B in

spodumene, making spodumene the second largest concentrator of this element, albeit a distant second, behind tourmaline, in the Tip Top pegmatite in South Dakota. They further state that B either substitutes for Si in the structure, or occurs in fluid inclusions (*cf* London, 1986b). In the case of the former, the presence of a divalent cation, such as Fe^{2+} or Mn^{2+}, is required to offset the charge imbalance (Shearer and Papike, 1986).

It is known that spodumene is commonly altered in lithium pegmatites and that this alteration represents an important part of the subsolidus evolution of these pegmatites (London and Burt, 1982c). London and Burt (1982c) summarizes some of the spodumene alteration assemblages observed in many lithium pegmatites throughout the world. The most common alteration products mentioned in this summary are eucryptite, albite and mica. Altered spodumene in the Little Nahanni pegmatite group most often occurs with massive, cleavelanditic albite, muscovite/lepidolite ± cookeite, ± apatite, ± beryl, which is consistent with what has been previously been described with respect to spodumene alteration assemblages in lithium pegmatites (e.g. Černý, 1972; London and Burt, 1982b,c).

Completely altered spodumene in the Little Nahanni Pegmatite Group ranges from a vibrant light pink to dark purple, and to green and black in colour and does not exhibit any cleavage (Fig 5.17). These alteration products are pseudomorphs of spodumene such as illite-montmorillonite, kaolinite, mica (muscovite and lepidolite) and albite. Eucryptite has not been identified in this pegmatite group. Samples (150, 162 and 358) examined by powder XRD were mixtures of these minerals. Zeolites such as stilbite and heulandite are also found in cavities left by the alteration and removal of spodumene (e.g. samples 115, 153, 163). It is important to keep alteration, particularly the pseudomorphic alteration, in mind for exploration purposes, as some dikes may deceivingly appear to be full of colourful spodumene. Careful inspection is sometimes necessary to distinguish the two.

Gem spodumene samples have been classified as "triphane" (colourless to yellow), "kunzite" (pink, lilac), and "hiddenite" (green) (e.g. Jahns and Wright, 1951). Claffy (1953) showed that

Table 5.11: Average electron probe microanalyses of spodumene.

Sample	161	188	176	230	191	281	357
# of analyses	10	8	22	15	11	9	18
SiO_2	64.27(35)	64.98(17)	64.91(33)	64.69(24)	64.83(23)	63.73(47)	64.57(27)
Al_2O_3	27.87(17)	28.04(14)	27.90(18)	28.00(12)	27.81(11)	26.61(11)	27.84(14)
FeO	0.12(8)	0.13(10)	0.11(2)	nd	0.05(9)	1.21(6)	0.04(3)
MnO	0.02(4)	0.05(4)	0.11(3)	0.05(3)	0.11(6)	nd	0.11(4)
MgO	nd	nd	nd	nd	nd	0.05(1)	nd
Na_2O	0.09(3)	0.09(3)	0.11(1)	0.11(2)	0.11(3)	0.07(1)	0.12(2)
Li_2O [a]	8.05(2)	8.13(2)	8.11(3)	8.10(2)	8.10(2)	7.94(5)	8.07(3)
Total	100.42	101.42	101.26	100.93	101.01	99.61	100.75
	Formula contents on the basis of 6 anions (O).						
Si^{4+}	1.986	1.988	1.989	1.987	1.991	1.995	1.988
Al^{3+}	1.015	1.011	1.008	1.014	1.007	0.982	1.010
Fe^{2+}	0.003	0.003	0.003	nd	0.001	0.032	0.001
Mn^{2+}	0.001	0.001	0.003	0.001	0.003	nd	0.003
Mg^{2+}	nd	nd	nd	nd	nd	0.002	nd
Na^{+}	0.005	0.005	0.007	0.007	0.007	0.004	0.007
Li^{+}	1.000	1.000	1.000	1.000	1.000	1.000	1.000

Note: K_2O, CaO, Cs_2O and Cr_2O_3 sought but not detected.
a Determined by stoichiometry.
() Standard deviation of averages.
nd Not detected.

Figure 5.16: A photograph of sample 167 showing a spodumene crystal that broke and was reset in a bent form. Specimen is about 6 cm across.

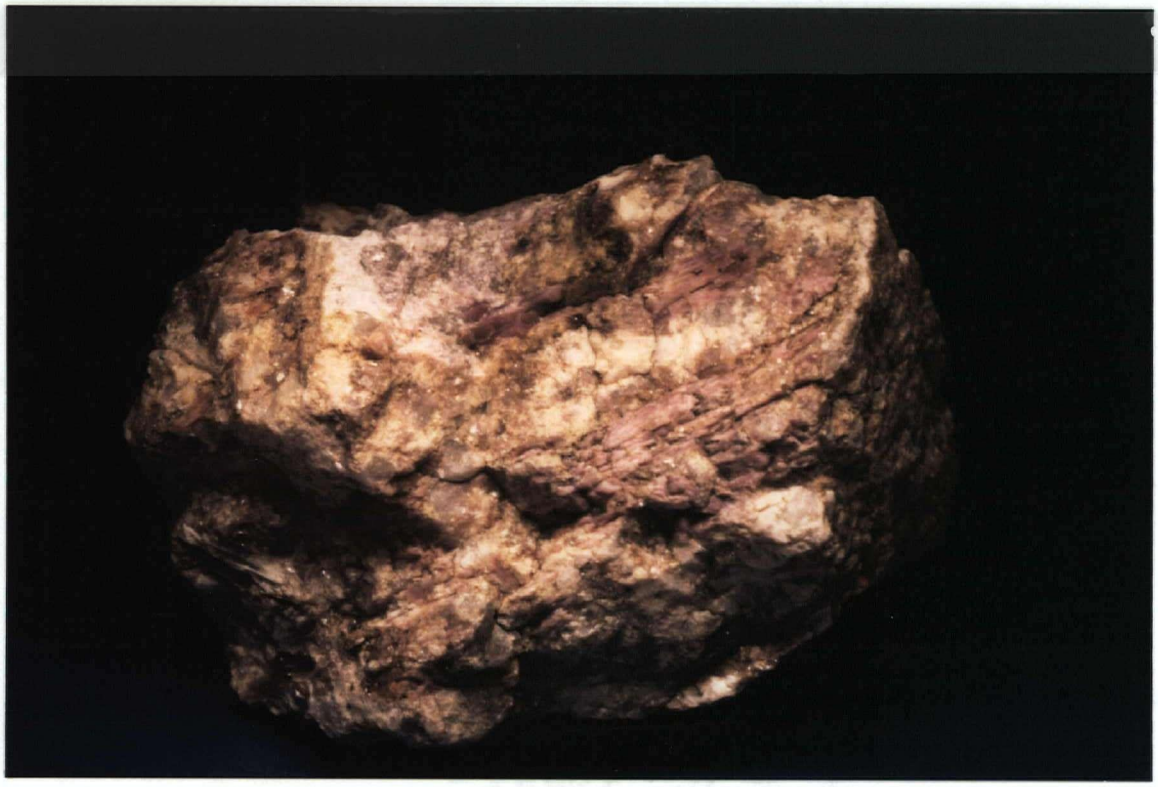

Figure 5.17: A photograph of sample 122 (B) showing the purple alteration products pseudomorphs after spodumene. Specimen is about 9 cm across.

this classification does not always correspond to differences in chemical composition and optical behaviour, and that spodumene has two types: chromian and non-chromian. According to Claffy (1953), the green colour of North Carolina "hiddenite" is due to chromium and the pink colour of "kunzite" due to the presence of Mn, or more especially to a low Fe:Mn ratio. However, a reversible green colour may also be induced in non-chromian spodumene by irradiation. This is attributed to effect of irradiation on the oxidation state of Mn. The green colour of chromian spodumene is unaffected by irradiation or by attempts to fade the colour by exposure to daylight, ultraviolet light or heat treatment. Chromian spodumene does not have the luminescent properties that non-chromian spodumene does (Claffy, 1953).

Two samples of colourless to light pink spodumene (191 and 193) from the Little Nahanni pegmatites were subjected to irradiation. Both samples turned green. The samples returned to their former colour when left in full sunlight for two days. The naturally green sample (281) was found on a boulder, exposed to the elements, so one may safely assume that its colour is unaffected by sunlight. Heat treatments were not attempted. Examination under short and long wave ultraviolet light showed all fresh surfaces of spodumene crystals to fluoresce pinkish-orange, except sample 281. The degree of fluorescence varies, and in some cases (e.g. sample 167), spodumene crystals are strongly zoned. The behaviour of colourless to pink spodumene crystals from the Little Nahanni Pegmatite seems to be consistent with Claffy's (1953) findings. Spodumenes of lower Fe:Mn ratios tend to be deeper pink, if not weathered. Again, the exception is sample 281. While sample 281 and the green hiddenite analyzed by Claffy are similar in colour and luminescent/tenebrescent behaviour, the hiddenite is a chromian spodumene where as sample 281 is entirely free of Cr and Mn. This seems to shed doubt as to whether the colouration and luminescent/tenebrescent properties is a function of Cr content. However, the hiddenite samples analyzed by Claffy (1953) do have the highest Fe contents of all the analyses reported in that paper (i.e. the only values that reach the "X.0 %" range). It is interesting to note, then, that sample 281 is also the only Little Nahanni Pegmatite Group sample with Fe values reaching the "X.0 %" level.

5.5 Beryl

Beryl occurs throughout the Little Nahanni Pegmatite Group in a variety of habits and colours. It is common for beryl to occur in different zones of a single, highly differentiated pegmatite. This does not generally present any problems for the previously mentioned classification scheme as the beryls do follow similar trends and fall within a single or two neighbouring classes (Černý, 1975). Differences in habit within the Little Nahanni Pegmatite Group are reflected by different relative *Z*:*X* aspect ratios (*Z* parallel to *c* axis; *X* parallel to *a* axis). For the purposes here, tabular refers to a low aspect ratio (< 0.5:1), blocky refers to an approximately 1:1 ratio and elongate refers to a high aspect ratio (> 2:1).

Water-clear, colourless beryl "goshenite" occurs as tabular and blocky crystals. Tabular crystals were found in cirque 6, in a calcite-filled vug lined with muscovite, on a boulder in the talus (sample 309). The blocky, colourless crystals were found spatially related to a late-stage cross-cutting quartz vein in dike LMM-5-8 (samples 88 and 390). A large section of the dike had broken away along the plane of the quartz vein. Beryl samples were found along that surface, in the quartz vein and in the pegmatite adjacent to the quartz vein. These crystals differ from sample 309 in that no Fe was detected in them and that no calcite filled the small vugs along the plane.

Large talus boulders on the ridge between cirque 10 and 11 produced the largest beryl crystals found (sample 197; Fig. 5.18). Up to 4 cm in diameter and 6 cm long, these crystals are associated with patchy, fine-grained lepidolite and fine-grained, granular (saccaroidal) albite. Weathered crystals appear slightly pinkish but fresh specimens are all chalky to translucent white.

Opaque white, blocky to elongate beryl crystals were found in cirque 4. These occur as euhedral prisms to 3 cm long at the contact between the wall unit and the intermediate units. They grew normal to the contact and are surrounded by coarse, anhedral quartz and

Figure 5.18: Photograph of sample 197 showing occurrence of Cs-bearing beryl with saccharoidal albite and lepidolite-quartz.

potassium feldspar. Except for colour, these crystals are similar in appearance to those in sample 330 (see below).

Pale blue-green "aquamarine", blocky to elongate crystals came from cirque 1N in the talus just below dike 4 (sample 330). They occur in a calcite-filled vug, associated with K-feldspar and smoky quartz in the intermediate unit (though less than 15 cm from the host rock pegmatite contact). Potassium feldspar crystals in the same vug had been partially resorbed as is evidenced by their "boxwork" etched nature.

Beryl has an ideal formula of $Be_3Al_2Si_6O_{18}$. However, nonessential water, inert gases and alkalis are usually contained in the channels of the beryl structure. Channel constituents may consist of: the alkalis (Na, K, Rb, Cs and Ca), water, OH^-, carbon dioxide and iron (Fe^{2+}, Fe^{3+}). Igneous beryl can have a total alkali content as high as 5 to 7% (Deer *et al.*,1986). Analyses by other workers, of samples from many different beryl localities show that beryl commonly contains Na, ranging from less than 1% to approximately 2% Na_2O (e.g. Aurisicchio *et al.*, 1988; Černý and Turnock, 1975; Feklichev, 1963; Bakakin and Belov, 1962). The maximum sodium content is reported to be 4.22 wt % (Feklichev, 1963). Wood and Nassau (1968) found molecular water to exist as two types, based on the molecule's orientation in the channels. Type-I water is unbonded, with the hydrogen atoms oriented parallel to the *c* axis of the beryl, whereas type-II water is coordinated to alkali ions in the channel and rotated 90° due to the interaction between the dipole and the nearby alkali ion.

A number of substitutions occur in the beryl structure. When present, Li^+ generally substitutes for Be^{2+} at the tetrahedral sites (Sherriff *et al.*, 1991; Aurisicchio *et al.*, 1988; Hawthorne and Černý, 1977; and Bakakin *et al.*, 1969). This substitution is coupled with the presence of alkali ions (e.g. Na^+, Cs^+) in channel sites. Sherriff *et al.* (1991) consider Li^+ "essential" in the

substitution in Be-deficient beryl because of a combination of local bond-valence and long-range charge balance requirements. Sherriff *et al.* (1991) also found Li^+ to exist in the channels and Li^+ is very rarely found in the spaces between the silicate rings (Bakakin and Belov, 1962). Where they are in excess, small amounts of Si and/or Al (max. 0.115 and 0.077 atoms, respectively) may complete the tetrahedral site (Aurisicchio *et al.*, 1988). Fe^{2+} and Mg^{2+} are the most important, and Mn^{2+}, Fe^{3+}, Cr^{3+}, V^{4+}, Sc^{3+} and Ti^{4+} are minor substituting ions for Al^{3+} at the octahedral sites (Aurisicchio *et al.*, 1988).

Aurisicchio *et al.* (1988) describe three types of beryl based on the *c/a* ratios. The ratios are affected by substitutions at either the Be^{2+} site ("tetrahedral" type) or the Al^{3+} site ("octahedral" type), or at both sites ("normal" type). They suggest two kinds of controlling factors that favour one type or the other. First, and most important, is the chemistry of the environment in which the beryl crystal grew (i.e. bulk-rock chemistry and fluid-phase composition). The second factor is pressure and/or temperature, in that increased pressure may favor the incorporation of Li^+ into the structure and decreased pressure may favour the incorporation of elements such as Fe^{2+} and Mg^{2+}.

Five samples were analyzed for Al and Si as well as Na, K, Cs, Ca, Mg, Mn, Sc, V, Cr and Fe using electron microprobe techniques. Four of these samples were analyzed for Li using wet chemical methods. The samples with their locality information are listed in Appendix A. Microprobe data are provided in Appendix B (diskette). Wet chemical data are provided in Appendix C. Table 5.12 summarizes average compositions for the five beryls analyzed by electron microprobe.

The oxide totals of the analyses range from 97.17 to 98.98 %. Water has not been analyzed or calculated for these beryls. Water is most often present in beryls and usually ranges from 1.44 to 2.26 wt % (Deer *et al.*, 1966), which would make up for the shortcoming in these analyses.

All the beryl samples were enriched in Na, which ranges from 0.52 to 1.69 % Na_2O. Cs_2O contents range from 0.07 to 0.93 %. Li_2O ranges from 0.07 to 0.30 %. This is consistent with

Table 5.12 Average electron-probe microanalyses of beryl.

Sample	88	197	390	330	309
# of analyses	4	5	4	4	4
SiO_2	65.30(27	64.49(33	64.36(2	64.53(4	64.92(2
Al_2O_3	18.51(14	18.37(13	18.09(9)	18.33(9)	17.79(3
MgO	nd	nd	0.02(2)	nd	0.21(1
V_2O_3	0.02(1)	0.03(1)	0.02(0)	0.01(1)	0.02(2)
Fe_2O_3	nd	0.01(3)	0.15(5)	nd	0.25(1
BeO *a*	13.69(5)	13.15(6)	13.02(1	13.36(6)	13.45(4)
Li_2O *b*	na	0.15	0.30	0.12	0.07
Na_2O	1.07(4)	1.03(3)	1.55(4)	1.13(3	0.85(1
K_2O	0.02(3)	0.02(2)	nd	0.02(3)	0.02(2)
Cs_2O	0.19(5)	0.55(31	0.36(3)	0.12(3)	0.20(1
Total	98.80	97.80	97.87	97.62	97.78
	Formula contents based on 18 anions (O).				
Si^{4+}	5.984	5.959	5.963	5.961	5.987
Al^{3+}	1.954	2.001	1.975	1.996	1.934
Mg^{2+}	nd	nd	0.003	nd	0.029
V^{3+}	0.001	0.002	0.001	0.001	0.001
Fe^{3+}	nd	0.001	0.010	nd	0.017
Be^{2+}	3.000	2.944	2.888	2.955	2.974
Li^+	na	0.056	0.112	0.045	0.026
Na^+	0.19	0.185	0.278	0.202	0.152
K^+	0.002	0.002	nd	0.002	0.002
Cs^+	0.007	0.022	0.014	0.005	0.008

Note: MnO, Sc_2O_3, Cr_2O_3 and CaO sought, but not detected.
a Determined by stoichiometry.
b Determined by wet chemistry.
na Not analyzed.
nd Not detected.

what has been previously stated about the coupled existence of Li and Cs-Na in beryl in that alkali contents match or exceed that of Li in order to maintain charge neutrality (e.g. Sherriff *et al.*, 1991 and Bakakin and Belov, 1962). Vanadium contents range from undetectible to 350 ppm and generally seem to have a positive correlation with cesium. The reasons for this correlation remain unclear. Li^+ and V^{3+} do not share a relationship similar to that of Li^+ and Cs^+ as vanadium is assumed to be trivalent and substituting for Al^{3+} in beryl (Feklichev, 1963), thereby posing no charge balance problems. Geochemically, V^{3+} and Al^{3+} are unrelated (e.g. Rankama and Sahama, 1950).

Two samples were analyzed for Mn and Cs using wet chemical methods. No Mn was detected by probe analysis. Mn values determined wet chemically are interpreted to reflect physical contamination from inclusions, particularly apatite.

Sample 88 (mount 77) shows very faint zoning under BSE imaging. The rim of this crystal contains K and V whereas these elements were undetected in the core. Cs is slightly elevated in the rim area as well (Fig. 5.19).

Sample 390 (mount 151) comes from the same dike as the crystal used for mount 77. The two are similar in composition except that this sample has a slightly lower Cs content and a slightly higher Na content than that of sample 88. No zoning was observed.

Subtle zoning in sample 197 (mount 66) is evident under BSE imaging where Cs- and V-rich bands show up lighter (Fig. 5.20). Of the beryls analysed, this is the richest in cesium.

Sample 330 (mount 178) predictably had the highest Fe content. This is consistent with its blue-green "aquamarine" colour which is caused by the presence of Fe (Sinkankas, 1981 and references therein).

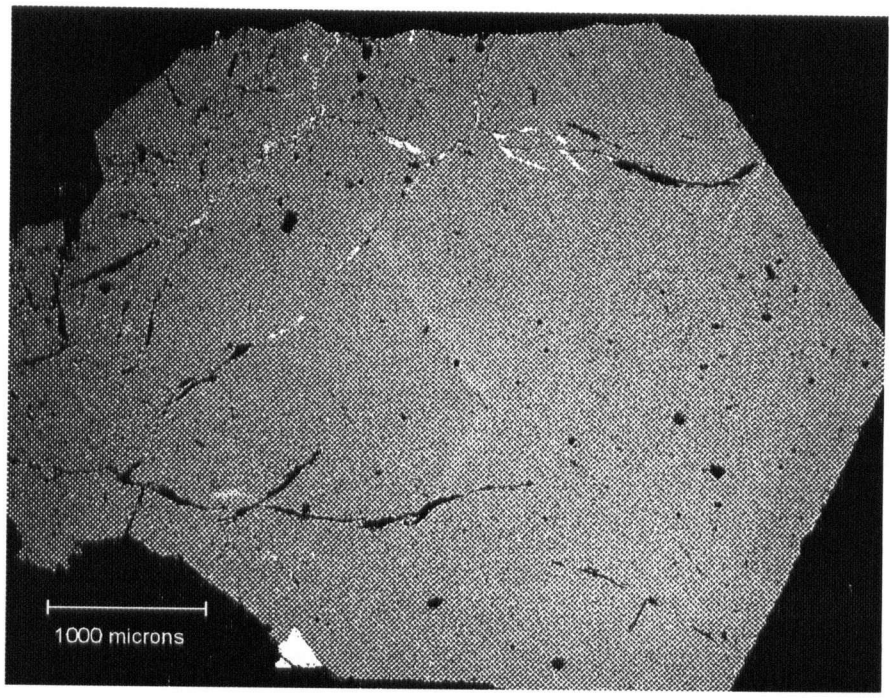

Figure 5.19: A backscattered electron image of beryl sample 390 (mount 77; LMM-5-8). The lighter bands (parallel with the edges of the crystal) correspond with higher Cs values.

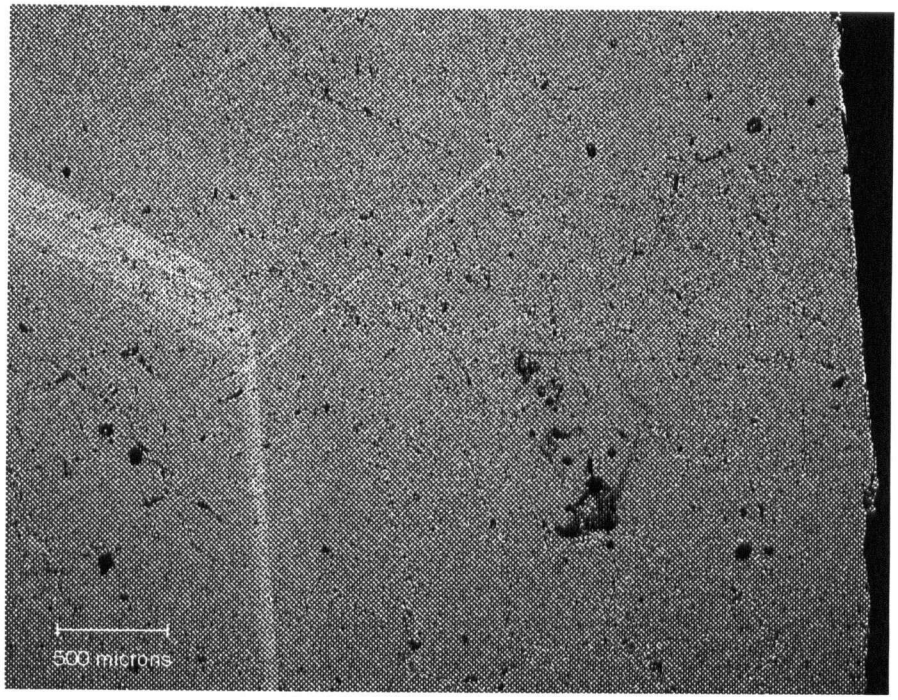

Figure 5.20: A backscattered electron image of beryl sample 197 (mount 66; LMM-10^11-t). The lighter bands correspond with higher Cs values.

The Na content of Sample 309 (mount 179) was significantly higher (up to 1.59% Na_2O) than any others analysed. These goshenites also had the second highest Fe content. This was at first surprising because of the total lack of colour in the crystals. Some of the crystals may have been subject to the bleaching effects of weathering, but others were etched out of the remaining calcite and are likewise totally colourless. This beryl sample (309) was the only one in which no K was detected. No zoning was evident in a BSE image. However, several different inclusions were identified. Muscovite occurs as euhedral blades, albite occurs as tiny veinlets and uranmicrolite occurs as an anhedral grain. The overgrowth growth of beryl on muscovite (i.e. muscovite inclusions in the beryl) is also visible in the hand sample.

While the number of beryl samples available for analysis is not large enough to be conclusive about regional trends, the few that are available come from a wide and linear spread of localities along a north-south trend, but with no east-west spread, in the field area. Considering this, no regional north-south zoning was evident in the beryl trace element geochemistry. The samples available were not at all appropriate to determine any east-west zoning. It is worthy to note that the two "vug" beryls were the only ones to contain Fe and Mg. Only one analysis, out of six points analyzed, on another sample (197) showed a small amount (0.004 pfu) of Fe, but no Mg. Considering their occurrence in late-stage, calcite-filled "pods", it is reasonable to assume that the mineralizing fluids from which these crystals grew had, in part, assimilated Fe and Mg from the host rocks. It is also interesting to consider the controlling factors mentioned by Aurisicchio *et al.* (1988). It is equally reasonable to assume that the late-stage fractures would produce a local decrease in pressure as they formed. The crystals grown in the new space would then have done so in a lower pressure environment than in other parts of the dike. The fact that the two beryl samples with the highest Fe and Mg values grew in such an environment is consistent with the suggestions made by Aurisicchio *et al.* (1988).

Černý (1975) determined alkali variations in beryl to be a useful tool in geochemically characterizing pegmatites, in terms of relating possibly genetically similar pegmatite groups and in terms of the internal evolution of single pegmatites.. A classification scheme, adapted by Černý (1975) from Beus (1960), based on alkali variation in beryls from uncontaminated granitic pegmatites is given in table 5.13. Beryls from the Little Nahanni Pegmatite Group fall into the sodic-lithian beryl category.

Na-Cs-Li plots of the Little Nahanni beryls (figures 5.20a-d) are somewhat scattered and do not, with the possible exception of the Li versus Na plot, exhibit any well-defined trends. The plots show minor similarities to those of Černý (1975), especially with the data from the Greer Lake beryl samples. However, Černý's (1975) work does not include data from albite-spodumene type pegmatites and, as he himself suggests, more work needs to be done to test the trends and discrepancies described in his work. As the analyses in this thesis are few and of beryls from a pegmatite type not included in Černý's (1975) work, it would be prudent to gather more data from Little Nahanni Pegmatite Group beryl samples and from other albite-spodumene pegmatites before evaluating the usefulness of alkali variations with respect to albite-spodumene type pegmatites.

All samples were examined with an ultraviolet lamp (short and long wave). Some beryls from the Little Nahanni pegmatite group fluoresce white and some do not. What is of note is that some of the crystals (sample 197) had fluorescent bands within them (figures 5.22a and b) and, in one particular crystal, this rim corresponds to the Cs-V-rich band noted under back-scatter electron imaging seen in figure 5.20. This suggests that the degree of fluorescence is indicative of elevated cesium and/or vanadium content which, if true, would represent a useful exploration tool in the field.

Table 5.13 Beryl types based on alkali content.

Beryl Type	Alkali Content	Occurrence
Alkali-free	Total alkalis < 0.1 wt %	Vugs of predominantly graphic pegmatites, and schlieren- and pocket-type bodies in granites.
Alkali-poor potassic, and sodic-potassic	K predominant, but only 0.2 to 0.5 wt %	Schlieren- and pocket-type bodies in granites, and quartz cores of simple blocky pegmatite
Sodic	Na predominant, 0.5-1.0 wt %	Pegmatites with albite-rich assemblages but very poor in rare alkalis.
Sodic-lithian	Na X-2.0 wt %; Li up to 0.6 wt%; Cs low	Li-bearing pegmatites
Lithian-cesian beryl	High Na and Li with Cs > 0.5 wt%	Extremely differentiated Li-rich pegmatites with metasomatic lepidolite units, frequently pollucite-bearing; also as late hydrothermal crystals in vugs of these pegmatites.

After Černý (1975) modified after Beus (1960) and Feklitchev (1964).

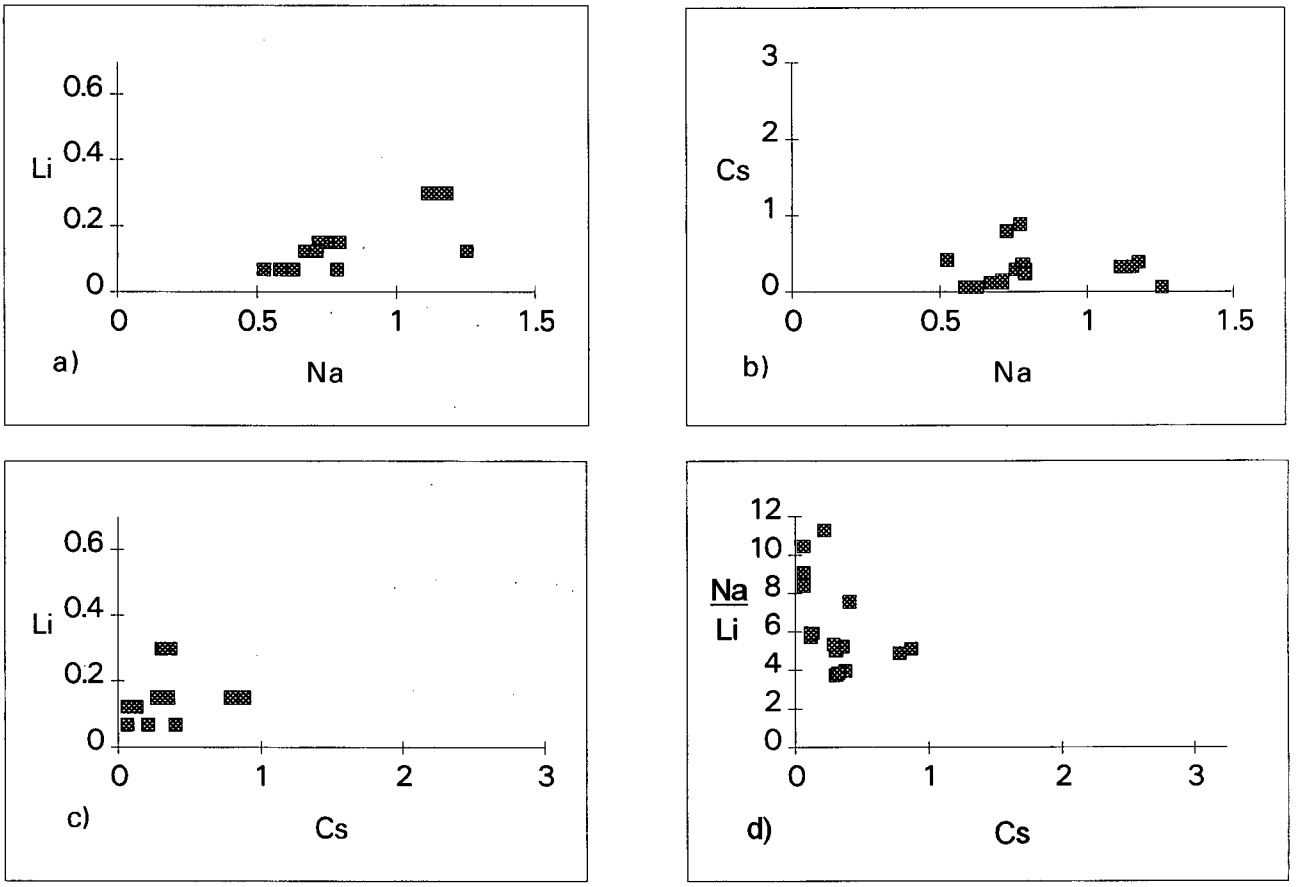

Figure 5.21: Plots of Na-Li-Cs (wt %) from Little Nahanni Pegmatite Group beryl samples.

Figure 5.22a: Photograph of beryl sample 197 taken under plain light.

Figure 5.22b: Photograph of beryl sample 197 taken under ultraviolet light. The outer, fluorescent rim corresponds to the higher Cs content detected under backscattered electron imaging. The crystal is 6 cm across.

5.6 Mica Group Minerals

5.6.1 Lepidolite

Pale to deep purple lepidolite occurs as: 1) fine-grained (mm-sized), massive, irregular units associated with similarly fine-grained quartz and albite (e.g. 197, 180); 2) coarse-grained (2mm to 2 cm) aggregates associated with pink spodumene, quartz and feldspar; and 3) very coarse (2 cm to 10 cm), cone-shaped aggregates with a botryoidal "ball-peen" habit. The latter type of lepidolite shows strong directional growth as evidenced by the widening of the cone-shaped crystals toward the centre of the dike; as well, the botryoidal surfaces are convex towards the centre of the dike.

Four lepidolite samples were analyzed for Al and Si as well as Na, K, Ca, Rb, Cs, Mn, Mg, Sr, Ba, Fe and F using electron microprobe techniques. Another sample (197) was analyzed, together with a batch of feldspars, for Al and Si as well as Na, K, Ca, Rb, Cs, Mn, Sr, Ba, Fe and P. Four samples were analyzed for Li, and B using wet chemical methods. The samples with their locality information are listed in Appendix A. Microprobe data are provided in Appendix B (diskette). Wet chemical data are provided in Appendix C. Table 5.14 summarizes average compositions for the five samples analyzed by electron microprobe.

There is a discrepancy between calculated Li values (by stoichiometry) and those obtained by wet chemical methods. Wet chemical analyses show the lepidolite to contain up to 3.83% Li_2O (and up to 0.077 % B_2O_3), whereas values obtained by stoichiometry range from 5.98 to 6.52% Li_2O. K/Rb ratios range from 13.18 to 33.93. There seems to be a trend of increasing Rb and Cs from north to south. Samples 197 and 9, both from the southern end of the field area, had the highest Cs contents; K/Cs ratios for these range from 31.03 to 413. Sample 197 contains significantly more Na than any other sample.

Table 5.14: Average compositions of lepidolite.

Sample	114 [a]	183 [a]	9 [a]	199 [a]		197 [b]
# of analyses	8	7	13	3		2
SiO_2	49.00(128)	48.26(22)	49.80(64)	49.03(56)	SiO_2	50.79(30)
Al_2O_3	27.83(283)	29.57(64)	27.82(110)	27.74(67)	Al_2O_3	26.70(42)
FeO	0.08(4)	0.04(3)	nd	nd	Fe_2O_3	0.06(3)
MnO	0.77(17)	0.76(9)	0.26(7)	0.24(3)	MnO	0.34(3)
Na_2O	0.21(6)	0.28(5)	0.29(4)	0.29(4)	Na_2O	1.22(21)
CaO	0.01(2)	nd	nd	nd	CaO	0.01(1)
K_2O	11.06(30)	11.21(7)	10.84(11)	11.10(14)	K_2O	9.66(12)
Rb_2O	0.86(13)	0.81(4)	1.53(9)	0.90(10)	Rb_2O	1.10(7)
Cs_2O	0.01(2)	0.03(4)	0.39(19)	0.04(6)	Cs_2O	0.11(1)
SrO	0.03(5)	0.05(6)	0.06(6)	0.03(5)	SrO	0.07(1)
F	4.99(91)	5.00(41)	6.05(61)	6.02(41)	BaO	0.01(1)
					P_2O_5	0.02(2)
Li_2O [c]	6.25(19)	6.17(4)	6.27(9)	6.16(9)	Li_2O [c]	6.43(5)
H_2O [c]	2.21(49)	2.25(21)	1.75(30)	1.71(19)	H_2O [c]	4.63(0)
Total	101.22	102.33	102.51	100.73	Total	101.15
		Formula contents based on 12 anions.				
Si^{4+}	3.207	3.130	3.233	3.222	Si^{4+}	3.289
Al^{3+}	2.147	2.260	2.129	2.149	Al^{3+}	2.038
Fe^{2+}	0.004	0.002	nd	nd	Fe^{2+}	0.003
Mn^{2+}	0.043	0.042	0.014	0.013	Mn^{2+}	0.019
Na^{+}	0.027	0.035	0.037	0.037	Na^{+}	0.153
Ca^{2+}	0.001	nd	nd	nd	Ca^{2+}	0.001
K^{+}	0.924	0.928	0.898	0.931	K^{+}	0.798
Rb^{+}	0.036	0.034	0.064	0.038	Rb^{+}	0.046
Cs^{+}	nd	0.001	0.011	0.001	Cs^{+}	0.003
Sr^{2+}	0.001	0.002	0.002	0.001	Sr^{2+}	0.003
Li^{+}	1.646	1.610	1.638	1.629	Li^{+}	1.674
					Ba^{2+}	nd
					P^{5+}	0.001
F^{-}	1.033	1.026	1.242	1.251		
OH^{-}	0.967	0.974	0.758	0.749	OH^{-} [d]	2.000

a Ba and Mg sought but not detected.
b Fe^{2+}, Mg, and F not sought (part of feldspar analysis run)
c Determined by stoichiometry.
d This site assumed as entirely OH- only because F not analyzed.
nd Not detected.
() Standard deviation of averages.

5.6.2 Muscovite

Muscovite occurs as fine-grained to coarse-grained (1 mm to 2.5 cm) crystals in the wall zones and aplitic units of many pegmatite dikes. Very fine-grained (<1 mm) muscovite occurs in the border zones of some dikes.

Three muscovite samples were analyzed for Al and Si as well as Na, K, Rb, Cs, Ca, Sr, Ba, Mn, Mg, Fe and F using electron microprobe techniques and one sample was analyzed for Li, and B using wet chemical methods. Appendix A lists the samples with their locality information. Microprobe data are provided in Appendix B (diskette). Wet chemical data are provided in Appendix C. Average compositions for the three muscovite samples analyzed by electron microprobe are summarized in table 5.15.

5.6.3 Cookeite

Cookeite is found as irregular stringers or fracture-fillings that cut across dike zonation. It is generally pale green. Identification was made by XRD and by EDS using an SEM or an electron microprobe.

Table 5.15: Average compositions of muscovite.

Sample	360	314	325
# of analyses	7	1	5
SiO_2	45.01(48)	49.20	44.71(11)
Al_2O_3	38.07(41)	32.74	38.46(32)
FeO	0.61(5)	0.48	0.45(4)
MnO	nd	nd	0.15(3)
MgO	0.17(2)	0.04	nd
Na_2O	0.48(5)	0.36	0.66(14)
K_2O	11.09(10)	13.05	10.87(16)
Rb_2O	0.45(10)	0.12	0.30(20)
Cs_2O	0.06(6)	nd	nd
SrO	nd	0.09	0.04(6)
F	0.52(10)	nd	0.49(32)
H_2O [a]	4.27(5)	4.51	4.28(16)
Total	100.51	100.59	100.21
Formula contents based on 12 anions.			
Si^{4+}	2.987	3.270	2.970
Al^{3+}	2.977	2.565	3.011
Fe^{2+}	0.034	0.027	0.025
Mn^{2+}	nd	nd	0.008
Mg^{2+}	0.017	0.004	nd
Na^{+}	0.062	0.046	0.085
K^{+}	0.939	1.107	0.921
Rb^{+}	0.019	0.005	0.013
Cs^{+}	0.002	nd	nd
Sr^{2+}	nd	0.003	0.002
F^{-}	0.109	nd	0.103
OH^{-}	1.891	2.000	1.897

Note: Ba and Ca sought but not detected.
() Standard deviation.
a Determined by stoichiometry.
nd Not detected.

5.7 Tourmaline group

The most common tourmaline group mineral is schorl. The most abundant occurrence of schorl is in black, exocontact selvages at the contact between pegmatite dike and host rock (Fig. 5.23). These selvages are at most a few centimetres wide and usually less than 1 centimetre wide. In some dikes, schorl occurs as euhedral, prismatic crystals within the border, wall or intermediate zones of the pegmatite dike. These occurrences are either tourmalinized screens, fracture fillings perpendicular to dike contacts or single crystals rooted in the border zone and growing inward. Tourmalinized screens are planar features, parallel to dike contacts, along which the tourmaline crystals are usually aligned. A few examples in which the schorl crystals had grown radially along the plane of a fracture were found in a dike (NMM-1N-7s) which also hosts single crystals at the contact. All occurrences of schorl are, in some way, related to the contact and/or host rock. Tourmalinized screens appear to be pieces (slices) of host rock that have been incorporated into the main body of the pegmatite. Close inspection reveal that minerals typical of the border and wall zone are present along the contact between the screens and the enclosing pegmatite. Zoning is evident around some thicker, xenolithic fragments of the schist host rock. Single, euhedral crystals of schorl observed away from the contact (i.e. in the inner wall or intermediate zones) may have broken off and been carried inward by later, still mobile magma. Samples from a dike in the NMM-1N-7 swarm contain schorl crystals that have been broken and slightly rotated, but surrounding schorl crystals remain unaffected (Fig. 5.24).

Tourmaline (schorl-dravite) very rarely occurs as euhedral, acicular crystals associated with euhedral albite and muscovite, and overgrown by clear, euhedral quartz in calcite-filled, or mica/clay partially-filled fractures cross-cutting pegmatite dikes.

One specimen (#326) of green schorl came from the intermediate zone of a dike in the LMM-2s swarm, proximal to the Cali claims in cirque 2. This schorl is anhedral and intimately intergrown with spodumene and feldspar.

Eleven species comprise the tourmaline group of trigonal, chemically complex borosilicates. The general formula for the group is $XY_3Z_6(BO_3)_3Si_6O_{18}(O,OH,F)_4$, where X = Na, K, Ca; Y = Li, Al, Mg, Mn^{2+}, V^{3+}, Fe^{2+}, Fe^{3+}; Z = Al, Fe^{3+}, Fe^{2+}, Mg, Ti (Grice and Ercit, 1993). Schorl, $NaFe^{2+}{}_3Al_6(BO_3)_3Si_6O_{18}(OH)_4$ forms a series with two other members of the group: dravite, $NaMg_3Al_6(BO_3)_3Si_6O_{18}(OH)_4$; and elbaite, $Na(Li,Al)_3Al_6(BO_3)_3Si_6O_{18}(OH)_4$. These two series have complete compositional ranges between the end-members of each. However, Mg and Li are almost immiscible in tourmaline and no series exists between dravite and elbaite (Deer *et al*, 1966).

Two samples were analyzed for Al and Si as well as Na, K, Ca, Mg, Mn, Fe, Ti, V, Cr and F using the electron microprobe. One of these samples, and one other, were analyzed for Li using wet chemical methods. The samples with locality information are listed in Appendix A. Microprobe data are provided in Appendixes B-2 (diskette). Wet chemical data are provided in Appendix C. Table 5.16 summarizes average compositions for the two tourmalines analyzed by electron microprobe.

Certain difficulties were encountered while attempting to calculate formulas from the electron microprobe data and these have as yet not been resolved. Oxide totals remain low even after calculating for H_2O and the calculated formulas are not consistent with the empirical formulas determined by Grice and Ercit (1993). The observations made hereafter regarding the chemistry of the tourmalines should be viewed as general overviews that are included in this thesis because a even general idea of the behaviour of tourmaline chemistry is still an important one. Tourmaline group minerals, especially of the schorl-elbaite series, rarely occur in albite-spodumene pegmatites.

The black tourmaline (sample 318) is schorl. It is Mg- and Fe-rich and contains significant Ti and F, minor Ca and Mn, and trace K and V; Li was not determined for this sample. However, Li was detected in a sample (334) of the same type and occurrence, taken from a dike close to that of sample 318. It was found to contain only trace amounts of Li (275 ppm). It may be important to note that the Li value obtained is comparable to those values obtained for whole rock analyses for Li for the tourmaline selvage at a dike contact (188 ppm), a sample of the host rock 5 centimetres from the contact (230 ppm), and a sample taken 1 metre away from the contact (136 ppm). This may be noteworthy only in that the latter two samples do not contain significant (i.e. visible) tourmaline.

The green tourmaline (sample 326) is schorl-dominant in the schorl - elbaite series (i.e. Li+Al (in the *X* site) < Fe). This sample contains no Mg, V or Ti, and F, Mn, Na and Al contents are higher than those of sample 318. Lithium contents were determined to be 0.33 % Li_2O.

Figure 5.23: A sample from dike NMM-1N-5 showing well-developed tourmaline exocontacts. Note that where the dike is parallel to the host rock foliation, the exocontact is regular, and where the dike is discordant, the contact is irregular.

Figure 5.24: Schorl from dike NMM-1N-7s (sample 318). The large crystal is broken and partially rotated whereas neighbouring crystals are intact.

Table 5.16: Average compositions of tourmaline samples.

Sample	318	326
# of analyses	10	8
SiO_2	34.23(23)	35.30(21)
TiO_2	1.07(14)	nd
Al_2O_3	31.26(33)	37.34(54)
V_2O_3	0.04(4)	nd
MgO	3.48(33)	nd
MnO	0.32(3)	0.92(4)
FeO	11.10(33)	6.32(82)
CaO	0.59(5)	0.12(7)
Na_2O	2.17(4)	2.42(18)
K_2O	0.04(2)	0.01(1)
F	0.90(10)	1.20(31)
B_2O_3	9.98(0)	9.98(0)
Fe_2O_3 [a]	nd	nd
Li_2O [b]	na	0.33(0)
H_2O [c]	3.04(5)	2.89(16)
O = F	-0.38(4)	-0.51(13)
Total	97.84	96.33

Formula contents based on 31 anions (O, OH, F) and
18 cations (Si^{4+}, Ti^{4+}, Al^{3+}, V^{3+}, Cr^{3+}, Mn^{2+}, Fe^{2+}, Fe^{3+},B^{3+} ,Li^{+}).

Si^{4+}	5.884	5.965
Ti^{4+}	0.138	nd
Al^{3+}	6.332	7.436
V^{3+}	0.006	nd
Mg^{2+}	0.893	nd
Mn^{2+}	0.046	0.132
Fe^{2+}	1.596	0.894
Fe^{3+}	nd	nd
Li^{+}	na	0.224
Ca^{2+}	0.109	0.022
Na^{+}	0.724	0.794
K^{+}	0.009	0.001
B^{3+}	2.961	2.911
F^{-}	0.487	0.642
OH^{-}	3.509	3.341

Note: Cr sought but not detected
- a Determination of Fe3+ contents attempted by methods of Grice and Ercit, 1993.
- b Determined by wet chemistry.
- c Determined by stoichiometry.
- nd Not detected
- na Not analyzed.

5.8 Garnet Group

Two kinds of garnet occurrences have been noted in the Little Nahanni Pegmatite Group. The most frequent occurrence is as anhedral to euhedral, orange-red to reddish-brown, grainy to glassy crystals at or very close to the pegmatite-wall rock contact. These garnets are associated with quartz, muscovite ± albite ± schorl. They are generally cm-sized, though may range from several mm up to 2.5 cm. Where associated with schorl, garnet crystallized after the schorl and before muscovite. Figure 5.25 shows this sequence of crystallization well. Some samples seem to show evidence of resorption (e.g. sample 225). They have a very grainy texture, as does the host feldspar, and the contact between the garnet and the host feldspar is irregular and diffuse.

The second type of garnet occurs as pods of dull reddish-brown to almost brown-black, well-defined dodecahedral crystals associated with medium to fine-grained albite-quartz. This material has an altered appearance and seems to intrude or replace blockier K-feldspar-quartz-spodumene. The garnet crystals, particularly the larger ones, may be glassy, but heavily fractured. Grain sizes of this type are similar to the first type.

The garnet group has a general formula $A_2B_3(SiO_4)_3$, where: A = (major) Ca, Mn, Fe^{2+}, Mg, and (minor) Zn, Y^{3+} and Na; B = (major) Al, Cr, Fe^{3+}, and (minor) $Ti^{4+,3+}$, V^{3+}, Fe^{2+}, Zr, and Sn. Si may in part be replaced by minor Al, $Fe^{3+,2+}$,Ti^{4+} and P (Meagher, 1980; Deer *et al.*, 1966).

Eight samples were analyzed for Al and Si as well as Mn, Fe, Ca, Mg, Ti, Na, Zr, Sn, P, V, and Cr using electron microprobe techniques. The samples with their locality information are listed in Appendix A. Microprobe data are provided in Appendixes B-2 (diskette). Table 5.17 summarizes average compositions for the eight garnets analyzed by electron microprobe.

Figure 5.25: Photograph of sample 318 showing the crystallization sequence, tourmaline → garnet → muscovite.

While it is possible to make some broad generalizations when relating garnet chemistry and host lithologies, many authors have discussed the difficulties of subjecting the garnet group to a simple classification or interpretive scheme with respect to genetic relationships, for example, establishing the relationship between compositional zoning trends and pegmatite evolution (*cf* Clarke, 1981). Foord (1976) showed garnet from the Mesa Grande district, California to have great variability with respect to Fe-Mn zoning. Three major trends were: an Fe-enrichment toward the rim, an Mn-enrichment toward the rim and an Mn-enrichment followed by an Fe-enrichment. Two minor trends included: an Fe-enrichment followed by Mn-enrichment, and no discernible zonation. Some of the analyses of Baldwin and von Knorring (1983) showed similar Fe-Mn trends. A Ugandan garnet sample, studied by Baldwin and von Knorring (1983), contained an outward Ca-depletion and concurrent Mn-enrichment; Fe remained constant throughout. Analyses from the present study do little to clarify the situation and, in fact, add complexity by presenting significant variability within a single pegmatite group.

All but one of the samples analyzed are spessartine. The exception, sample 399, has a core of almandine and a rim of spessartine. There is extreme variation with respect to Mn, Ca and Fe contents of the samples analyzed. Where zoning is evident in individual crystals, Mn contents generally increase outward, in relation to Fe, from the centre of a crystal (e.g. figures 5.26 and 5.27). This seems to be at odds with what has been reported as common zonation trends found in pegmatitic/granitic garnet crystals (e.g. Černý *et al.*, 1985; Baldwin and von Knorring, 1983; Leake, 1967). An exception to the trend at the Little Nahanni Pegmatite Group, and more consistent with that of the above references, was found in sample 84: Fe is slightly enriched with respect to Mn, although Mn and Fe are very depleted relative to Ca, which increases (Fig. 5.31). When viewed in BSE mode, there is a very subtle lightening in shade between the core of this crystal and its euhedral edge, then a stark change (darker) between the euhedral crystal and an irregular, outer zone (Fig. 5.30). Whether this outer zone represents an irregular, late-stage overgrowth or a replacement texture is open to interpretation.

The behaviour of Mn, Ca and Fe in sample 225 appears to be similar to a Ugandan sample analyzed by Baldwin and von Knorring (1983) in that the major variations are with respect to Mn and Ca, whereas Fe remains relatively constant throughout the crystal. This sample exhibits several discernible zones with respect to Ca/Mn (Fig. 5.27). The Ca/Mn ratio decreases outward from the core of the crystal, then rises sharply and stays level in the next zone before it gradually decreases to a level roughly equivalent to that of the core. What is notable in sample 255 (Fig. 5.26) is the lighter grey, inner zone in that the contact between it and the more Ca-rich, inner part of the outer zone exhibits some textures which may be interpreted as being of replacement in nature. As well, the garnet in contact with the calcite in-fillings (black inclusions in figure 5.26) is euhedral.

All samples except 399 and 160 show a negative correlation between Ca and Mn (Fig. 5.32). A similar correlation between Fe and Mn is evident in samples 399 and 160, whereas other samples show no such correlation (Fig. 5.34). Samples 160, 299 and possibly 318 are negatively correlated with respect to Ca and Fe (Fig. 5.33). An Fe/Mn *versus* Mn plot for the Little Nahanni Pegmatite Group (Fig. 5.34) matches a similar plot published by Černý *et al.* (1985): Fe/Mn for this group ranges from 1.44 to 0.11. Titanium contents in the Little Nahanni garnet samples range from 0.00 to 0.27 weight % TiO_2.

Table 5.17: Averaged electron-probe microanalyses of garnet samples

Sample	318	84	160	299	114	225	399
# of analyses	3	7	4	20	5	35	16
SiO_2	36.09(12)	36.12(51)	35.92(19)	35.98(34)	36.57(18)	36.70(32)	35.77(23)
Al_2O_3	20.38(7)	20.38(19)	20.54(12)	20.45(24)	20.64(6)	20.65(17)	20.28(12)
TiO_2	0.09(2)	0.06(7)	0.22(4)	0.13(6)	0.13(3)	0.12(3)	0.14(4)
V_2O_3	nd	0.01(2)	nd	nd	nd	0.02(3)	na
Fe_2O_3	0.60(46)	0.75(65)	0.29(34)	0.68(51)	0.83(14)	0.76(46)	0.52(37)
MnO	23.09(44)	23.96(741)	26.55(67)	23.00(448)	21.43(100)	17.22(201)	18.32(252)
FeO	15.67(34)	10.88(344)	12.35(90)	14.77(775)	10.21(17)	12.81(72)	23.01(238)
CaO	2.63(44)	5.84(553)	2.67(64)	3.74(328)	8.73(84)	10.15(215)	0.65(19)
MgO	0.46(5)	0.34(22)	0.27(11)	0.17(10)	0.42(1)	0.45(3)	0.27(7)
Total	99.01	98.35	98.80	98.92	98.96	98.89	98.94
Si^{4+}	5.966(28)	5.962(23)	5.950(29)	5.948(29)	5.953(12)	5.957(29)	5.960(28)
Al^{3+}	0.034(28)	0.038(23)	0.050(29)	0.052(29)	0.047(12)	0.043(29)	0.040(28)
Al^{3+}	3.937(31)	3.928(62)	3.960(11)	3.933(38)	3.913(7)	3.908(42)	3.943(26)
Ti^{4+}	0.012(2)	0.008(9)	0.028(5)	0.016(8)	0.016(4)	0.015(4)	0.017(5)
V^{3+}	nd	0.001(2)	nd	nd	nd	0.002(3)	na
Fe^{3+}	0.074(57)	0.093(79)	0.036(42)	0.084(62)	0.102(17)	0.093(56)	0.065(47)
Mn^{2+}	3.233(56)	3.365(1091)	3.725(87)	3.217(606)	2.955(147)	2.369(292)	2.585(351)
Fe^{2+}	2.166(45)	1.502(479)	1.711(128)	2.051(1092)	1.390(20)	1.739(106)	3.207(336)
Ca^{2+}	0.466(78)	1.021(959)	0.474(114)	0.657(573)	1.523(143)	1.762(360)	0.116(33)
Mg^{2+}	0.113(13)	0.083(53)	0.066(26)	0.041(25)	0.101(1)	0.109(8)	0.067(17)
Mole % Spe	0.54	0.56	0.62	0.54	0.50	0.40	0.43
Mole % Alm	0.36	0.25	0.29	0.34	0.23	0.29	0.54
Mole % Pyr	0.08	0.17	0.08	0.11	0.26	0.29	0.02
Mole % Gro	0.02	0.01	0.01	0.01	0.02	0.02	0.01

Note: Na, Zr, Sn and P sought but not detected.
() Standard deviation of averages.
nd Not detected.
na Not analyzed

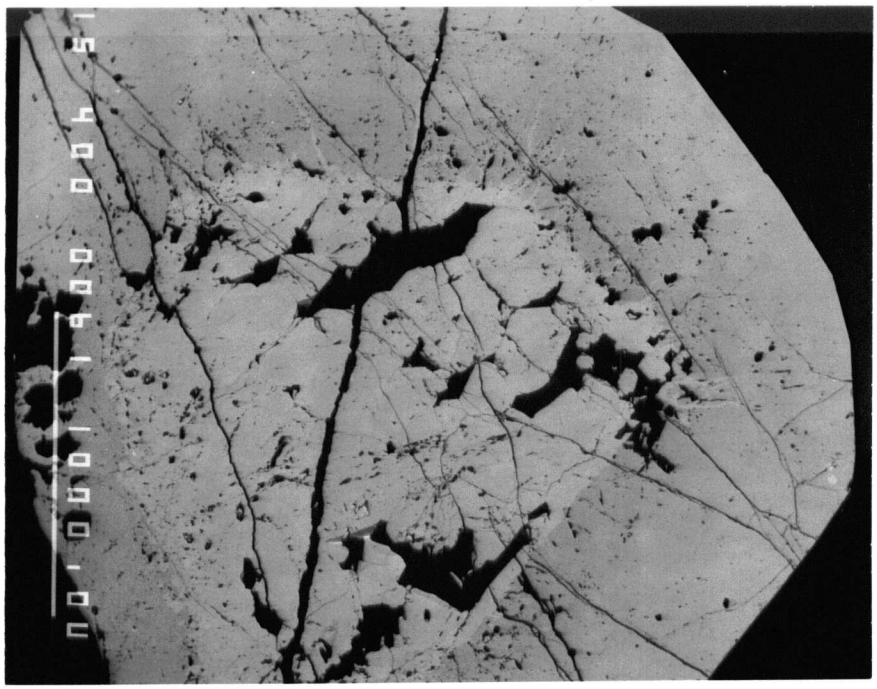

Figure 5.26 Back-scatter electron image of sample 225 (mount 153). The black areas inside the garnet crystal are calcite. Note the euhedral garnet in the interior of the crystal, and the texture at the contact between the lighter core and darker rim.

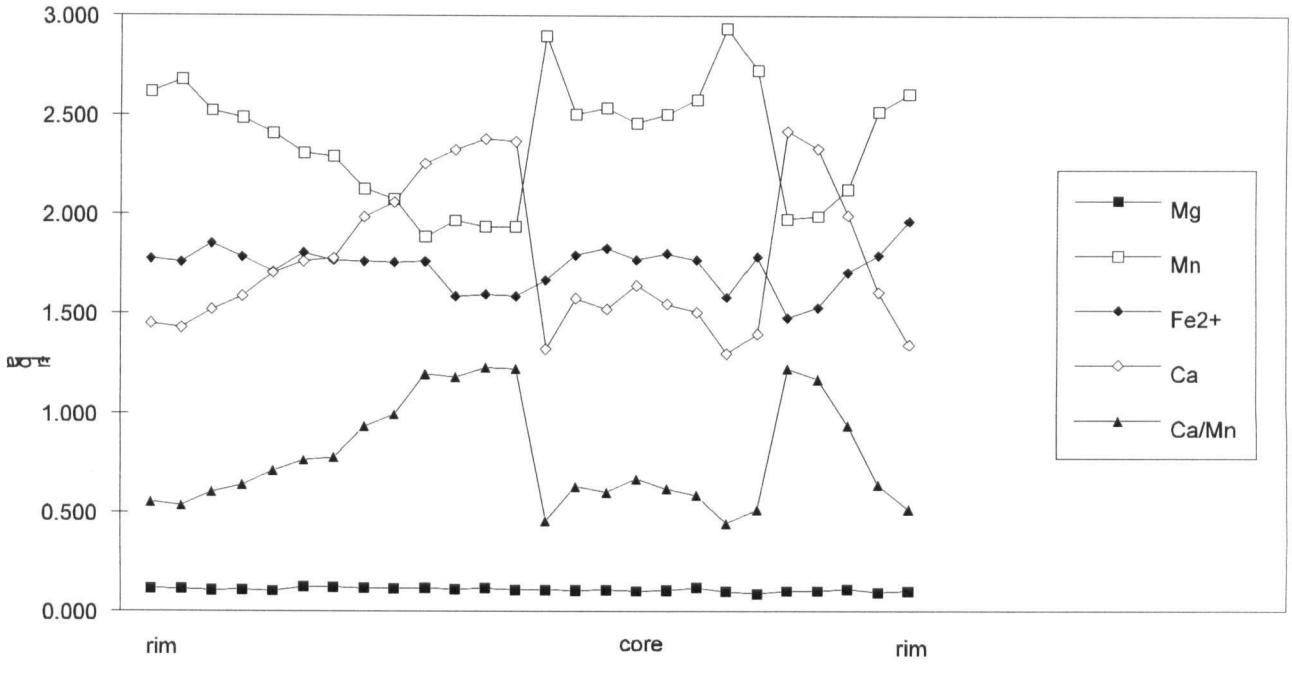

Figure 5.27: Analyses of garnet sample 225 showing zonation.

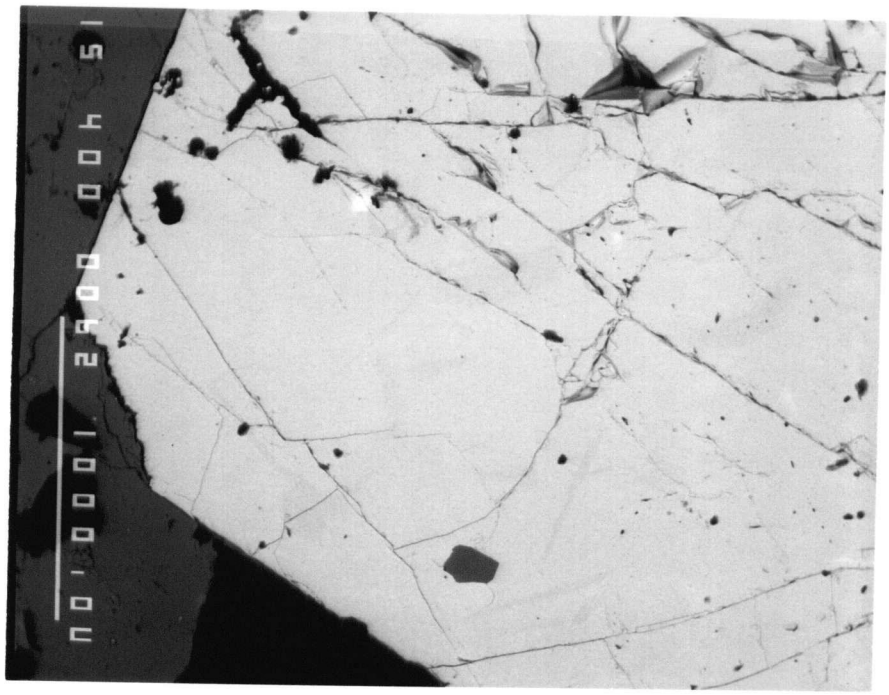

Figure 5.28 Back-scatter electron image of sample 399. The atomic masses of Fe and Mn are too close for the zoning to be seen under BSE mode. However, this shows the euhedral habit of the crystal well. The enclosing minerals are albite and quartz.

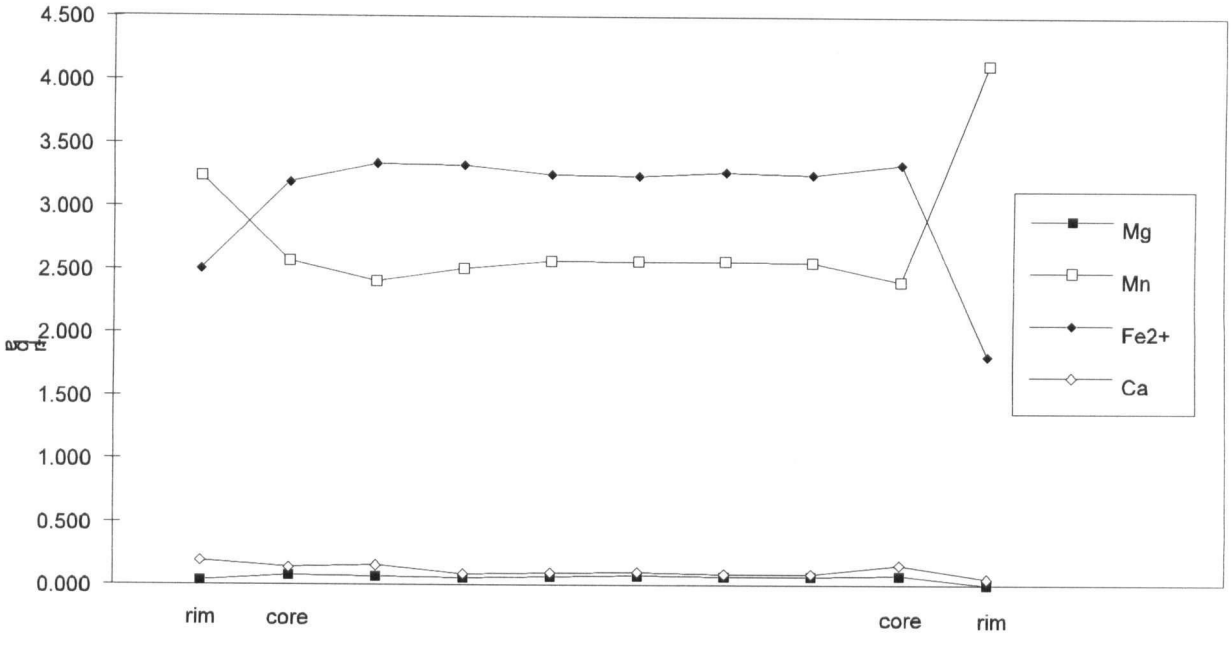

Figure 5.29: Analyses of garnet sample 399 showing zonation. There is a positive correlation between Fe and Mg; both are negatively correlated with Mn.

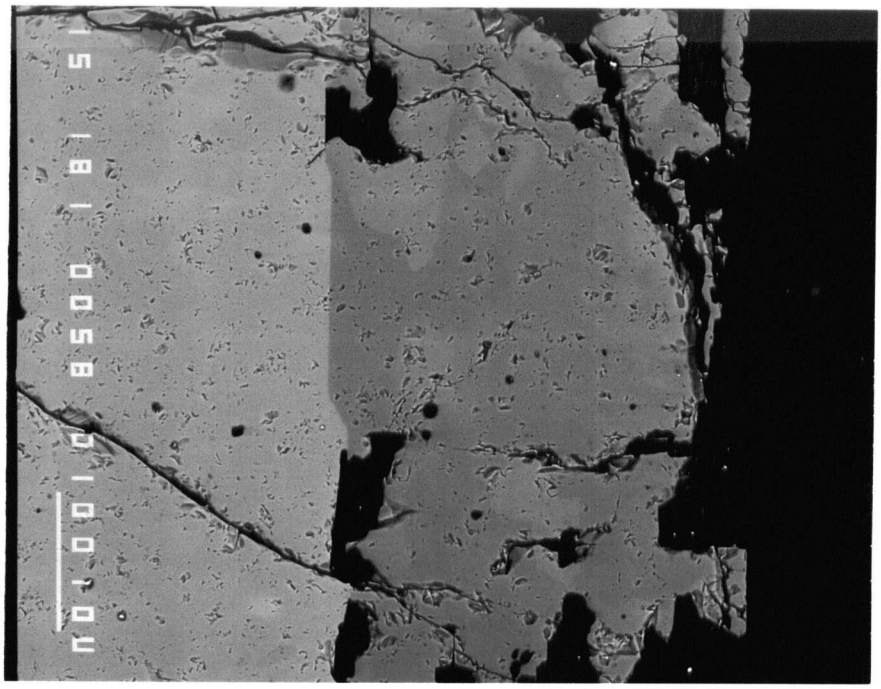

Figure 5.30 Back-scatter electron image of the edge of a garnet crystal in sample 84. The light-grey zone to the left corresponds to the "edge" shown in figure 5.29, the darker area is the "rim", and the black region is the enclosing plagioclase (Na-Ca-bearing [EDS analysis only]).

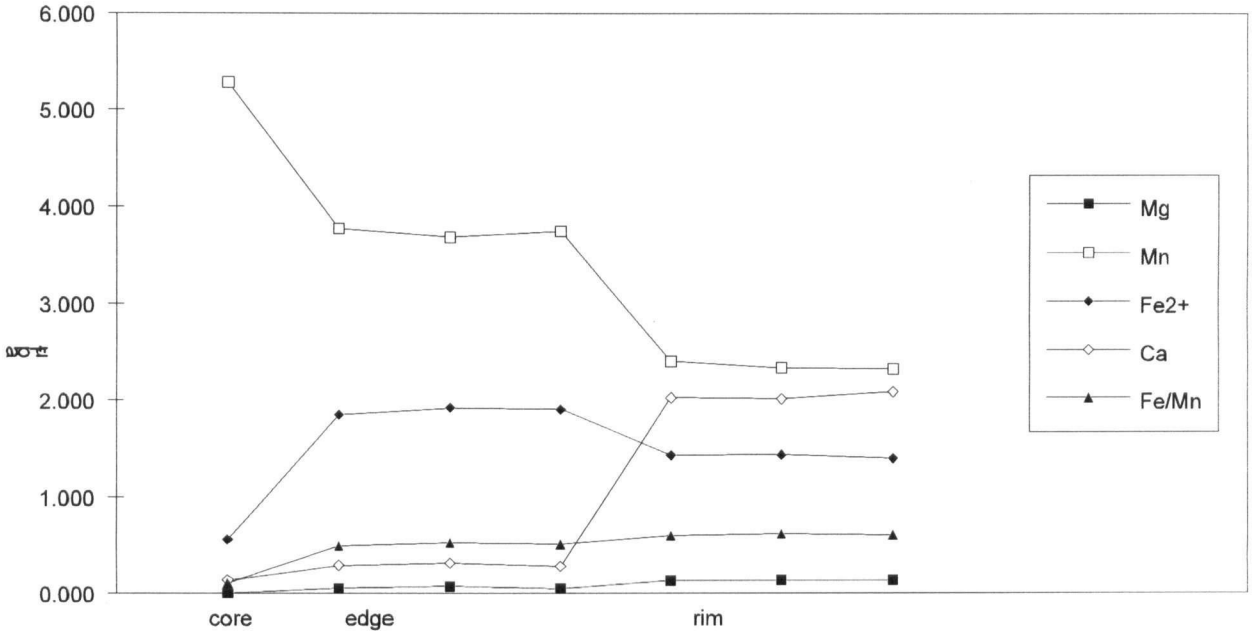

Figure 5.31: Analyses of garnet sample 84 showing zonation. Note the depletion of Mn with respect to Ca and the enrichment of Fe with respect to Mn toward the rim.

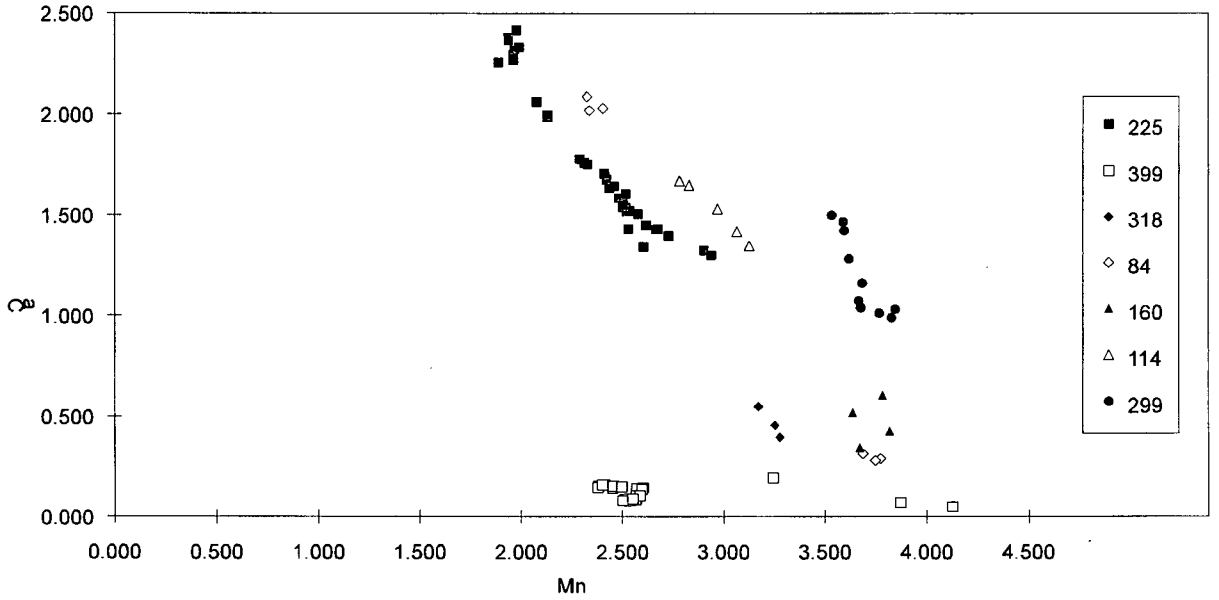

Figure 5.32: A plot of Ca *versus* Mn for garnet. Units are in atoms per formula unit.

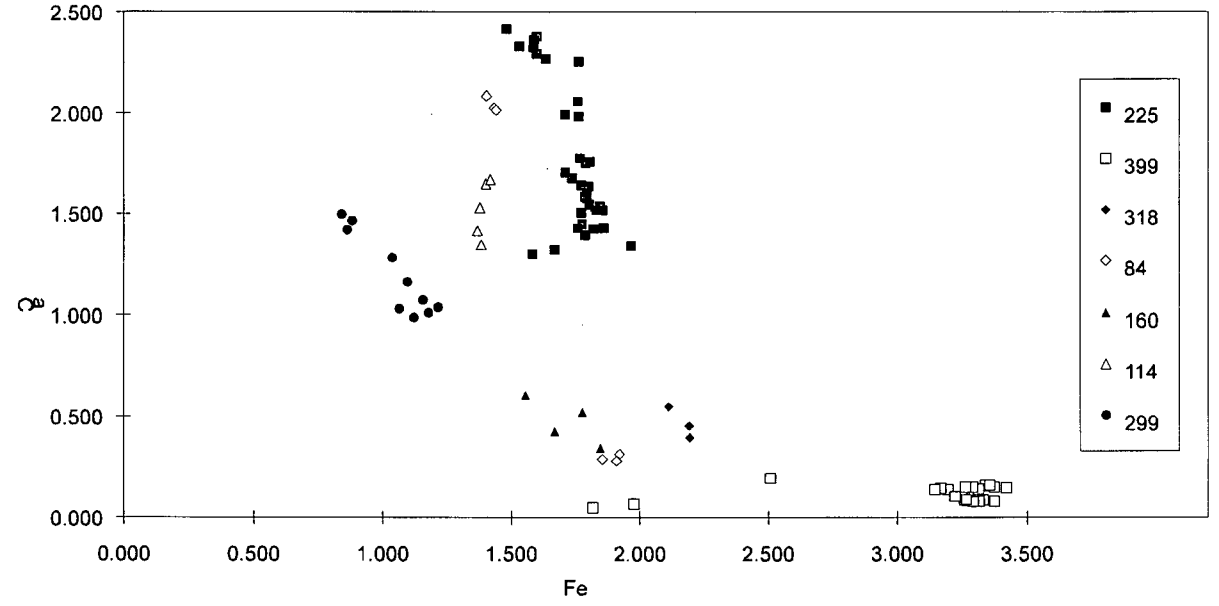

Figure 5.33: A plot of Ca *versus* Fe for garnet. Units are in atoms per formula unit.

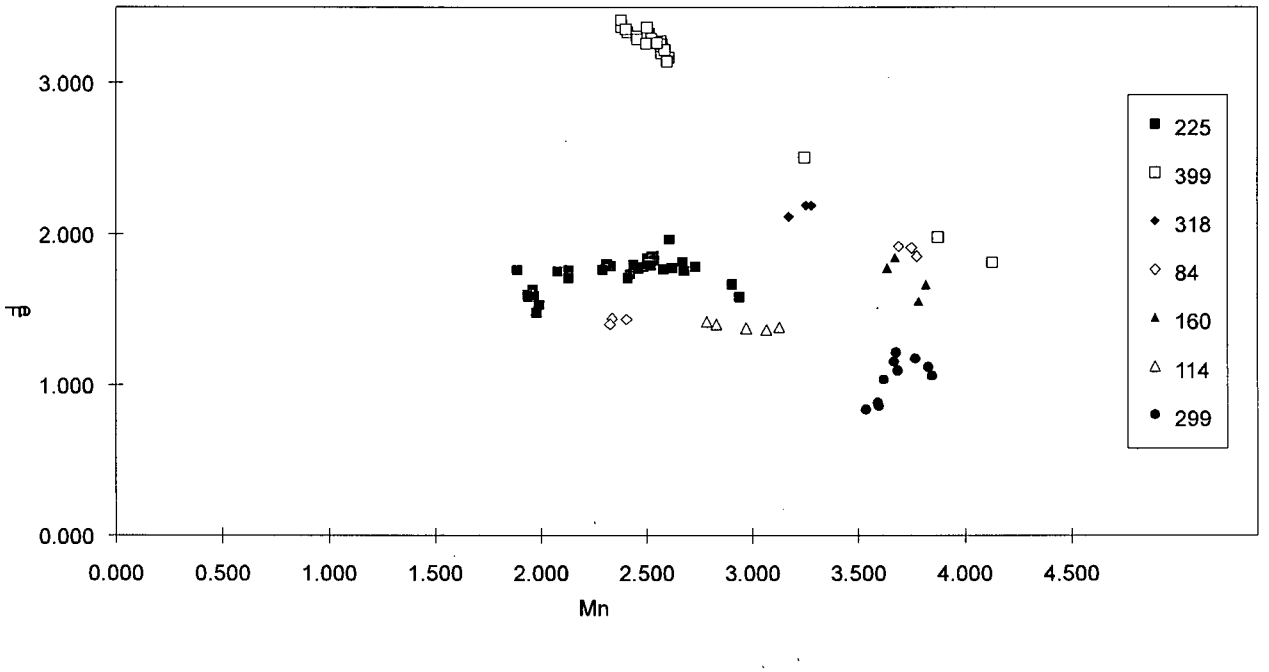

Figure 5.34: A plot of Fe *versus* Mn for garnet. Units are in atoms per formula unit.

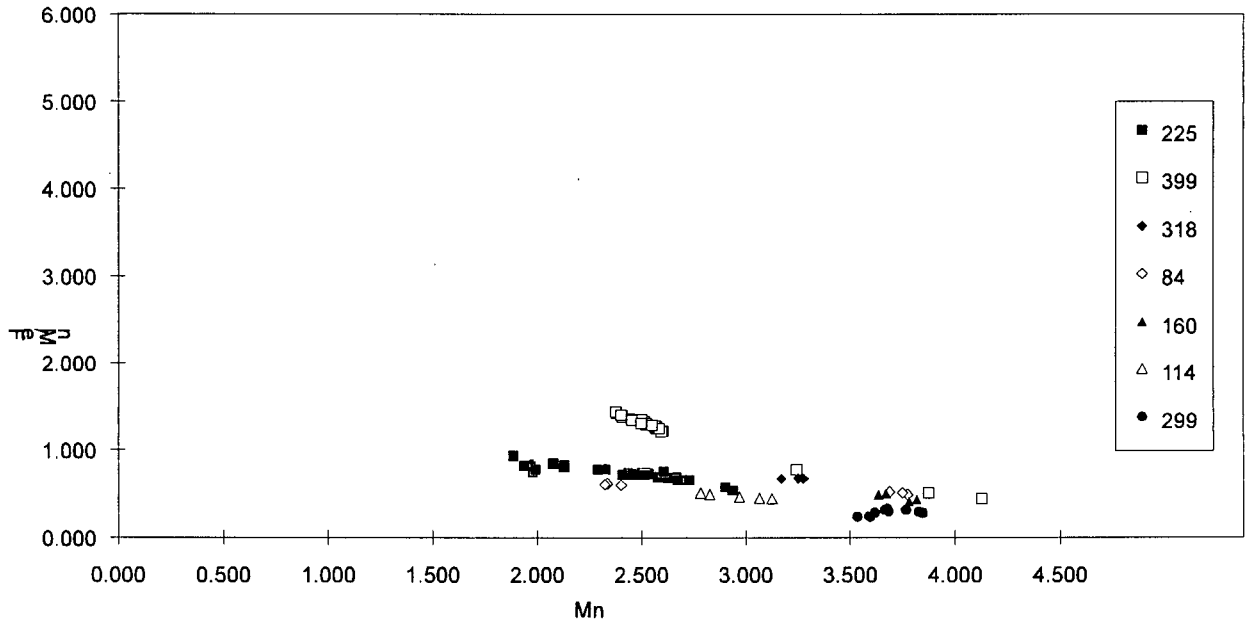

Figure 5.35: A plot of Fe/Mn *versus* Mn for garnet. Units are in atoms per formula unit.

5.9 Zeolite Group Minerals

Zeolites are a group of hydrous aluminosilicates generally forming in relatively low temperature environments. Several members of the zeolite group occur in the Little Nahanni pegmatite group. They occur as late-stage minerals lining vugs, overgrowing all minerals except calcite in calcite-filled fractures. The species that have been identified are: chabazite (Ca), stilbite (Na,Ca), stellerite (Ca), laumontite (Ca), heulandite (Na,Ca), dachiardite (Ca,Na,K). Chabazite, stellerite and stilbite are commonly associated with apatite and beryl in late-stage fractures and pockets. Laumontite and heulandite occur in albite-rich units with open-spaced vugs and voids left by altered spodumene.

These minerals were visually identified and confirmed either by powder Xray diffraction, scanning electron microscope or electron microprobe using electron dispersive (qualitative) chemical analysis. No quantitative chemical analysis was made. However, the fact that these are all Ca-bearing minerals in late-stage features suggests some degree of assimilation with the host rock.

5.10 Minor accessory minerals

5.10.1 Sulphides

Galena occurs as micron-size inclusions in K-feldspar (e.g. sample 246) and as discrete grains in feldspar (e.g. sample 329). Sphalerite occurs as anhedral blebs associated with cleavelanditic albite and K-feldspar (e.g. sampe 345, 122). Pyrrhotite and pyrite occur at the pegmatite/host rock contact, associated with schorl and/or garnet.

5.10.2 Fluorite

Small, anhedral, purple crystals up to 1 mm were found in a calcite-filled fracture. The crystals have a distinct "etched" appearance. The fluorite was identified by microprobe, using energy dispersive spectroscopy.

5.10.3 Helvite

Orange-yellow to orange-brown helvite occurs as tetrahedral crystals on "skeletal", etched K-feldspar in calcite-filled pockets in specimens from cirque 1N (samples 329 & 330). It is associated with grey-green apatite, "aquamarine" beryl, albite and chabazite.

6. PETROGRAPHY

Petrographic investigations included optical microscopy, SEM studies of polished blocks and feldspar staining in addition to careful hand sample description. Notes made during these investigations are compiled in appendix D.

6.1 Border Zone

The border zone was not observed to exceed 1.5 to 2 centimetres in width and was usually less than 0.5 cm. SEM and optical petrographic study revealed that the contact is generally defined, on the pegmatite side (i.e. border zone), by quartz (35 - 100%), muscovite (0 - 25%) and/or plagioclase (0 - 50%), plus or minus apatite or tourmaline. The contact between the clearly more mafic constituents (e.g. biotite) of the host rock schist and pegmatite mineralization (e.g. muscovite) in sample 246 is defined by a very distinct band of apatite crystals. This dike is asymmetrically zoned and the apatite band is at the contact between the aplitic side of the pegmatite and the host rock as may be seen in figure 6.1.

A real border zone does not seem to be present in some dikes. For example, sample 348 shows 0.5 to 1 cm-sized albite laths that grew away from, but in contact with, the host rock, leaving no room for a defined border "zone" (Fig. 6.2).

6.2 Wall Zone

Wall units vary considerably in thickness and texture but are typically from 2-3 mm to several cm in width and granitic to aplitic in texture. In many dikes, a wall unit is not apparent at all.

Particularly in cases where the pegmatite has been emplaced in pelitic metasedimentary rocks, the wall zone can be subdivided into an outer wall zone and an inner wall zone, based on the presence or lack of muscovite, respectively. Figure 3.2 shows an excellent example of this. In that dike (LMM-5-1), there is a clear zonal progression from a thin (1-2 mm) border unit to a

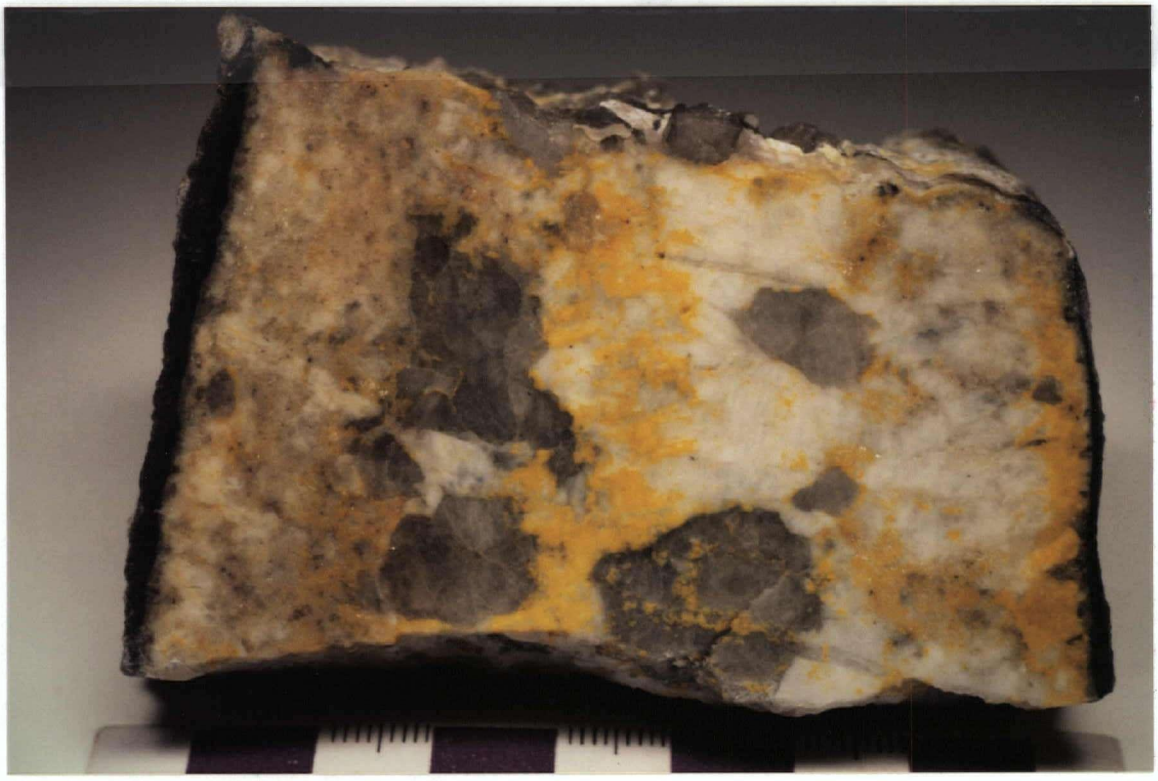

Figure 6.1: Dike cross-section (sample 246). Note the asymmetric zonation. This sample has been stained to identify K-feldspar. The scale is in cm.

Figure 6.2: Dike cross-section (NMM-1N^1S-25: sample 348). Colouration on left side is due to natural iron oxides, not feldspar staining techniques. Note inner aplitic unit.

roughly 2 cm outer wall zone, followed by a muscovite-absent inner wall zone (about 1.5 cm), then an intermediate zone in which grain size dramatically increases. Pegmatites emplaced in calcareous metasedimentary rocks may also contain calcite in the wall (and border) zone. Sample 318, shown in figure 5.25, has a wall zone consisting of 50% quartz, 30% calcite, 15% albite, and 5% muscovite.

Feldspar contents of wall zones may be entirely plagioclase (albite), entirely K-feldspar, or a mixture of both. Figures 6.1 and 6.3 are photographs of dike cross-sections that have been stained to show K-feldspar contents. Sample 315 (Fig. 6.3) exhibits concentric zoning where quartz and plagioclase comprise a thin border zone, and K-feldspar (60%) and quartz (40%) make up the 2 - 3 mm thick wall zone. Sample 246, in figure 6.1 has a similar wall zone only on one side if the dike. The wall zone in sample 132 (figure 6.4) consists of quartz (60%) and muscovite (40%). Sample 348 is an example of a K-feldspar absent dike (the colouration seen on the left hand side in figure 6.2 is due to iron-oxide stains, not feldspar staining dyes). The wall zone is less than 0.5 cm thick and composed of albite (59%), quartz (39%) and muscovite (2%).

6.3 Intermediate Zone

The contact between the wall unit and the intermediate unit is not sharp, but is generally defined by a coarsening of mineral textures towards the centres of dikes. For many dikes, the first appearance of spodumene can be used as a reliable indicator of the start of the intermediate unit. In general, the intermediate unit consists of K-feldspar and/or plagioclase, quartz and spodumene, with or without lepidolite. Grain sizes vary greatly: from cm-sized crystals on thin dikes to crystals up to 70 - 80 cm in larger dikes.

Figures 5.1, 5.2 and 6.4 show examples of intermediate zone mineralogy.

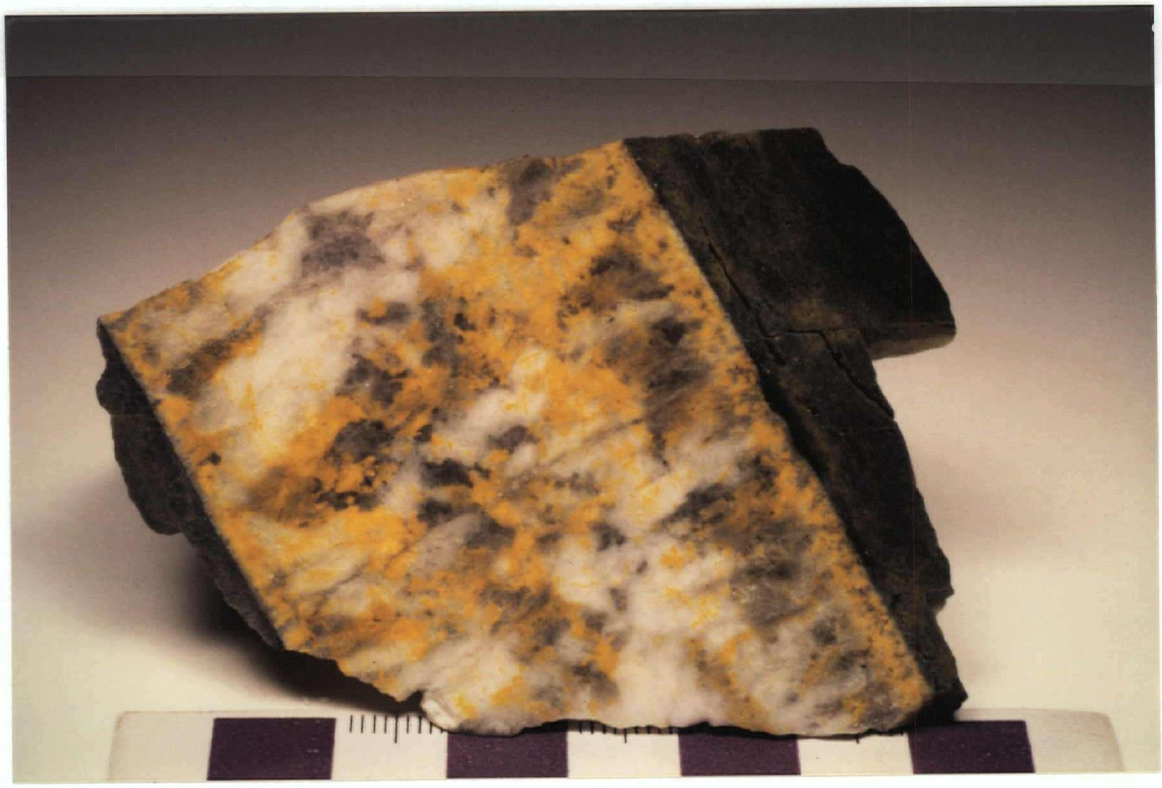

Figure 6.3: Dike cross-section (sample 315). Note the concentric zonation. This sample has been stained to identify K-feldspar. The scale is in cm.

Figure 6.4: Dike cross-section (sample 132). Same cross-section as figure 5.2.1, except this has been stained for K-feldspar identification.

6.4 Aplite

Albite (25 - 85%) and quartz (10 - 45%) are the dominant minerals comprising the aplitic units. Mica (muscovite or lepidolite) is generally present (5 - 25%) and oxide minerals such as cassiterite and columbite-group minerals are common. Less common are relict fragments of spodumene and/or K-feldspar; the latter occurs more as remnants of large (cm scale) blocky crystals rather than 'fragments'.

Aplitic units are equigranular; contacts are generally sharp and free of alteration textures. An exception to this are the relict spodumene fragments that some aplitic material contains. Large, blocky K-feldspar or other minerals of the wall and intermediate zones that are in contact the aplitic material, commonly show embayment or other signs of resorption and/or alteration. Aplitic units differ from wall zone mineralization in that the minerals such as quartz and albite do not generally exhibit strain features such as undulatory extinction, like those of the wall zone commonly do. As well, the general appearance of the aplitic material is "cleaner", more pristine, than that of the wall zone material. Except as somewhat altered 'phenocrysts' of blocky, intermediate zone K-feldspar, K-feldspar is not noted as a constituent within the aplitic material.

Aplitic stringers or layers commonly cut through larger, elongate crystals such as the spodumene crystals seen figures 3.3 and 6.5. In hand sample and in thin section, the spodumene crystals exhibit alteration/resorption textures where they are in contact with the aplitic material (Fig. 6.6). The fragments often have highly irregular contacts with the aplitic material. Sample 382 (thin section 6) contains a plumose, micaceous mineral that appears to have grown into (embayed), and at the expense of spodumene. Other samples, such as 201 (thin section 29), contain relict fragments of almost completely altered spodumene (Fig. 6.7). The K-feldspar crystals shown in figure 6.8 also exhibit a white alteration rim where in contact with the aplitic material. The aplitic material is not necessarily cutting a single K-feldspar crystal in this case, but such a feature has been noted in several dikes (e.g. NMM-1N-27s).

Figure 6.5: Photograph of sample 265 showing aplite stringer cutting spodumene crystals. The field of view is about 4 cm across.

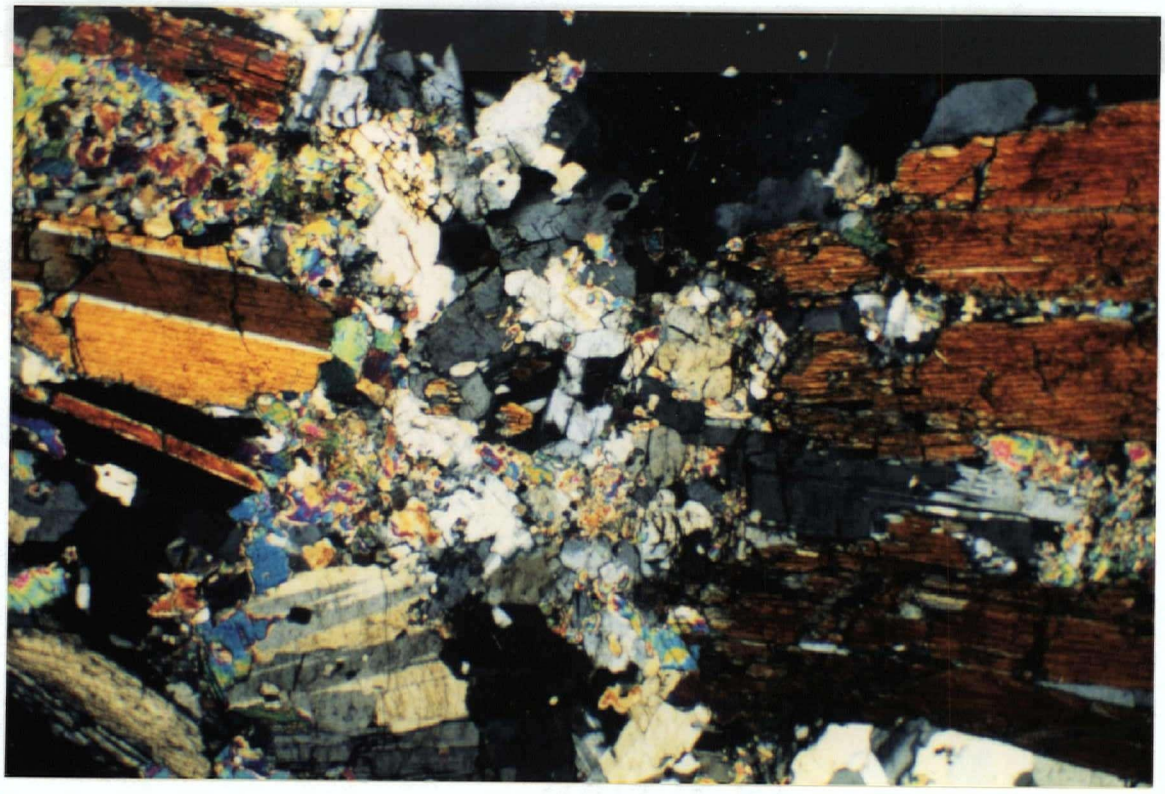

Figure 6.6: Photomicrograph of thin section of same feature as in figure 6.5. (Crossed polarized light; field of view = 5.1 mm across.)

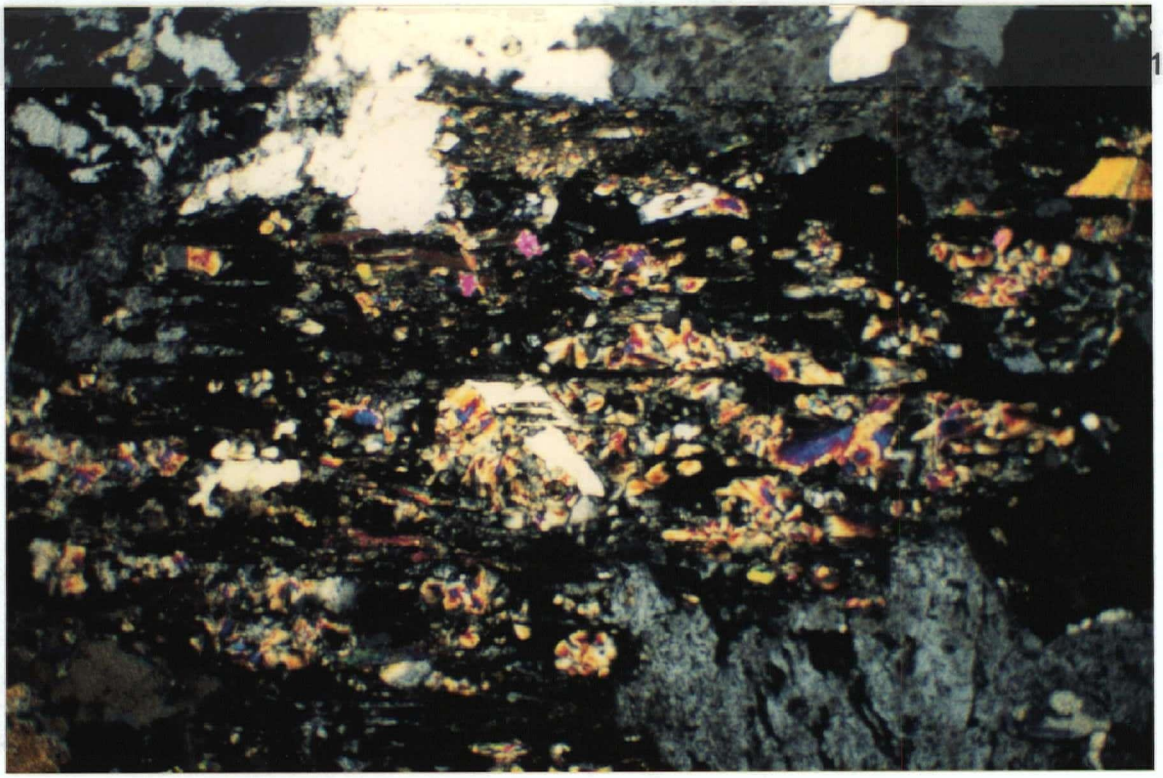

Figure 6.7: Photomicrograph of sample 201 showing a spodumene crystal that is completely altered to Lpd + Ab + Qz. (Crossed polarized light; field of view = 5.1 mm.)

Figure 6.8: Photograph of sample 123 showing aplite - blocky K-feldspar contacts. Note the white alteration rim around the K-feldspar. The scale is in cm.

6.5 Exocontacts

Exocontacts where dikes are hosted by pelitic schists are commonly enriched in biotite and very commonly contain tourmaline. Some exocontacts consist almost entirely of these minerals. Quartz is another major component of the exocontacts. Where the dike attitude is parallel to host rock bedding/foliation, dark exocontacts have a uniform width along the contact. Where the dike attitude is at an angle to that of the host rock, schorl and biotite have crystallized along the planes of weakness/ composition (e.g. Fig. 6.9) in the host rock (i.e. foliation, bedding) giving the exocontact an irregular appearance (Fig. 5.23). Allanite, monazite, zircon and titanite, associated with biotite and tourmaline were identified by SEM (EDS) in the exocontact within the pelitic schist near the contact in sample 246.

6.6 Host Rock

Three thin sections of the porphyroblastic biotite schist were examined. All have a predominant, strong foliation with respect to the biotite-quartz-muscovite matrix. This foliation has been overprinted by: 1) random biotite and chloritoid porphyroblasts, and 2), a subtle kinking. Staurolite prophyroblasts with curved inclusion trails and biotite inclusions similar to those in the matrix are present in sections 4 and 5 (Fig. 6.10). Section 3 contains cordierite porphyroblasts with biotite inclusions. Muscovite, chlorite and tourmaline are present around the edges of the cordierite. None of the sections show much evidence of retrogression.

Two metamorphic events are clearly evident. The first, represented by the predominant, strong, syntectonic foliation with syndeformational staurolite porphyroblasts implies a peak (mid-amphibolite) metamorphic temperature of 500 to 550 C. A second, post-tectonic event of 400+ C is evidenced the presence of the biotite and chloritoid porphyroblasts that cut the main foliation and the subtle kinking. The timing of the cordierite porphyroblasts is equivocal; biotite inclusions in the cordierite may be overgrowths or contemporaneous with the cordierite. The staurolite porphyroblasts are so skeletal that the included biotite could easily have formed within the staurolite during the second event (Dipple, personal communication).

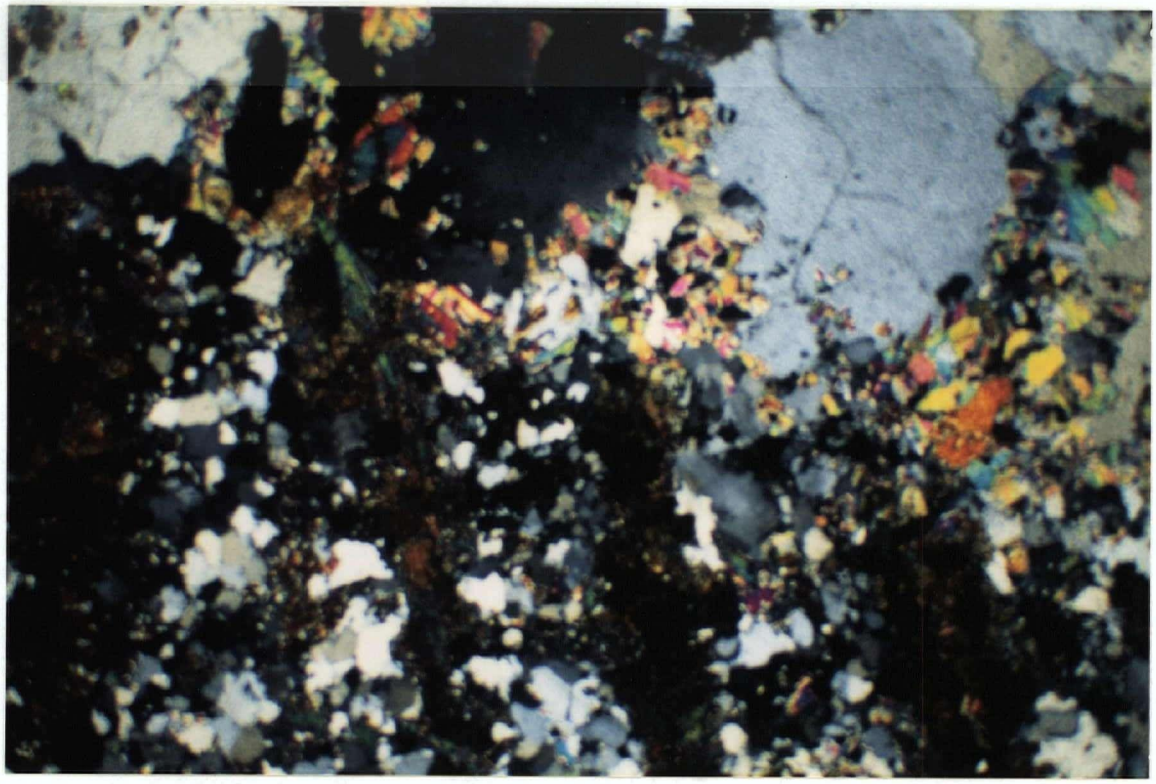

Figure 6.9: Photomicrograph of sample 198 showing pegmatite-host rock contact. The dark bands meeting the contact at an angle are tourmaline and biotite that have crystallized along compositional planes (e.g. mafic-bearing bedding) in the host rock. Note also the recrystallized quartz in the lighter coloured bands.

Figure 6.10: Photomicrograph of a staurolite porphyroblast in section 4. Note the curved inclusion trails in the staurolite and the biotite prohyroblasts cutting the major foliation.

7 GEOCHRONOLOGY

7.1 Samples

Columbites were separated from four samples (113, 167, 233, 227) Some of the grains showed visible color zoning, which appear to correlate with wide variations in Nb and Ta contents based on electron microprobe studies (see also chapter 5.2.1).

Two lepidolite (197 and 230) and one white muscovite were chosen for K-Ar dating. One lepidolite sample (197) chosen came from an unusual dike which consisted of fine-grained, massive lepidolite associated with large Mn- and Cs-rich beryls and very fine-grained, creamy white albite. The lepidolite in sample 230 was coarse-grained (4 to 8 mm) and more representative of lepidolite found throughout the pegmatite group. The white muscovite was also coarse-grained (2 to 4 mm) and came from the wall zone of the columbite-bearing dike.

7.2 Columbite Dates

U-Pb analyses of eleven fractions of columbite were completed, comprising three fractions from each of three samples and two fractions from a fourth sample (Table 7.1). The Pb isotopic composition of coexisting feldspar was also measured for each of the first three samples (Table 7.2), and used as an estimate for the initial common Pb composition for data reductions. Measured U-contents for the columbites range from 279 to 2972 ppm, with all but three of the fractions containing between 279 and 947 ppm U. Most of the fractions contain a significant proportion of common Pb (2.5 to 5.5%). Th/U ratios for each analysis, calculated using measured $^{208}Pb/^{204}Pb$ and $^{206}Pb/^{204}Pb$ ratios and an assumed age of 82 Ma, are very low (0.01). Seven of the fractions plot on or near concordia at about 82 Ma (Fig. 7.1). Two of the fractions (233-A and 233-C) give slightly younger $^{206}Pb/^{238}U$ ages. The remaining two fractions (227-B and 227-C) give highly anomalous Pb/U and Pb/Pb ages, and plot well outside of the field shown in figure 7.1.

SEM investigations of the columbite grains showed samples 227 and 233 to include several fine (mainly <1 μm in diameter) inclusions of uraninite. Sample 233 displayed strong zoning, and the uraninite inclusions were observed to occur only within Ta-rich zones. Such a correlation is less clear for sample 227, which also contained uraninite inclusions, but in which the Ta/Nb zoning is not as extreme. No inclusions of any kind were observed in samples 113 and 167, although sample 113 was strongly zoned. There appears to be a close correlation between fractions that display disturbed U-Pb isotopic systematics and the presence of uraninite inclusions. The two fractions analysed from sample 227 also gave the highest U-contents (1584 and 2972 ppm). The only other fraction whose measured U-content approached these levels was 113-C; however this sample apparently did not contain uraninite inclusions, and shows no obvious disturbance of the U-Pb system.

On $^{238}U/^{204}Pb$ *vs.* $^{206}Pb/^{204}Pb$ isochron diagrams in figures 7.2a to d (plotting parameters for isochrons are given in Table 7.4), isochron ages calculated for each of the samples incorporate the measured Pb isotopic composition of coexisting feldspar to estimate the initial $^{206}Pb/^{204}Pb$ ratio. The dates range from 82.2 to 81.6 Ma and an age calculated using the seven columbite analyses mentioned above, is 81.6 ± 0.5 (MSWD = 7.9), with a model initial ratio of 20.22. The Pb isotopic compositions of the feldspars (Table 7.2) are more radiogenic than predicted from the "shale curve" of Godwin and Sinclair (1982), which is an average crustal growth curve for mid-Proterozoic and younger sedimentary units in the miogeocline in northwestern North America. This corroborates the peraluminous or "S-type" character inferred from the mineralogy of the pegmatites, to suggest that they represent crustal melts.

7.3 Mica Dates

K-Ar analytical data and calculated ages are given in Table 7.3. The muscovite sample (235) gave an age of 65.4 ± 4.0 Ma and the two lepidolite samples (197 and 230) gave ages of 65.8 ± 3.4 Ma and 65.4 ± 3.6 Ma and are more than 15 Ma younger than the U-Pb dates for the columbite.

Table 7.1: U-Pb analytical data.

Sample Description	Wt .(mg)	U (ppm)	Pb^a (ppm)	$^{206}Pb/^{204}Pb$ (meas.)^b	total common Pb (pg)	% $^{208}Pb^b$	$^{206}Pb/^{238}U^c$ (± % 1σ)	$^{207}Pb/^{235}U^c$ (± % 1σ)	$^{207}Pb/^{206}Pb^c$ (± % 1σ)	$^{206}Pb/^{238}U$ age (± % 2σ)
						Sample 113				
B: med. red-brn	0.120	279	3.35	403	69	7.0	0.01291(0.14)	0.08508(0.26)	0.04778(0.17)	82.7(0.2)
C: pale red-brn	0.025	1383	16.1	2626	11	0.3	0.01292(1.22)	0.08487(1.32)	0.04765(0.42)	82.7(2.0)
D: pale red-brn	0.015	736	8.4	79.2	146	27.2	0.01284(0.18)	0.08389(1.75)	0.04739(1.60)	82.2(0.3)
						Sample 167				
A: med. red-brn	0.140	652	7.53	1305	56	2.30	0.01291(0.80)	0.08441(0.84)	0.04780(0.18)	82.0(1.3)
B: med. red-brn	0.059	695	7.97	651	51	4.05	0.01274(0.11)	0.08332(0.35)	0.04745(0.27)	81.6(0.2)
C: med. red-brn	0.021	665	7.58	473	24	2.11	0.01277(0.98)	0.08199(1.81)	0.04655(1.49)	81.8(1.6)
						Sample 233				
A: pale red-brn	0.116	478	5.34	858	50	3.13	0.01238(8.64)	0.08233(8.65)	0.04825(0.43)	79.3(13.6)
B: med. red-brn	0.043	658	7.33	309	77	6.91	0.01279(0.33)	0.07067(1.57)	0.04008(1.42)	81.9(0.5)
C: med. red-brn	0.021	947	10.0	724	20	0.66	0.01176(1.24)	0.08899(1.72)	0.05488(0.95)	75.4(1.9)
						Sample 227				
B: dark red-brn	0.286	2972	23.9	571	884	0.00	0.00920(0.31)	0.05514(0.54)	0.04349(0.35)	59.0(0.4)
C: dark red-brn	0.159	1584	29.6	6878	47	0.27	0.02070(16.5)	0.13742(16.5)	0.04816(0.05)	132.1(43.2)

a Radiogenic Pb; corrected for blank, initial common Pb, and spike
b Corrected for spike and fractionation.
c Corrected for blank Pb and U, and common Pb.

Table 7.2: Feldspar Pb isotopic compositions.

Sample	$^{206}Pb/^{204}Pb^{a}$	$^{207}Pb/^{204}Pb^{a}$	$^{208}Pb/^{204}Pb^{a}$
#113	19.678	15.802	39.925
#167	19.658	15.775	39.807
#233	19.751	15.785	39.864

[a]All errors on Pb/Pb ratios are < 0.03 % at a 1σ level.

Table 7.3: K-Ar analytical data.

Sample	Species	K (wt.%)	Rad ^{40}Ar cc/gm·10^{-6}	% Rad ^{40}Ar	Age ± 2σ
#230	lepidolite	8.50 ± 0.05	22.009	85.4	65.4 ± 3.6 Ma
#235	muscovite	7.96 ± 0.11	20.596	80.2	65.4 ± 4.0 Ma
#197	lepidolite	8.56 ± 0.09	22.298	91.7	65.8 ± 3.4 Ma

Table 7.4: U-Pb analytical data (isochron parameters).

Fraction	$^{238}U/^{204}Pb$ (± 1σ, %)	$^{206}Pb/^{204}Pb$ (± 1σ, %)	Correlation coefficient	Isochron age (± 2σ, Ma)	MSWD
		Sample 113			
columbite B	37970(1.29)	510.1(2.31)	0.33	82.2 (0.3)	0.3
columbite C	4186000(28.6)	54071(28.6)	1.00		
columbite D	5186(0.22)	86.2(0.24)	0.85		
feldspar	n.m.	19.68(0.03)			
		Sample 167			
columbite A	137280(0.99)	1778(0.62)	0.60	81.6 (0.5)	7.6
columbite B	70460(0.63)	917.0(0.65)	0.99		
columbite C	94180(5.67)	1222(5.62)	0.99		
feldspar	n.m.	19.66(0.03)			
		Sample 233			
columbite A	96590(1.50)	1215(1.5)	0.17	81.6(2.3)	19.3
columbite B	28125(1.30)	379.4(1.33)	0.97		
columbite C	227800(7.37)	2699(7.47)	0.99		
feldspar	n.m.	19.75(0.03)			

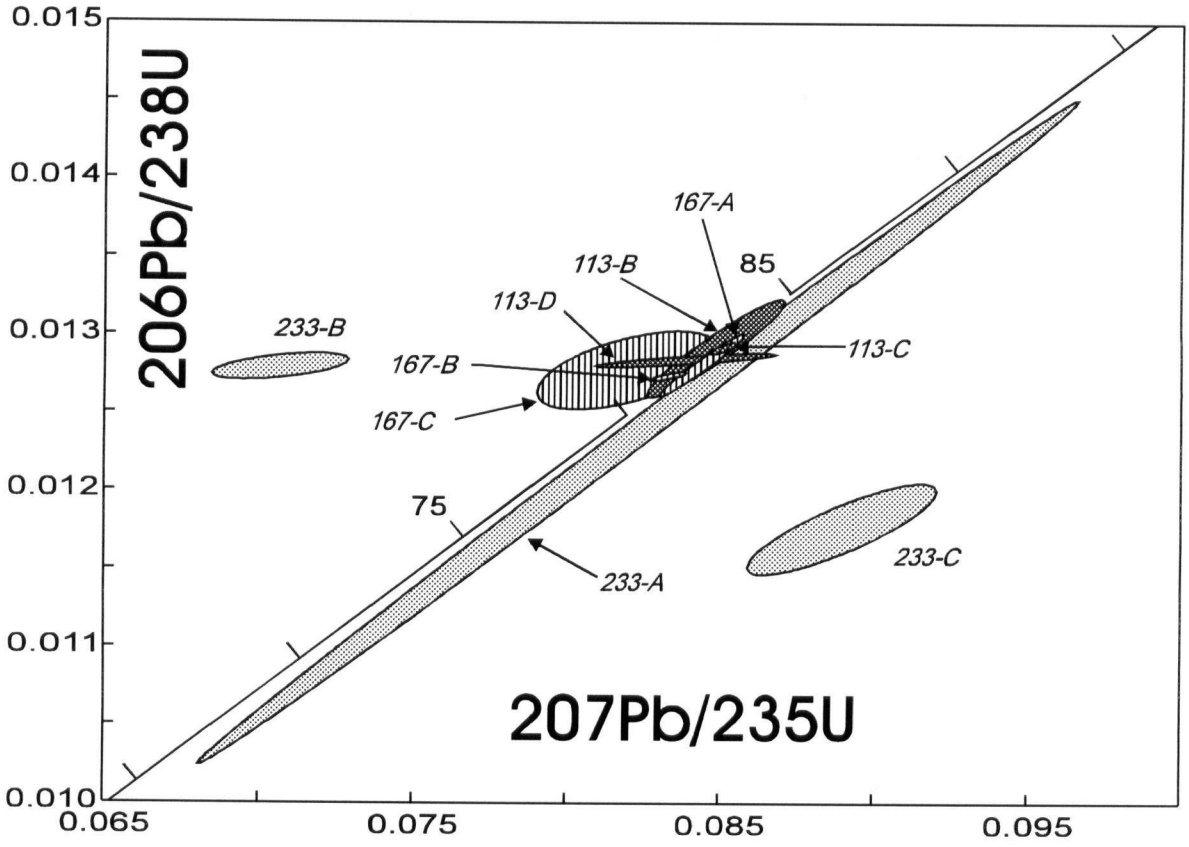

Figure 7.1: Concordia plot of U-Pb for columbite samples.

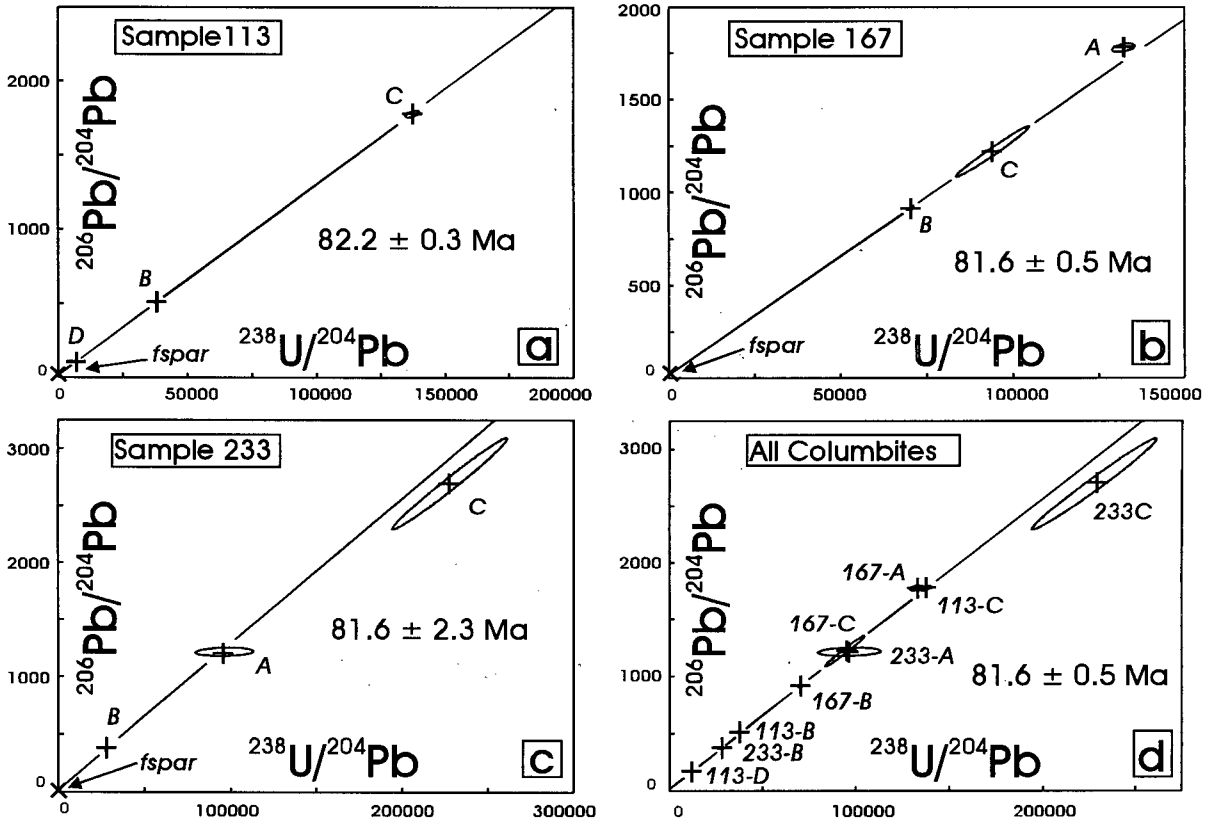

Figure 7.2: (a) to (c) U-Pb isochron diagrams for columbite samples.

8. DISCUSSION AND CONCLUSIONS

The Little Nahanni Pegmatite Group belongs to the LCT family of pegmatites as classified by Černý (1991a). The dikes have a peraluminous mineralogy and are strongly enriched in Li and F, moderately enriched in P, weakly enriched in B, Mn, Be, Ta and Nb, and contain trace levels of Rb and Cs.

The mineralogy, dike geometry and style of internal structure is typical of albite-spodumene pegmatites. Compared with other examples world-wide, the Little Nahanni Pegmatite Group may well be the best example of the type because of the relatively pristine (i.e. unmetamorphosed or otherwise tectonized) nature and excellent exposure of the group.

8.1 Internal Evolution

Two predominant models of pegmatite evolution exist. Jahns and Burnham (1969) proposed that pegmatite (and replacement) textures could be explained by a slowly cooling, low-viscosity, hydrous pegmatitic melt, crystallizing in a more-or-less closed system during which a supercritical aqueous fluid was produced. London (1987) offered a disequilibrium crystallization model involving the effects of volatile components such as Li, P, F and B on liquidus and solidus temperatures, and silicate melt-H_2O solubility. This model allowed the development of pegmatite textures at relatively low temperature and pressure conditions with relatively rapid crystallization. The latter model is invoked for the internal evolution of the dikes in the Little Nahanni Pegmatite Group. Indeed, many of the general processes involved in the evolution of the Tanco pegmatite, as described by London (1987, and references therein), would credibly account for features observed in the Little Nahanni Pegmatite Group.

Pegmatite fluid interaction with the host rock was minimal and the pegmatite dikes evolved, for the most part, as a closed system, with fractionation promoting the enrichment of Li, Na, B, P, and F in the melt. The trend with respect to Li content in rare-element pegmatites as stated by Černý (1989a) is apparent in this pegmatite group: wall zone muscovites are relatively poor in Li compared to intermediate zone/replacement unit lepidolites and cookeites, concentrations of

lithiophilite and associated Li-phosphates are more prevalent in the inner wall zone to outermost intermediate zone, and spodumene dominates the intermediate zone with respect to Li mineralogy. Late-stage albite- and lepidolite-rich units attest to the enrichment of Na and F respectively, in the melt

8.1.1 The roles of B, F, P

The effects of volatile elements such as B, F and P on granitic melts are well known (e.g. Chorlton and Martin, 1978; Pichavant, 1987; Manning, 1981; Dingwell, 1985; London, 1987, 1992b). The intent of this thesis is not to extensively review this body of literature (i.e. redo the work of much more competent and experienced workers) and the reader is referred to reviews such as Černý (1991a,b, 1992) or London (1987, 1990, 1992a, 1995).

Boron

The apparent absence of tourmaline in the Little Nahanni Pegmatite Group (or other rare-element pegmatites) does not necessarily mean that the pegmatite magma was barren of boron (London,1987; London *et al.*, 1994) The stability of tourmaline in pegmatite melts is partly inhibited by low Fe-Mg activities (Morgan and London, 1987a). The occurrence of tourmaline in the Little Nahanni Pegmatite Group is very similar to the tourmaline mineralization observed in other rare-element pegmatites (e.g. London, 1986) and to textures experimentally derived (London, 1987). This occurrence is consistent with an initial, and short-lived, exchange between newly emplaced pegmatite fluid and an Fe-Mg-bearing host rock, and a late-stage (post-vapour saturation) B metasomatism of the host rock (London, 1987). With the depletion of initially scavenged Fe and Mg, the capacity of tourmaline to buffer boron content is diminished and the melt becomes enriched with respect to B until vapour saturation is attained and boron leaves the system (Benard *et al.*,1985; London, 1987).

A boron-enriched pegmatitic melt for the Little Nahanni Pegmatite Group is also evidenced by the presence of rare schorl-elbaite in the intermediate zone and trace levels of B in spodumene, mica group minerals and albite (see Appendix C). Boron contents in minerals not

containing essential B are typically at low, trace levels (Oftedahl, 1964; Shearer and Papike, 1986) as B is preferentially partitioned into vapor relative to a melt (Pichavant, 1987). As well, the occurrence of the exocontacts is also indicative of a removal of B from the pegmatite melt into the host rocks. Even given a fluid gradient into the pegmatites, it does not make sense that all of the components required for tourmaline crystallization would move through the host rock toward the pegmatite, then crystallize out before reaching it. The exocontact is a "meeting place" of several components that would not have been together before: boron from the melt joined with Fe-Mg and others to produce schorl-dravite.

The tourmaline-rich exocontacts are not very extensive, suggesting that, given a boron enriched melt, the boron contents were still not very high. However, present within the pegmatite group are sporadic, grey (smoky) quartz veins containing abundant black tourmaline. These veins are undeformed, unlike many, whiter quartz veins in the field area which exhibit extensive, syntectonic deformation (boudinage, rotation and shearing). A model proposed by Mulja *et al.* (1995) suggests a pegmatite melt-derived hydrothermal fluid as the source for molybdenite-bearing quartz veins that are spatially related to the spodumene pegmatites in the country rocks around the Lacorne and Lamotte plutons. The quartz-tourmaline veins in the Little Nahanni Pegmatite Group have, unfortunately, not recieved as much attention in this study as they perhaps deserve. Boron isotopic and fluid inclusion comparisons between these veins and pegmatite quartz cores and tourmaline may reveal a relationship not yet known, which, if true, would suggest a much higher boron content for the pegmatite melt.

Fluorine and phosphorus

As with the initial formation of tourmaline (i.e. the removal of B, which would decrease H_2O-silica melt solubility), the early crystallization of apatite observed in the Little Nahanni pegmatites and other albite-spodumene pegmatites (*cf* Kessler, 1961; Sundelius, 1963; Göd, 1989) may similarly serve to further H_2O saturation in an H_2O undersaturated melt (London, 1987). F depresses the solubility of H_2O in granitic melts (Manning, 1981; Sorapure and Hamilton, 1984; Dingwell, 1985) and the presence of P increases H_2O solubility in granitic melts (Huffman *et al.*, 1986). The removal of F from the melt by apatite allows an increase in the solubility of H_2O, and the removal of P increases the saturation of H_2O in the melt. Crudely, the crystallization of apatite (assuming end-member fluorapatite) would require three times as much P as F, and using this logic, one could assume that the net effect would be that the melt becomes enriched in F with respect to P, thereby depressing the solubility of H_2O. This does not, however, take into account initial concentrations of the two elements. The reverse effect might in fact take place if the F budget is depleted first, even if at a third of the rate that P is. There is no data available at this time for the Little Nahanni pegmatite group to be able to discuss the extent to which these processes would balance one another out.

Late-stage fluids are F-rich as evidenced by the late-crystallization of lepidolite (*versus* the early crystallization of muscovite) and fluorapatite. Phosphorus contents of alkali feldspars consistent with the findings of Pan and Černý (1989) are also indicative of P-enriched melts The presence of montebrasite and relict spodumene in the late, albite-lepidolite quartz replacement unit seen in cirque 10^11 (sample 197) suggests that the activity of P may have increased to levels high enough to destabilize spodumene and allow montebrasite to crystallize (*cf* London and Burt, 1982c).

8.1.2 Mineral zonation

Several accessory minerals are zoned. In particular, the columbite group minerals, beryl, and garnet show the strongest zonation. Detailed examination or interpretation of the oxide minerals has not been a focus for this thesis. Such work will be the subject of a paper by Drs. T.S. Ercit and L. Groat and others, and is currently underway.

The Cs-rich rims in some beryl samples, particularly sample 197, indicates an enrichment in Cs in the melt. That most beryl is associated with late-stage assemblages (replacement units and late-stage fractures) suggests that Be was partioned in the melt phase until the final stages of crystallization. It may also be that late-stage fluids resorbed earlier crystallized beryl, however, there is no evidence of resorption in any of the beryl crystals found, including earlier, rock-forming beryl associated with quartz and K-feldspar.

Garnet crystals also show strong zonation, which is visible in hand specimen in some cases. Baldwin and von Knorring (1983) state that in lithium-rich pegmatites, pure spessartine garnet is typical of replacement and quartz core zones. The sudden change to a spessartine rim composition in sample 399 may then represent renewed growth during the replacement of the host pegmatite by Mn-enriched fluids. However, sample 225 shows a definite, steady increase in Mn in its outermost zone more likely caused by a gradual Mn-enrichment in the melt.

8.1.3 Spodumene crystallization

The spodumenes are interpreted to have grown at a high rate from the wall zone substrate into a low viscosity melt. Spodumene crystals dominantly occur at a high angle to wall rock contacts, but coexisting parallel-to-contact spodumene crystals also occur (Fig. 5.4.1). This feature has also been observed in other albite-spodumene pegmatites (e.g. the Volta Grande pegmatites, Heinrich, 1964). In the subhorizontal Volta Grande pegmatites, spodumene crystals appear to have grown perpendicularly from the hanging wall, but spodumenes of various orientations occur closer to the footwall. This would also suggest that the spodumenes grew into a fluid of low viscosity and when a crystal did break off, it would have settled towards

the bottom, or footwall. As most of the dikes in the Little Nahanni pegmatite group are sub-vertical to vertical, broken crystals would not necessarily settle to one side or the other and would more likely just settle downwards through the least viscous part of the dike. If the magma was still mobile at the time of the crystallization of the spodumene laths, it is possible that some may have aligned themselves, then settled in an orientation parallel to the flow direction of the magmatic fluid.

8.1.4 Late-stage/replacement units

Late stage/replacement aplitic units have been recognized in many pegmatite dikes (e.g. Černý, 1991a; London, 1992a). More importantly, the textures and relationships between the aplitic units and pegmatite zones, even individual crystals, observed in the Little Nahanni Pegmatite Group are similar to those reported from other albite-spodumene type pegmatites. For example, Sundelius (1963) describes fine-grained units that cut across individual perthite crystals in dikes from the Peg Claims in Maine and Göd (1986) describes a late-stage aplitic unit that occurs as irregular bodies and stringers that cut dike zonation.

Aplitic units in the Little Nahanni Pegmatite Group are commonly characterized by high Na content, alteration features and "invasive" replacement textures. The very common occurrence of phosphate and Nb-Ta minerals, and lepidolite in these units indicates elevated levels of P, Li, F, and Ta-Nb in the melt responsible for the aplitic bodies. For example, sample 197 is the product of extreme Na-P-F and concomitant Cs-Rb enrichment in the melt as evidenced by the presence of massive lepidolite (high Na, F), montebrasite and relict Spd, which suggest P activity levels high enough to cause the instability of Spd, and Cs-rich beryls. Columbite group minerals are also present in the albitic bands and pods. These units represent the latest stages of the magmatic evolution of the pegmatite dikes.

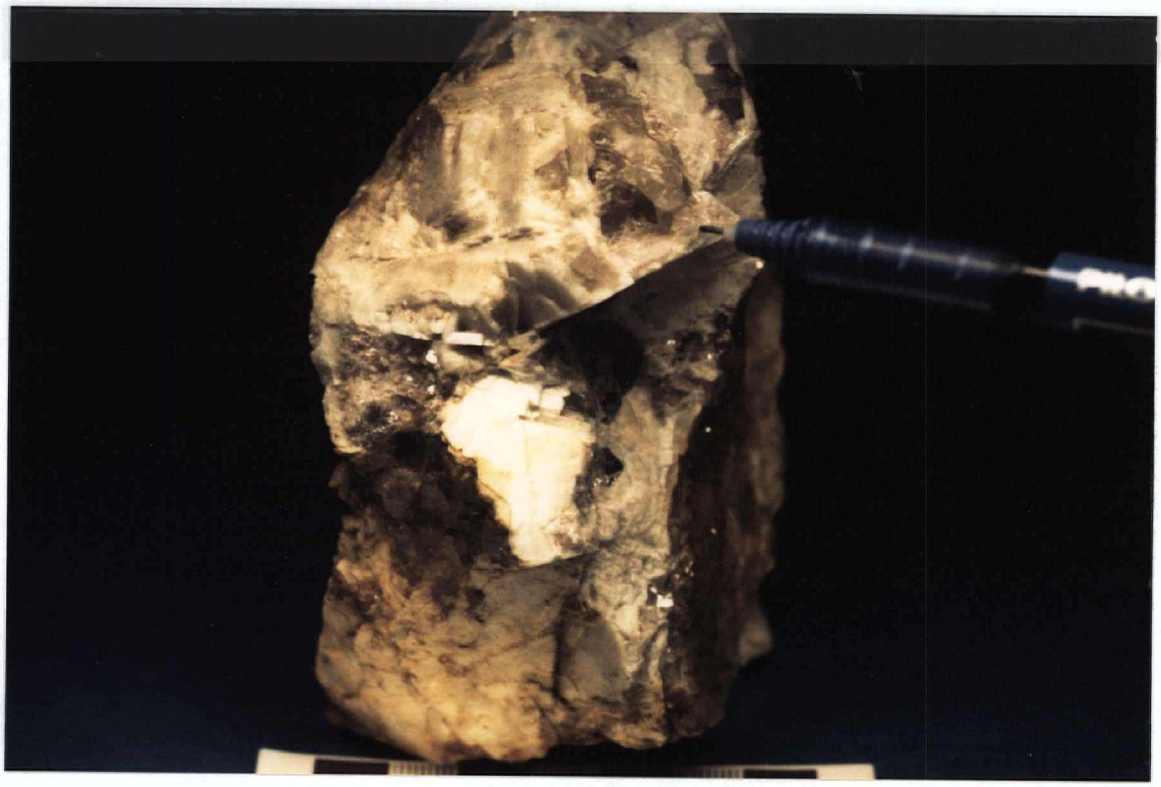

Figure 8.1 Coarse cleavelanditic albite from cirque 1N (sample 363). The pen is pointing to an open-space "vug" containing "popcorn"-like purple mica (lepidolite). Another such vug is visible to the left of the bright white cleavelandite blade in the centre.

Whether or not some of the massive cleavelandite units are primary or replacement is debatable. There is little doubt though, that these units represent very late crystallization in the evolution of those particular dikes. For example, sample 363, shown in figure 8.1, is an example of very coarse cleavelandite and quartz. The cleavelandite blades are randomly crystallized, giving the sample a "house of cards" appearance. Notable in the sample are the open spaces between some of these crystals. Some of these open-space "vugs" are partially filled with "popcorn"-like masses of lepidolite (light purple mica) indicating the presence of some vapour phase.

8.1.5 Rhythmic banding

Rhythmic banding remains one of the more enigmatic features in aplite and pegmatite dikes. As mentioned in chapter three, banding in the Little Nahanni pegmatites is not all of the same type, hence a single model is probably insufficient to explain these occurrences. Mechanisms for some of the banding types, for example, Type E banding, which involves alternating bands of aplitic and non-spodumene-bearing pegmatitic material, and type B banding, in which bands of spodumene exist in an otherwise homogeneous dike, remain unclear. These types of banding have the appearances of being "primary" in nature, in that they seem to be unaffected by late-stage or subsolidus reactions. That is not to completely rule out the possibility of an influence from such processes, but compared to "secondary" banding, those influences, if present, are not as clear.

"Secondary" banding, particularly type F, shows clear evidence of "invasive" emplacement of aplitic material into previously crystallized spodumene/blocky K-feldspar bearing pegmatite (see also chapters 3.3.2, 5.4, 6.4 and 8.1.4). This type of banding is not always "banding". Aplite and pegmatite components may alternate rhythmically as banding or are intimately and irregularly mixed. This texture has been observed in other spodumene-bearing pegmatites (e.g. Göd, 1989; Charoy et al, 1992). It is concluded that these textures are the result of late-stage, more-or-less *in situ* aplitic replacement at the expense of spodumene-bearing

pegmatite. The relatively regular spodumene-aplite bands seen in figure 3.16 are interpreted to result from the "invasion" and replacement by residual melt material (as opposed to multiple injection by new charges of magma) between previously crystallized, type B spodumene bands. Dike NMM-1N-9 is an excellent example (Figs. 3.16 to 18). Within a distance of five to six metres, the dike changes from an irregular mixture of pegmatitic and aplitic material, through an intermediate section in which spodumene crystals appear significantly altered and cut by aplitic material (Figs. 3.17 and 3.18), to a section that exhibits seemingly even banding. Where the late-stage fluids appear to have travelled within the dike, they have not travelled far (i.e. less than several metres). One notable difference between irregularly "banded" sections and those that are more evenly banded is the density of spodumene crystals. The migrating fluids may have taken the path of least resistance in the case of densely packed spodumene bands, that is, between the bands. In contrast, dikes with sparse or more elongate spodumene crystals are likely to have aplitic stringers irregularly transecting those crystals and the dike in general.

However, this still leaves many questions about the "primary" banding unanswered. How are the spodumene bands in type B banding formed? Type E banding, like type F banding, involves alternating pegmatitic and aplitic layers, but the pegmatite layers are spodumene-free and show more prominent directional growth; how are these explained?.

London (1992a) evaluates four mechanisms commonly used to account for layering in intrusive rocks: 1) cumulus processes, 2) pressure fluctuations, 3) nonequilibrium sequential crystallization caused by significant undercooling below the liquidus, and 4) flow segregation. Of these, London (1992a) dismisses cumulus processes as a viable option and the states that while any one of the remaining three may be invoked given a certain situation, they also do not present a general or viable account.

Rose (1981) described the multi-step emplacement of the Brabant pegmatite (Namibia). Multiple injection emplacement of some of the Little Nahanni Pegmatite Group dikes has been

previously suggested (Ahlborn, 1977b). However, none of the evidence Rose (1981) cites has been observed or determined for this locality.

The detailed description of "segregation banding" by Matrosov (1978) very closely resembles some of the banding, particularly type E banding (Fig. 3.15), that occurs in the Little Nahanni Pegmatite Group. According to Matrosov (1978), "segregation banding" is most commonly observed in lepidolite-albite pegmatites and less commonly in spodumene-albite dikes and is formed "by the internal energy resources of the developing pegmatite", (i.e. in a closed system). Matrosov (1978) invoked pressure fluctuations in a closed system as a primary mechanism in the formation of this style of banding. London (1992a, and references therein) cites experimental work done by other investigators that invalidates pressure fluctuations as a mechanism for layering in aplites. However, the pressure fluctuations suggested by Matrosov (1978) are related to the cooling shrinkage of the relatively thin dikes, as opposed to the vapour loss by overpressure process that London (1992a) discussed. Shrinkage due to cooling has been previously discussed in this thesis to explain the presence of cross-cutting fractures and quartz veins.

8.2 Regional Variation and Emplacement History

Regional zonation is important in determining the fractionation histories of pegmatite populations. Various zones, characterized by specific suites of rare-element minerals, occur at relative distances from the source granitoid. The closest (commonly internal) to the source granitoid are generally barren. At further distances from the granite, barren pegmatites are followed by Be, Be-Nb-Ta, Li-Be-Ta-Nb, and finally, Li-Cs-Be-Ta-Nb bearing pegmatites (Černý, 1991). There are only subtle trends that suggest any unidirectional fractionation across the Little Nahanni Pegmatite Group.

8.2.1 Regional variation

Lepidolite and beryl samples from the southernmost part of the field area (cirques 10 and 11) were found to be the richest in Cs. The type of occurrence of these minerals in this area is also unique in the group. Dike LSE-10^11 contained large masses (metre scale) of botryoidal ("ball peen") lepidolite, and the Cs-beryl occurs in a unusual, fine-grained, saccharoidal albite and lepidolite-quartz matrix. Figure 8.2 shows the decrease in lepidolite K/Rb values (averaged for each sample) toward the south end of the group (cirque 11). The lepidolite K/Cs values show a similar decrease (Fig. 8.3). It must be noted, however, that this trend is based on the results of five samples analyzed, which may not be statistically valid. Nonetheless, this trend is consistent with the presence of a buried source granite near the north end of the pegmatite group, based on the increased size and abundance of andalusite toward the north (i.e. the most fractionated dikes being the furthest from the source granite).

Columbite group minerals from cirque 2 show a distinct enrichment in Fe with respect to Mn, and a concomitant enrichment in Ta with respect to Nb. As mentioned earlier, this trend is inconsistent with most trends described by Černý *et al.* (1985). Exsolved tantalian rutile, possible wodginite group minerals and U-oxides also occur associated with in this cirque. A north-south distribution plot of Ta/Ta+Nb (Fig.8.4) shows no trends. However, there is an enrichment of Mn with respect to Fe from north to south as can be seen in figure 8.5.

A plot of K-feldspar K/Rb values exhibits disappointingly wide scatter (Fig.8.6). A subtle increase in K/Rb may be interpreted from the main bulk of data points, which is contrary to the southward increasing fractionation indicated by lepidolite K/Rb and K/Cs data and by columbite Mn enrichment.

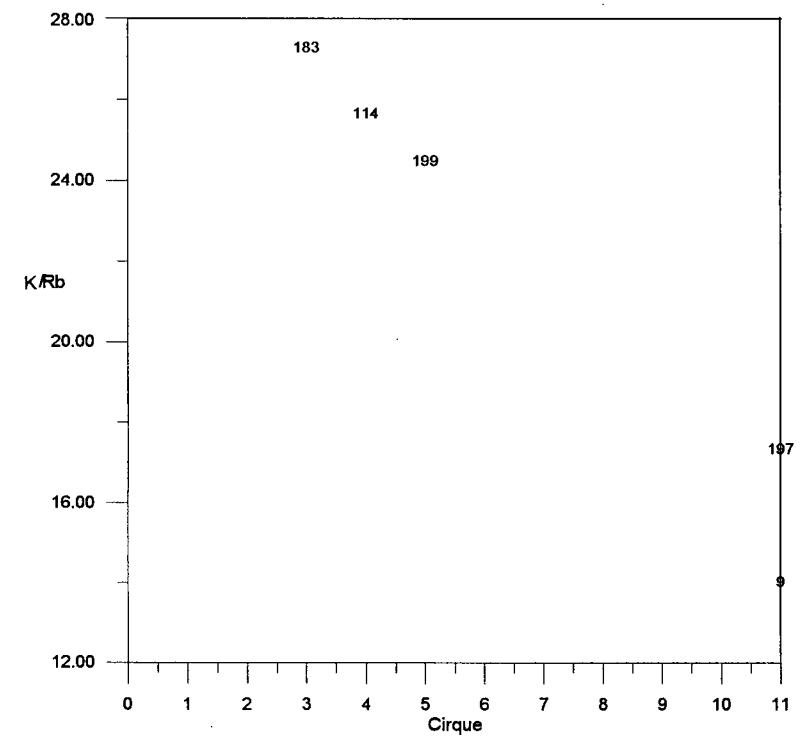

Figure 8.2: Lepidolite K/Rb plot (using apfu).

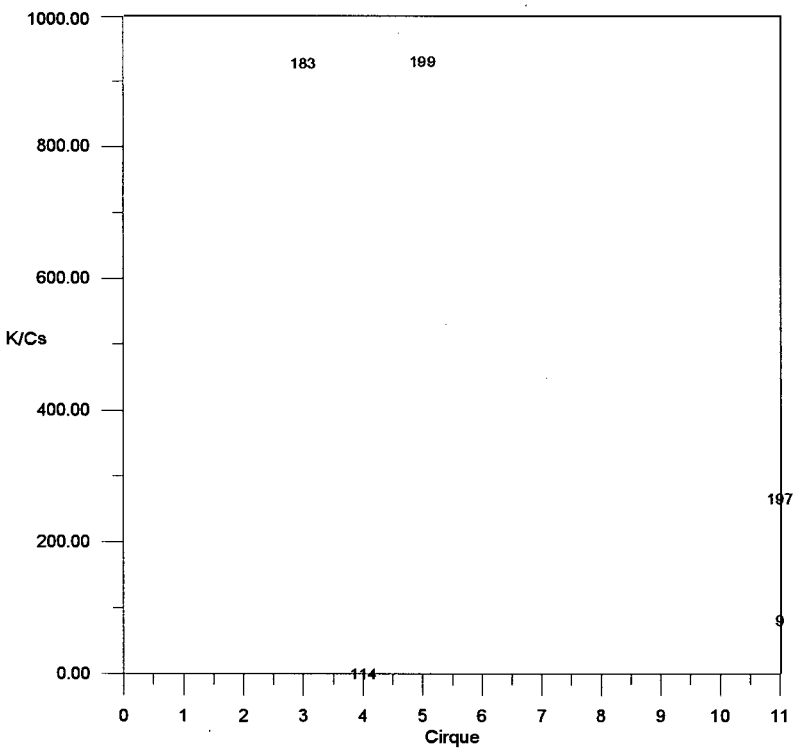

Figure 8.3: Lepidolite K/Cs plot (using apfu). Sample 114 contained no Cs and was arbitrarily given a value of "0" to plot it.

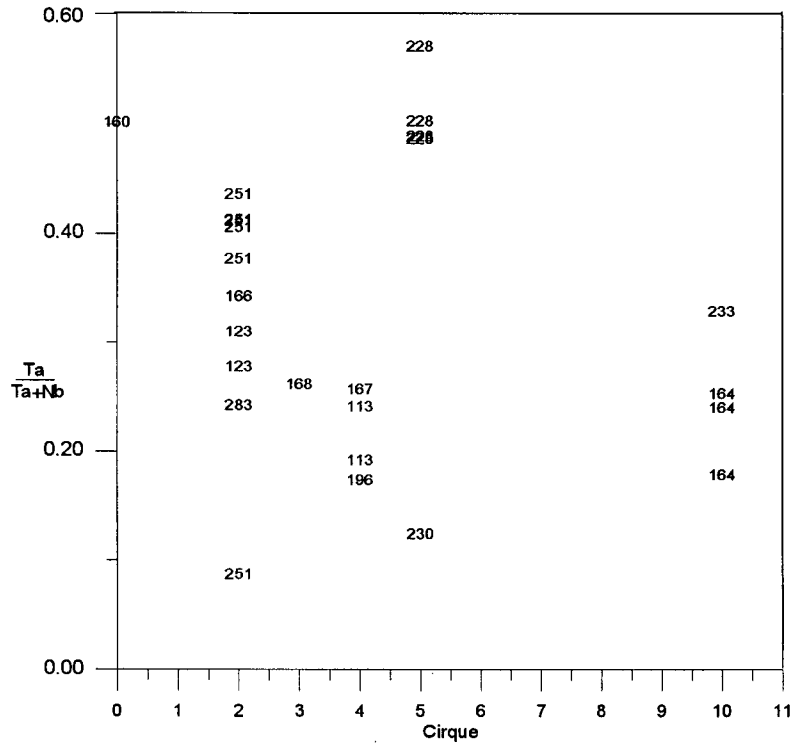

Figure 8.4: Plot of columbite Ta/Nb ratios (using apfu) along cirques.

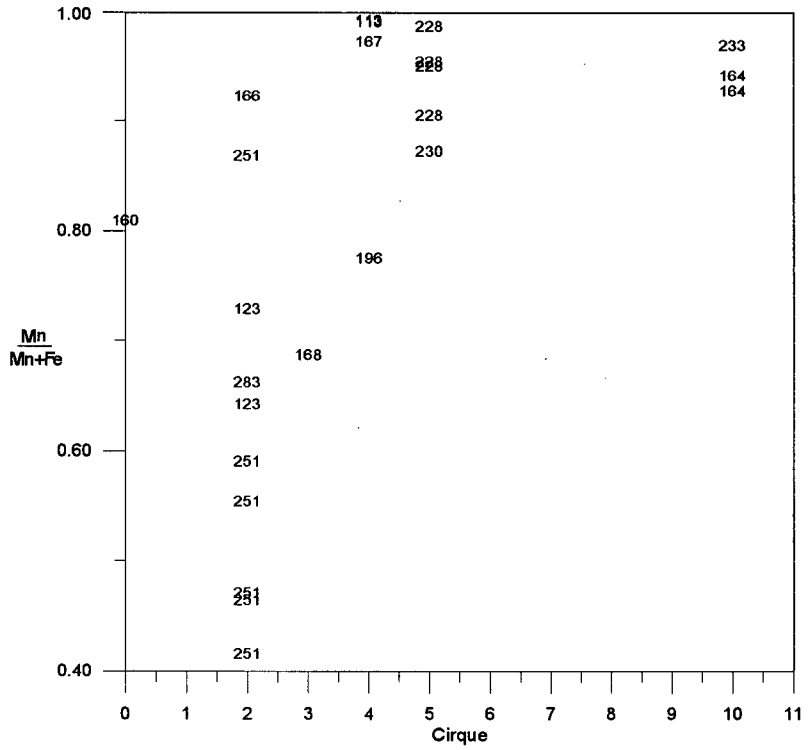

Figure 8.5: Plot of columbite Mn/Fe ratios (using apfu) along cirques.

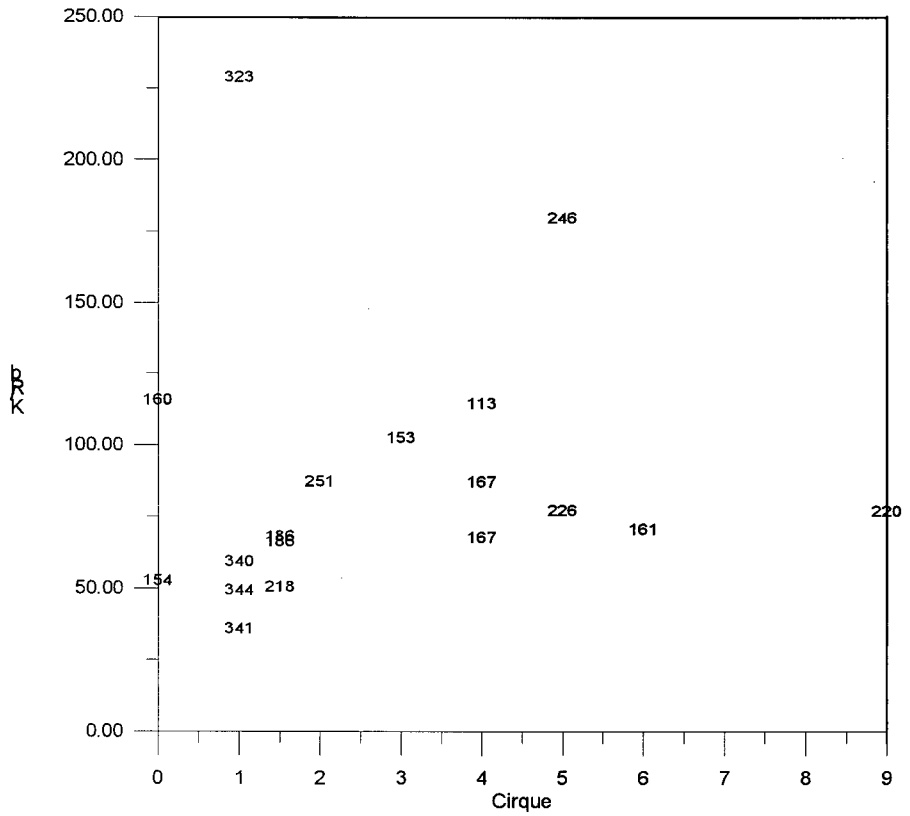

Figure 8.6: K-feldspar K/Rb versus cirque number plot. Ridges between cirque have been given an "X.5" designation (e.g. 1^2 = 1.5). Sample numbers are used as data points.

8.2.2 Pressure and temperature of emplacement

Lithium-aluminosilicate phase relations are useful in determining preliminary petrogenetic constraints for pegmatites (London, 1984). The fact that (1) primary petalite, (2) spodumene-quartz intergrowths, pseudomorphous after petalite, and (3) eucryptite have not been observed in the Little Nahanni Pegmatite Group suggests that the dikes were emplaced at a pressure and temperature higher than the Spd + Qtz ⇔ petalite stability curve, between 380 at 2 kb and 660 at 4 kb.

Structural states determined for alkali feldspars in the Little Nahanni Pegmatite Group are consistent with a relatively low temperature event. The high albite-low albite inversion is arbitrarily taken to be a first-order transformation occurring at 680 C for Ab_{100} (Ribbe, 1983 and references therein). All albite samples analyzed are near end-member, almost fully ordered, low albite indicating that the melt had cooled well below the high albite-low albite inversion temperature by the time albite began to crystallize.

Ribbe (1983) states that intermediate microcline has no stability field of its own because, like high albite-low albite, the sanidine-microcline inversion is also arbitrarily taken to be a first-order transformation. He adds that "orthoclase" is regarded as a structure that is kinetically stranded during that inversion. Figure S-1 in Smith (1974) shows the orthoclase ("low sanidine")-microcline boundary approximately between 460 to 510 C for Or_{90} and Or_{100}, respectively. Figure 8a in Ribbe's (1983) chapter gives a dashed line at about 350 C which represents "stranded structures", although "orthoclase" is not specifically mentioned. The Little Nahanni samples plotted between the orthoclase and maximum microcline lines on the 2Θ 060 *versus* 2Θ 204 plot (Fig. 5.1.4). This, combined with compositional data (Or_{90} to Or_{98}), suggests a crystallization temperature at or slightly higher than the range given for the inversion by Smith (1974).

As Smith (1974) points out, the alkali feldspar order transformation is not unique and is dependent on the temperature-time history of the particular feldspar. However, order transformations are also sluggish and a range of 475 to 525 C, given a relatively rapid

cooling history for the pegmatites, probably estimates the emplacement temperature reasonably acurately. Correspondingly, emplacement pressure may have ranged from 3.0 to 3.5 kb.

8.2.3 Post emplacement deformation and cross-cutting relationships

The Little Nahanni Pegmatite Group appears to be remarkably unaltered in terms of metamorphic or tectonic overprinting. However, the three features mentioned in chapter three suggest some degree of post-emplacement deformation. Perhaps the most significant of these is the NMM-1N-18s fault, which is traceable for approximately thirty metres along strike. The fault gouge zone is generally less than thirty centimetres thick and not more than one metre thick, and shows no discernible lateral displacement. Alteration within the dike, away from the gouge seems minimal; unaffected vugs of feldspar and stilbite were observed less than ten centimetres from slickensided surfaces in the gouge zone. However, the host rocks are pervasively iron-oxide stained up to two metres away from the fault zone for the length of the fault. In contrast, the displacement seen in dike NMM-1N-9 does not show any of the features that the NMM-1N-18s fault does and can probably be attributed to late Holocene erosional processes (i.e. mass movement).

Cross-cutting relationships are seen at two scales: 1) between two dikes, and 2) within the dikes. The only clearly cross-cutting dikes (1) are those in cirque 10 (LMM-10-6 and -7). However, these dikes originate from the same dike near the top of the cirque (Fig. 3.24). In fact, dikes LMM-10-1 to LMM-10-14 are all related to the same dike mass, which, closer to the main mass near the top of the cirque, splits and rejoins commonly. Dikes LMM-10-6 and -7 are therefore not likely to represent multiple-event intrusions.

Internal cross-cutting features (2) include: calcite-filled and open fractures, monomineralic quartz veins and late-stage aplitic units (irregular bodies, bands and stringers). These features do not extend into the host rocks and are interpreted to be the result of emplacement processes, such as cooling shrinkage.

8.3 Petrogenesis

Geochemical trends, the general peraluminous mineralogy and the Pb isotopic compositions of feldspars in the pegmatites suggest that the granitic magmas from which these pegmatites evolved are entirely crustally-derived (S-type), consistent with their derivation from small volumes of initial partial melt material formed during regional metamorphism. Low to nonexistent Cl and S, low to high F, and moderate to high B and P (London, 1992c) as well as the peraluminous composition (White and Chappell, 1987) also typify S-type (supracrustal) felsic magmas.

Garnet Fe/Mn ratios (1.4 to 0.1) are lower than the range given by Černý *et al.* (1985) for primitive pegmatites (6.1 to 1.8) but higher than the extreme value of 0.01 he gives for "highly fractionated" pegmatites. Low mica and K-feldspar K/Rb values are indicative of moderate to high levels of fractionation as are columbite Mn/Mn+Fe and Ta/Ta+Nb ratios (Černý *et al.*, 1985).

No granites that could be interpreted to be parental to the Little Nahanni Pegmatite Group were observed in the field area. Plutons belonging to the Selwyn Plutonic Suite are ruled out as candidates based on the fact that the youngest dates for these plutons (Gordey & Anderson, 1993) are more than 13 million years older than the columbite U-Pb ages determined for the pegmatite group. However, according to Gordey and Anderson (1993), the first appearance of andalusite (and commonly, biotite) in the pelitic host rocks occurs within 500 metres of the intrusive contact. Andalusite porphyroblasts in the host rocks of the Little Nahanni Pegmatite Group, particularly in the northern end of the field area, suggest the the presence of a pluton at depth.

8.4 Geochronology and Regional Implications

Both the U-Pb and K-Ar ages obtained in this study are surprisingly young compared with K-Ar and Rb-Sr geochronology for the region's granitic rocks. The young U-Pb columbite ages represent either emplacement ages of the pegmatites; prolonged cooling ages following emplacement; or thermally reset ages. The timing of pegmatite emplacement is interpreted to be late syn-tectonic, and the pegmatites intrude wall rocks that have experienced metamorphic temperatures in excess of 500°C. It is considered highly unlikely, however, that pegmatite samples from three widely separated (up to 3.5 km apart) localities would yield identical regional, post-metamorphic cooling ages. The relatively high closure temperature inferred for the U-Pb system in columbite by Romer and Wright (1992) also argues against the U-Pb ages being cooling ages. The similarity among U-Pb columbite ages and high discordancy with the K-Ar mica ages rules out partial resetting related to the thermal event recorded in the K-Ar mica ages. The U-Pb ages must therefore represent either an older, high-temperature thermal event that completely reset the U-Pb columbite systems, or the actual emplacement ages of the pegmatite bodies. The U-Pb columbite ages are 8 to 13 Ma younger than most isotopic ages obtained thus far for other granitic intrusions in this region (Gordey and Anderson, 1993); however the pegmatites are also mineralogically distinct from any of the other plutonic rocks. In the absence of any evidence for an ~82 Ma thermal event in this region, the U-Pb columbite ages are therefore interpreted to date the emplacement of the pegmatites. This indicates that the pegmatites represent a magmatic event that has not previously been recognized in this region. A metamorphic event of this age has also not been recognized in this area, although the Mackenzie fold-and-thrust belt was possibly still active at this time (Gordey and Anderson, 1993).

The K-Ar mica ages are interpreted as the time at which the pegmatite bodies last passed through the blocking temperature of the K-Ar system in muscovite and lepidolite (~350°C). The Late Cretaceous-Paleocene K-Ar mica ages for the pegmatites probably reflects a thermal overprint related to a relatively young intrusive event. No plutons of this age have been

recognized thus far in the immediate study area; however, two small plutons about 100 km southeast of the study area, yielded K-Ar ages for biotite between 60 to 69 Ma (D.A. Archibald, unpublished data). Late-Cretaceous-Paleocene U-Pb dates on zircon and monazite and K-Ar ages for biotite were obtained from plutons of the McQuesten plutonic suite in the McQuesten River area in west-central Yukon (Murphy and Héon, 1994; Murphy et al., 1995). Late Cretaceous-Paleocene plutons of the McQuesten area, thermal overprinting in this study area and coeval plutons southeast of the study area form a distinct belt within the overall arc of the Mackenzie fold-and-thrust belt.

The results of this study suggest that U-Pb columbite dating is a valuable geochronological technique for relatively young rocks that lack conventionally datable accessory phases such as zircon, titanite or monazite. Samples with very high U-contents (>1000 ppm) tend to yield anomalous and non-reproducible ages, as do samples that contain uraninite inclusions. This finding differs from that of Romer and Wright (1992) and Romer and Smeds (1994a), who concluded that the most reliable ages were obtained from the uraninite inclusions contained within the columbite, and that the columbite itself generally yielded disturbed isotopic systematics. These conclusions were based on studies of much older (Early Proterozoic) samples, and it is possible that over such a long period of time the columbite structure may have accumulated sufficient radiation damage to render it more susceptible to isotopic disturbance. The columbite fractions analysed here show high optical clarity; thus it is unlikely that significant metamictization has affected the grains. The main criteria suggested for selection of columbite for U-Pb dating of young samples are the transparency of the grains and the absence of inclusions (especially uraninite). Examination of the grains by SEM is recommended, prior to analysis, because the uraninite grains are commonly too small to be detected visually. There also appears to be a correlation between high-Ta grains (or portions of grains), high U-contents, and the presence of uraninite inclusions; we therefore recommend avoiding the more Ta-rich endmembers of the columbite-group minerals.

8.5 Further Work

1) A more detailed zonational study with respect to the feldspars. Thin section analysis of Little Nahanni Pegmatite Group samples showed the presence of tartan twinning, typical of microcline, in wallzone K-feldspar. This suggests some zonal variation exists and perhaps warrants further exploration to determine the nature of this variation more accurately. Studies should include XRD analyses using Gandolfi or Debye-Scherrer camera methods to reduce the effects produced by perthitic contamination. Gathering enough grains to produce a slide mounted powder for analysis is impractical for finer grained feldspars as albite and K-feldspar are commonly indistinguishable and are easily mixed together.

2) Detailed study on the Great Wall dike. It extends from cirque 10 to cirque 2, and incorporates the dikes which have been mapped as NMM-10-15&16&17, the GWC proper (cirques 8-9), LMM-5-8, NMM-3-4s, and the western dikes on the Cali (1^2) ridge. This may be seen on stereo-paired airphotos.

3) A more thorough study of apatite may bring to light more information regarding the behaviour of F, P and H_2O during the internal evolution of the pegmatite dikes. Many crystals are visibly zoned as are bands of apatite at the edge of calcite-filled fractures, near the wallrock contact.

4) Boron isotopic and fluid inclusion studies of the tourmaline-bearing quartz veins and pegmatite tourmaline and quartz cores may reveal a petrogenetic relationship between the quartz veins and pegmatite dikes.

5) Evaluation in this thesis of the models to explain the presence of rhythmic banding in the Little Nahanni Pegmatite Group has been preliminary at best. Further investigation of the "segregation banding" and "nonequilibrium sequential crystallization" models to explain some of the type F banding is warranted. As well, very detailed sampling, petrography and chemical analysis along several dikes to gain a better understanding of the interaction of late-stage fluids and previously crystallized pegmatite would be useful. Whole rock analysis of the finer-

grained zones and units may help in identifying variations between, for instance, aplitic wall zone and late-stage replacement aplitic material.

6) Further geochronoligical studies may answer more conclusively the questions regarding the two dates determined in this study.

8.6 Conclusion

This thesis is the first as part of a larger research project that represents the first attempt to conduct original investigations into pegmatites of the Canadian Cordillera on a regional scale. In general terms, the primary objective of this thesis is to provide a broad, preliminary study of a significant Cordilleran pegmatite group: to further the characterization of the particular "type" to which the group belongs, and to place the group in its regional geological context. This objective has been met. Numerous opportunities for further study have also been revealed and it is hoped that future workers will pick up where this work rests.

9. REFERENCES

Ahlborn, V.H. (1977a): Assessment report for CALI claims, Erex Int. Ltd.

Ahlborn, V.H. (1977b): Preliminary geological survey of the CALI 1-9 claims. Canadian Superior Exploration Ltd.

Aldrich, L.T., Davis, G.L., Tilton, G.R. and Wetherill, G.W. (1956): Radioactive ages of minerals from the Brown Derby Mine and the Quartz Creek Granite near Gunnison, Colorado. *Journal of Geophysical Research*, v. 61, pp. 215-232.

Appleman, D.E. and Evans, H.T.Jr. (1973): Job 9214: Indexing and least-squares refinement of powder diffraction data. *U.S. Geol. Surv. Comput. Contrib.* 20 (NTIS Doc. PB2-16188).

Aurisicchio, C., Fioravanti, G., Grubessi, O. and Zanazzi, P.F. (1988): Reappraisal of the crystal chemistry of beryl. *American Mineralogist*, v. 73, pp. 826-837.

Bakakin, V.V. and Belov, N.V. (1962): Crystal chemistry of beryl. *Geochemistry*, #5, pp. 484-500.

Baldwin, J.R. and von Knorring, O. (1983): Compositional range of Mn-garnet in zoned granitic pegmatites. *Canadian Mineralogist*, v. 21, pp. 683-688.

Bakakin, V.V., Rylov, G.M. and Belov, N.V. (1969): Crystal structure of a lithium-bearing beryl. *Doklady Acad. Sci. USSR*, v.188, pp. 659-662.

Bambauer, H.U., Corlett, M., Eberhard, E. and Viswanathan, K. (1967): Diagrams for the determination of plagioclases using X-ray powder methods. *Schweizer Mineralogische und Petrogische Mitteilungen*, v. 47, pp. 333-349.

Beavon, R.V. (1977): Preliminary geological survey of the CALI 1-9, 11 mineral claims, Cantung area, District of Nahanni, NWT. Canadian Superior Exploration Ltd.

Benard, F., Moutou, P. and Pichavant, M. (1985): Phase relationships of tourmaline leucogranites and the significance of tourmaline in silicic magmas. *Journal of Geology*, v. 93, pp. 271-291.

Beus, A.A. (1960): *Geochemistry of Beryllium and Genetic Types of Beryllium Deposits*. Publishing House Academy of Science, Moscow.

Cameron, E.N., Jahns, R.H., McNair, A.H. and Page, L.R. (1949): Internal Structure of Granitic Pegmatites. *Economic Geology* Monograph 2.

Černý, P. (1972): Secondary minerals from the spodumene-rich zones. *Canadian Mineralogist*, v. 11, pp. 714-726.

Černý, P. (1975): Alkali Variations in Pegmatitic Beryl and their Petrogenetic Implications. *Neues Jahrbuch fuer Mineralogie - Abhandlungen*, v. 123, pp. 198-212.

Černý, P. (1989a): Characteristics of Pegmatite Deposits of Tantalum. In *Lanthanides, Tantalum and Niobium* (Moeller, P., Černý, P. and Saupe, F., eds.), Springer-Verlag.

Černý, P. (1991a). Rare Element Granitic Pegmatites. Part I: Anatomy and Internal Evolution of Pegmatite Deposits. *Geoscience Canada*, v. 18, # 2, pp. 49-67.

Černý, P. (1991b). Rare Element Granitic Pegmatites. Part II: Regional to global environments and petrogenesis. *Geoscience Canada*, v. 18, # 2, pp. 68-81.

Černý, Petr (1992): Geochemical and petrogenetic features of mineralization in rare-element granitic pegmatites in the light of current research. *Applied Geochemistry*, v. 7, pp. 393-416.

Černý, P. and Turnock, A.C. (1975): Beryl from the granitic pegmatites at Greer Lake, southeastern Manitoba. *Canadian Mineralogist*, v. 13, pp. 55-61.

Černý, P., Smith, J.V., Mason, R.A. and Delaney, J.S. (1984): Geochemistry and petrology of feldspar crystallization in the Vezna pegmatite, Czechoslovakia. *Canadian Mineralogist*, v. 22, pp. 631-651.

Černý, P., Meintzer, R.E. and Anderson, A.J. (1985): Extreme fractionation in rare-element granitic pegmatites: selected examples of data and mechanisms. *Canadian Mineralogist*, v. 23, pp. 381-421.

Charoy, Bernard, Francois, Lhote and Dusausoy, Yves (1992): The crystal chemistry of spodumene in some granitic aplite-pegmatite of northern Portugal. *Canadian Mineralogist*, v. 30, pp. 639-651.

Chackowsky, L.E. (1987): Mineralogy, geochemistry and petrology of pegmatitic granites and pegmatites at Red Sucker Lake and Gods Lake, northeastern Manitoba. Unpublished MSc thesis, University of Manitoba, 157 p.

Chorlton, L.B. and Martin, R.F. (1978): The effect of boron on the granite solidus. *Canadian Mineralogist*, v. 16, pp. 239-244.

Claffy, E.M. (1953): Composition, tenebrescence and luminescence of spodumene minerals. *American Mineralogist*, v.38, pp. 919-931.

Clarke, D.B. (1981): The mineralogy of peraluminous granites: a review. *Canadian Mineralogist*, v. 19, pp. 3-18.

Corlett, M. and Ribbe, P.H. (1967): Electron probe microanalysis of minor elements in plagioclase feldspars. *Schweizer Mineralogische und Petrographische Mitteilungen*, v. 47, pp. 317-332.

Deer, W.A., Howie, R.A. and Zussmann, J. (1966): *An Introduction to the Rock Forming Minerals*, Longman Group Ltd. London, 528 p.

Dingwell, D.B. (1985): The structure and properties of fluorine-rich silicate melts: implications for granite petrogenesis. In *Granite-Related Mineral Deposits* (R.P Taylor & D.F. Strong, eds.). Canadian Institute of Mining and Metallurgy, Extended Abstracts, pp. 72-81.

Feklichev, V.G. (1963): Chemical composition of minerals of the beryl group, character of isomorphism, and position of principle isomorphous elements in the crystal structure. Geochemistry, v. 4, pp. 410-421.

Feklichev, V.G. (1964): Beryl, morphology, composition, and structure of crystals [in Russian]. *Nauka Moscow*.

Foord, E.E. (1976): Mineralogy and petrogenesis of layered pegmatite aplite dikes in the Mesa Grande District, San Diego County, California. Ph.D. thesis, Stanford University, Stanford, California.

Göd, R. (1989): The spodumene deposit at "Weinebene", Koralpe, Austria. *Mineralia Deposita*, v. 24, pp. 270-278.

Godwin, C.I. and Sinclair, A.J. (1982): Average lead isotope growth curves for shale-hosted zinc-lead deposits, Canadian Cordillera. *Economic Geology*, v. 77, pp. 675-690.

Gordey, S.P. and Anderson, R.G. (1993): Evolution of the Northern Cordilleran Miogeocline, Nahanni Map Area (105I), Yukon and Northwest Territories. Geological Survey of Canada *Memoir* 428.

Grice, J.D. and Ercit, T.S. (1993): Ordering of Fe and Mg in the tourmaline crystal structure: The correct formula. *Neues Jahrbuch Mineralogische Abhandlungen*, v. 165, #3, pp. 245-266.

Groat, L.A., Ercit, T.S., Raudsepp, M. and Mauthner, M.H.F. (1994): Geology and Mineralogy of the Little Nahanni Pegmatite Group, NWT. *EGS 1994-14*, NWT Geology Division DIAND, Yellowknife.

Hawthorne, F.C. and Cerny, P. (1977): The alkali-metal positions in Cs-Li beryl. *Canadian Mineralogist*, v. 15, pp. 414-421.

Heinrich, E.Wm. (1964): Tin-Tantalum-Lithium Pegmatites of the Sao Joao del Rei District, Minas Gerais, Brazil. *Economic Geology*, v. 59, pp. 982-1002.

Huffman, M., Navrotsky, A. and Pintchovski, F.S. (1986): Thermochemistry and structure of low pressure chemically vapor deposited and bulk SiO2-P2O5 and SiO2-GeO2 glasses. *Journal of the Electrochemical Society*, v. 133, pp.431-439.

Jahns, R.H. and Burnham, C.W. (1969): Experimental studies of pegmatite genesis. I. A model for the derivation and crystallization of granitic pegmatites. *Economic Geology*, v.64, pp. 843-864.

Jahns, R.H. and Wright, L.A. (1951): Gem and lithium-bearing pegmatites of the Pala District, San Diego County, California. Div. of Mines, State of California Dept. of Natural Resources, *Special Report*, 7-A.

Kesler, T. (1961): Exploration of the Kings Mountain Pegmatites. *Mining Engineering*, v. 13. pp. 1062-1068.

Kroll, H. and Ribbe, P.H. (1983): Lattice parameters, composition, and Al/Si order in alkali feldspars. In *Feldspar Mineralogy* (P.H. Ribbe, ed.). Mineralogical Society of America Short Course Notes v. 2, 2nd edition, pp. 101-120.

Leake, B.E. (1967): Zoned garnets from the Galway granite and its aplites. *Earth and Planetary Sciences Letters*, v.3, pp. 311-316.

London, D. (1982): Stability of spodumene in acidic and saline fluorine-rich environments. *Carnegie Institution Geophysical Laboratory Annual Report*, v. 81, pp. 331-334.

London, D. (1984): Experimental phase equilibria in the system LiAlSiO4-SiO2-H2O: a petrogenetic grid for lithium-rich pegmatites. *American Mineralogist*, v.69, pp. 995-1004.

London, D. (1986): Magmatic-hydrothermal transition in the Tanco rare-element pegmatite: Evidence from fluid inclusions and phase-equilibrium experiments. *American Mineralogist*, v. 71. pp. 376-395.

London, D. (1987): Internal differentiation of rare-element pegmatites: Efects of boron, phosphorus and fluorine. *Geochimica et Cosmochimica Acta*, v. 51, pp. 403-420.

London, D. (1990): Internal differentiation of rare-element pegmatites; A synthesis of recent research. Geological Society of America *Special Paper* 246, pp. 35-50.

London, D. (1992a): The application of experimental petrology to the genesis and crystallization of granitic pegmatites. *Canadian Mineralogist*, v. 30, pp. 499-540.

London, D. (1992b): Phosphorus in S-type magmas: The P2O5 content of feldspars from peraluminous granites, pegmatites, and rhyolites. American Mineralogist, v. 77, pp. 126-145.

London, David (1992c): Volatile Characteristics of S-Type Felsic Magmas. *Eos*, v. 73, #14 (special supplement), p. 366.

London, D. (1995): Geochemical features of peraluminous granites, pegmatites, and rhyolites as sources of lithophile metal deposits. In *Magmas, Fluids, and Ore Deposits* (Thompson, J.F.H.ed), Mineralogical Association of Canada Short Course.

London, D. and Burt, D.M. (1982a): Lithium aluminosilicate occurrences in pegmatites and the lithium aluminosilicate phase diagram. *American Mineralogist*, v. 67. pp. 483-493.

London, D. and Burt, D.M. (1982b): Alteration of spodumene, montebrasite and lithiophilite in pegmatites of the White Picacho District, Arizona. *American Mineralogist*, v. 67. pp. 97-113.

London, D. and Burt, D.M. (1982c): Chemical models for lithium aluminosilicate stabilities in pegmatites and granites. *American Mineralogist*, v. 67. pp. 494-509.

London, D., Černý, P., Loomis, J.L. and Pan, J.J. (1990): Phosphorus in alkali feldspars of rare-element granitic pegmatites. *Canadian Mineralogist*, v. 28, pp. 771-786.

London, D., Loomis, J.L., Huang, W. and Morgan, G.B. VI (1990): Behaviour and effects of phosphorus in the system Ab-Or-Qz-H2O at 200 MPa (H2O). *Geological Society of America Abstracts with Programs*, v. 22, p. A302.

London, D., Wolf, M.B. and Morgan, G.B. IV (1994): Boron Saturation in Granitic Magmas: Tourmaline-Biotite-Cordierite Equilibria. Geological Society of America, *Abstracts with Programs*, 1994 Annual Meeting.

Manning, D.A.C. (1981): The effect of fluorine on liquidus phase relationships in the system Qz-Ab-Or with excess water at 1 kb. *Contributions to Mineralogy and Petrology*, v. 76, pp. 206-215.

Matrosov, I.I. (1978): The banded structures of the rare-metal pegmatites. *International Geology Review*, v. 20, pp. 177-186.

Meagher, E.P. (1980): Silicate garnets. In *Orthosilicates* (P.H. Ribbe, ed.) Mineralogical Society of America, Reviews in Mineralogy, v.5, pp. 25-66.

Meintzer, R.E. (1987): The mineralogy and geochemistry of the granitoid rocks and related pegmatites of the Yellowknife pegmatite field, Northwest Territories. PhD thesis, University of Manitoba, Winnipeg.

Morgan, G.B. VI, and London, D. (1987a): Behaviour of Boron and Tourmaline Stability in Granitic Systems. Geological Society of America *Program with Abstracts*, v. 19, p. 777-778.

Mulja, T., Williams-Jones, A.E., Wood, S.A. and Boily, M. (1995): The rare-element-enriched monzogranite - pegmatite - quartz vein systems in the Preissac-Lacorne batholith, Quebec. II. Geochemistry and petrogenesis. *Canadian Mineralogist*, v. 33, pp. 817-833.

Mulligan, R. (1965): Geology of Canadian Lithium Deposits. Geological Survey of Canada, *Economic Geology Series* #21.

Murphy, D.C., and Héon, D. (1994): Geological overview of Sprague Creek map area, western Selwyn Basin. In *Yukon Exploration and Geology 1993*, Exploration and Geological Services Division, Department of Indian Affairs and Northern Development, pp. 29-46.

Murphy, D.C., Mortensen, J.K., and Bevier, M.L. 1995. U-Pb and K-Ar geochronology of Cretaceous and Tertiary intrusions, western Selwyn Basin, and implications for the structural and metallogenic evolution of central Yukon. In Geological Association of Canada, *Program with Abstracts*, 20, A-74.

Oftedal, Ivar (1964): On the Occurrence and Distribution of Boron in Pegmatite. *Norsk Geologisk Tidsskrift*, v.44, #2, pp. 217-225.

Orville, P.M. (1967): Unit-cell parameters of the microcline-low albite and the sanidine-high albite solid solution series. *American Mineralogist*, v. 52, pp. 55-86.

Pan, J.C. and Černý, P. (1989): Phosphorus in feldspars of rare-element granitic pegmatites. GAC/MAC Annual Meeting *Program with Abstracts*, v. 14, p. A82.

Parrish, R.P. Bellerive, D. and Sullivan, R.W. (1992): U-Pb chemical procedures for titanite and allanite in the Geochronology Laboratory, Geological Survey of Canada. In *Radiogenic Age and Isotopic Studies: Report 1*; Geological Survey of Canada, Paper

Pichavant, M. (1987): Effects of B and H2O on liquidus phase relations in the haplogranite system at 1 kbar. *American Mineralogist*, v. 72, pp. 1056-1070.

Rankama, K. and Sahama, Th.G. (1949): *Geochemistry*. University of Chicago Press, Chicago, 912 p.

Ribbe, P.H. (1983): Aluminum-silicon order in feldspars; domain textures and diffraction patterns. In *Feldspar Mineralogy*, (P.H. Ribbe, ed.) Mineralogical Society of America, Reviews in Mineralogy, v. 2, 2nd edition, pp. 21-55.

Roddick, J.C. (1987): Generalized numerical error analysis with applications to geochronology and thermodynamics. *Geochimica et Cosmochimica Acta*, v. 51, pp. 2129-2135.

Romer, R. L. and Wright, J. E. (1992) U-Pb dating of columbites: A geochronologic tool to date magmatism and ore deposits. *Geochimica et Cosmochimica Acta*, v. 56, pp. 2137-2142.

Romer, R.L. and Smeds, S-A. (1994a): Columbite - A tool for U-Pb dating of Ta-Nb-Sn mineralization. in *Metallogeny of Collisional Orogens* (Seltmann, Kämpf and Möller, eds). Czech Geological Survey, Prague, pp. 399-404.

Romer, R.L. and Smeds, S-A. (1994b): Implications of U-Pb ages of columbite-tantalites from granitic pegmatites for the Paleoproterozoic accretion of 1.90-1.85 Ga magmatic arcs to the Baltic shield. *Precambrian Research*, v. 67, pp.141-158.

Rose, Dieter. (1981) Multi-step emplacement of a pegmatite vein - Brabant pegmatite, Namibia. *Neues Jahrbuch der Mineralogie.* Monatsheft, #8, pp. 355-373.

Rowe, Robert B. (1953): Pegmatitic Beryllium and Lithium Deposits, Preissac-Lacorne Region, Abitibi County, Quebec. Geological Survey of Canada *Paper* 53-3.

Shearer, C.K. and Papike, J.J. (1986): Distribution of boron in the Tip Top pegmatite, Black Hills, South Dakota. *Geology*, v. 14, pp. 119-123.

Sherriff, B.L., Grundy, H.D., Hartman, J.S., Hawthorne, F.C. and Černý, P. (1991): The incorporation of alkalis in beryl: Multi-nuclear MAS NMR and crystal structure study. *Canadian Mineralogist*, v. 29, pp. 271-285.

Sinkankas, J. (1981): *Emerald and Other Beryls*, Chilton Book Company, Radnor, PA.

Smith, J.V. (1974): *Feldspar Minerals*. I. Crystal Structure and Physical Properties. II. Chemical and Textural Properties. Springer Verlag, Heidelberg, 627 and 690 pp.

Solodov, N.A. (1962): Internal structure and geochemistry of rare-element granitic pegmatites. *Academy of Sciences of the USSR*, Moscow, 243 p.

Solodov, N.A. (1971): Scientific principles of perspective evaluation of rare-element pegmatites. *Nauka Moscow*, 292 p.

Sorapure, R. and Hamilton, D.L. (1984): The solubility of water in melts of albite composition with varying additions of fluorine. In *Progress in Experimental Petrology* (C.M.B. Henderson, ed.). Nat. Env. Res. Council Publ. Ser. D25, pp. 28-30.

Stewart, D.B. (1975): Lattice parameters, composition, and Al/Si order in alkali feldspars. In *Feldspar Mineralogy* (P.H. Ribbe, ed.). Mineralogical Society of America Short Course Notes v. 2, pp. St1-St22.

Stewart, D.B. and Wright, T.L. (1974): Al/Si order and symmetry of natural alkali feldspars, and the relationship of strained cell parameters to bulk composition. *Bull. Soc. franc. Minéral. Cristallogr.* v. 97, pp. 356-377.

Sundelius, H. W. (1963): The Peg Claims Spodumene Pegmatites, Maine. *Economic Geology*, v. 58, pp. 84-106.

Thomssen, R.W. and Anthony, J.W. (1977): Lithiophilite crystals from the Foote Mine. *Mineralogical Record*, v. 8, # 2, pp. 95-97.

Todt, W., Cliff, R., Hanser, A. and Hofman, A.W. (1984): 202Pb+205Pb double spike for lead isotopic analyses. *Terra Cognita*, v. 4, p. 209.

White, A.J.R. and Chappell, B.W. (1987): Some supracrustal (S-type) granites of the Lachlan Fold Belt. In *The Origin of Granites*. Trans. Royal Society of Edinburgh (Earth Sciences), 79 (2,3)

Wood, D.L. and Nassau, K. (1968): The characterization of beryl and emerald by visible and infrared absorption spectroscopy. *American Mineralogist*, v. 53, pp. 777-800.

Woodworth, G.J., Anderson, R.G. and Armstrong, R.L. Plutonic Regimes. In *Geology of the Cordilleran orogen in Canada* (H.Gabrielse and C.J.Yorath, eds). Geological Survey of Canada, Ottawa, pp. 491-531.

Wright, T.L. (1968): X-ray and optical study of alkali feldspar: II. An X-ray method for determining the composition and structural state from measurement of 2theta values for three reflections. *American Mineralogist*, v. 53, pp.88-104.

Wright, T.L. and Stewart, D.B. (1968): X-ray and optical study of alkali feldspar: I. Determination of composition and structural state from refined unit-cell parameters and 2V. *American Mineralogist*, v. 53, pp.38-87.

APPENDIX A

Hand-sample localities and descriptions. Note: not all samples collected and catalogued are listed here, only those samples referred to, or used, in this thesis are.

Abreviations used:

Ab	albite	Ap	apatite
Cass	cassiterite	Cc	calcite
Fsp	feldspar	Kfs	K-feldspar
Lit	lithiophilite	Lpd	lepidolite
M-col	manganocolumbite	Ms	muscovite
Qtz	quartz	Tur	tourmaline
Spd	spodumene		
HR	host rock	BZ	border zone
WZ	wall zone	OWZ	outer wall zone
IWZ	inner wall zone	INTZ	intermediate zone

Appendix A: Sample list.

Cat#	Species	Locality	Talus	Comments	Hand Specimen Petrology
9	Lepidolite	LSE-10^11-1	no		- coarse-grained (to cm across) books of Lpd in dominantly Qtz + minor Ab matirx
13	Lithiophilite	CC-1^2	yes	- no other sample (originally "CC-5")	
84	Garnet	LMM-5-lobe	no	- no other sample; at pegmatite/wall rock contact	
85	Beryl	LBW-7	yes		- "aquamarine" blue, acicular aggregate in "vug"+Ap, Ab, Qtz, and minor Ms; fluoresces bluish white
85	Cassiterite	LBW-7	yes	- in Ab+Qtz+Ms	- coarse cleavelandite + Qtz mixed with aplitic (Ab+Qtz+Ms); adjacent to vug
88	Beryl	LMM-5-8	no	- faint zoning; vial + 4 pieces	
91	Apatite	LMM-5	yes	- deep purple, in vug near contact	
92	Spodumene	LMM-10	yes	- pink	
93	Manganocolumbite	LMM-10	yes	- hosted by aplitic material	matrix = Ab 40%, Ms 40%, Qtz 20% ± other
98	Apatite	LMM-8-2	no	- deep purple; in vug near contact	
108	Chabazite	LMM-10	no		- off-white to colourless rhobohedral crystals in Cc-filled fracture; assoc. w/ Ap
113	Cross-section	LMM-4-1	no	- unbanded; unaltered	- dike is about 15 cm wide; concent. zoned; no WZ - BZ: 2-7 mm; Qtz (80%) - INTZ: Kfs(30%) + Qtz(25%) + Spd(25%) + Ab(20%)
113	Spodumene	LMM-4-1	no	- Spd perpendicular to contact	INTZ: Sp.25%, Qtz 25%, Kfs 50%; WZ: Ms, Fsp, minor Qtz; tourmaline exocontact
113	K-feldspar	LMM-4-1	no	- off-white, platy (looks like cleavelandite)	
113	Manganocolumbite	LMM-4-1	no	- dark reddish-brown-black	
114	Lepidolite	LMM-4-1	no	- fine-grained, irregular masses	- in Qtz+ Fsp
114	Garnet	LMM-4-1	no	- irregular pod of dull reddish-brown, very euhedral xls with altered appearance (Mn oxides); immediately associated with aplitic material & Ms, but grey blotchy Kfs & Sp also present: Spds appear more altered near garnets	matrix: Sp(20%) + Qtz(30%) + Fsp(50%)

Appendix A: Sample list.

Cat#	Species	Locality	Talus	Comments	Hand Specimen Petrology
115	Cassiterite	C-8	yes	- in coarse (cm-sized Ab+Qtz+Ms); alteration of Spd eveident	
118	Spodumene	C-3	yes	- end of 3?; glassy, slightly pink, variously oriented; pink alteration along cleavages	30% Spd, Qtz 25%, blocky Kfs 45%
119	Cassiterite	LSE-2-8	no	(A) in very coarse Qtz	(A) very coarse, almost massive Qtz (90%) + Mica (5%) + Cass (5%) (B) as above w/ salt&pepper aplitic material (Qtz+Fsp+Ms+Lit) as well
120	Tourmaline	LRG-7	no	- north half; with rich muscovite near contact with schist, but within pegmatite	Tur 40%, matrix 60%; matrix = 50% Ms, 30% Fsp, 20% Qtz
121	Spodumene	LRG-10	no	- centre of dike	
122	Garnet	C-2	yes	- zoned w/ some zones weathered out (mica layers??); rim of xls partially resorbed (diffuse contact between garnet and aplitic host); near clear, colourless apatite	
122	illite	C-2	yes	- dark purple; no cleavage	
122	Sphalerite	C-2	yes	- limonite-coated; best sphalerite; in cleavelandite assoc. w/ part. albitized (white-grey patchy) blocky Kfs	
122	Cassiterite	C-2	yes	- in partially albitized, blocky Kfs	
123	K-feldspar	LSE-2-5	no		-large, blocky Kfs + Sp in aplitic matrix
123	Spodumene	LSE-2-5	no	- like #159	-large, blocky Kfs + Sp in aplitic matrix
123	Beryl	LSE-2-5	no	- mildy fluorescent; in vial	
123	Lithiophilite	LSE-2-5	no	- vein	
123	Manganocolumbite	LSE-2-5	no	- 1-3 mm xl	- in (dirty, altered appearing) Ab+Qz matrix
123	Cassiterite	LSE-2-5	no		
132	Contact	LMR-5W	yes	- interesting cross-section; vug; unknowns; comes from top of cirque, on west side of range, just across from cirque 5	

Appendix A: Sample list (continued).

Cat#	Species	Locality	Talus	Comments	Hand Specimen Petrology
132	Cross-section	LMR	no	interesting cross-section; vug; unknowns	- dike is 12 cm wide; shows concentric zoning - BZ: 1 mm; Qtz (99%) + ?(1%) - WZ: 1 cm; Qtz (50%) + Ms (30%) + Ab (20%) - INTZ: 10 cm; Kfs (90%) + Qtz (10%); many fractures & stringers of cookeite(?); 2 cm, euhedral Qtz xls growth in almost from contact - CORE: Qtz (100%); in contact with euhedral Kfs
135	Andalusite	LLG-¯1-2	no	- fluoresces pale yellow	
137	Spodumene	LMR-4	yes	- anhedral (partially replaced); cut by aplite	Lpd 25%, Ab 35%, Qtz 20%, Spd 20%
140	Schist	LLG-¯1-2	no	- porphyroblasts fluoresce same pale yellow as andalusite in sample 135	
146	Spodumene	LRG-3-13	no	- centre of dike	
150	Kaolinite	LMM-0-3	no	- red, opaque kaolinite pseudomorphing after Spd; same as red UNK in #357	
150	Lepidolite	LMM-0-3	no	- purple	- coarse-grained; assoc. w/ Ab+Qtz+alt'd Spd
150	Spodumene	LMM-0-3	no	- pink, glassy Spd partially replaced by redder, opaque koalinite? (no cleavage)	- clevelanditic Ab(3-5 mm) 50%; Lep (3-5 mm) 15%; Spd + alt'n prod 15%; Qtz 20%
151	Spodumene	LMM-0^1-1	no	- pink, glassy; seem partially resorbed by aplitic material	
153	K-feldspar	LSE-3-1	no	(C)- fresh surface = coarse (large cleavage planes), anhedral, "dirty", blotchy beige-buff grey mottled appearance; weathered surface = appears whiter w/ needles (plates?) of clevelandite w/in white Kfs (albitization?); has CASS dotted over weathered (ie albite-containing) surface; aplitic (Qz+mica+Fsp) stringers between & thru large blocky Kfs	
153	Albite	LSE-3-1	no	(A) clevelanditic albite adjacent to crosscutting fracture (containing Ab+Ap+Ms); minor red/purple fluorescence (C) albitized Kfs	(A) Wall Zone = 55% Ab, 20% Qtz, 20% Ms: INTZ = 60% Ab, 30% Qtz, 10% alt Sp + UNK + zeolites (B) INTZ (altered) = 30% Ab, 30% Qtz, 30% Sp, 10% cavities (zeolites, cassitierite) (C) see "K-feldspar"

Appendix A: Sample list (continued).

Cat#	Species	Locality	Talus	Comments	Hand Specimen Petrology
154	K-feldspar	LSE-0-1	no	- large blocky xls (> 10cm) mottled, buff-grey, "dirty" appearance; white on weathered surface (xl marked (A) shows this well); outer rim of (A) fluoresces white; contains black oxide lined fractures (Mn-oxides?)	
156	Apatite	LMM-7^8	yes	- green & purple in Ab+Qtz+Ms	Ab(55%) + Qtz(35%) + Ms(10%)
159	Spodumene	LBW	yes	- fluoresces orange-pink; with large, blocky Kfs phenos in aplitic matrix	20 % Kfs phenos, 15% Spd, 35% Ab, 30% Qtz; Ab/Qtz = aplitic, salt & pepper
159	K-feldspar	LBW	yes	- fluoresces bluish-white; blocky Kfs	large blocky Kfs (20%) in matrix of aplitic material (65%: Ab 50%, Qtz 30%, speckled w/ oxides?) + Spd (15%); band of Spd + aplite -> Kfs crosscuts this
159	Cassiterite	LBW	yes	- in aplitic material	large blocky Kfs (20%) in matrix of aplitic material (65%: Ab 50%, Qtz 30%, speckled w/ oxides?) + Spd (15%); band of Spd + aplite -> Kfs crosscuts this
160	Albite	LMM-0-4	no	- clevelanditic; saccharoidal w/ major Cass (B)	
160	Apatite	LMM-0-4	no	- yellow fluorescent apatite band in Ab; light green core to darker green rim	- cm-sized apatite in milky Ab w/ minor Ms
160	Manganocolumbite	LMM-0-4	no	- 1-3 mm xls	- cleavelanditic Ab
160	Garnet	LMM-0-4	no	(E) orange-brown, gemmy, sub- to euhedral xls	- at contact w/ SST host; thin BZ (4 mm) of white, cleavelanditic Ab + Qtz; WZ same as BZ except coarser & + Ms
160	K-feldspar	LMM-0-4	no	(D) - dirty, white, blocky; fluoresces white	
160	Cassiterite	LMM-0-4	no		(A) - in saccharoidal Lep + Ab + Qtz; Spd is altered (replacement texture); (B) in saccharoidal Ab; C) as bands in massive Qtz
161	Spodumene	LSE-2-7	no	- pale pink, splintery Spd partially altered to pinkish, opaque, earthy stuff??; next to 5-7 cm blocky, white Kfs	
161	K-feldspar	LSE-2-7	no	- white-grey mottled, blocky	

Appendix A: Sample list (continued).

Cat#	Species	Locality	Talus	Comments	Hand Specimen Petrology
163	Spodumene	LSE-10^11-1	no	- highly altered, in vuggy, albitized matrix	
164	Cassiterite	LSE-10-1	no	- "morganite" dike	- in v. coarse Qtz + Fsp
164	Manganocolumbite	LSE-10-1	no	- "morganite" dike	"
164	Spodumene	LSE-10-1	no	- large (7 cm wide) glassy xls in massive, clevelanditic albite	20% Sp, 20% Qtz, 40% Ab, 10% Ms; other samples from same dike (this CAT#) are unaltered, clean, white blocky Kfs and Qtz
166	Lithiophilite	LSE-2-9	no		- w/ alt'd Spd + alt'd Fsp + aplite
166	Manganocolumbite	LSE-2-9	no		- w/ alt'd Spd + alt'd Fsp + aplite
167	Spodumene	C-4-1B	no	- Spd xl is bent; see also #167 Mn-columbite	(F) has strongly zoned orange(rim)-pink(core) fluorescence
167	K-feldspar	C-4-1B	no		- blocky (10+ cm) greyish, perthitic with a fine-grained, "sugary" interior; the outer rim (shows perfect cleavage, unlike the interior) fluoresces white (C) white, blocky; fluoresces white; perthitic (stringers to 0.5 mm wide and cm's long)
167	Albite	C-4-1B	no		- platy, cleavelanditic; w/ fine-grained Qtz + Ms - Ab (50%) + Qtz (25%) + Ms (25%)
167	Manganocolumbite	C-4-1B	no	- 5 cm Spd (relatively unaltered) embayed by 1.5 cm columbite xl; both hosted by off-white, aplitic to white-clevelanditic albite	
168	Garnet	C-3	no	(B) reddish-brown w/ Ab/Qtz + Kfs; (C) small gemmy, pink garnet in matrix which is interstitial to large (up to 6 cm) elongate Kfs	(C) matrix 40%: Ms 30%, Ab 30%, Qtz 40%
168	Tourmaline	C-3	no	- 8mm patch in saccharoidal to clevelanditic Ab next to large (4 cm) blocky Kfs.; no Spd or Lpd	Ab 30%, Kfs 30%, Qtz 30%, Tour+Gar+Mica 10%

Appendix A: Sample list (continued).

Cat#	Species	Locality	Talus	Comments	Hand Specimen Petrology
168	Cassiterite	C-3	no	- in aplitic material with large phenocrysts of Kfs (see samples (C) & (B))	
168	Manganocolumbite	C-3	no	- in aplitic material with large phenocrysts of Kfs (see samples (C) & (B)); C3-end B	
174	Albite				
176	Spodumene	CC-1^2	no	- clear, colourless to very pale pink	
178	Manganocolumbite	CC-1^2	no		- cm+ sized cleavelandite (50%) + Qtz (30%) + mod to highly alt'd Spd (15%); one piece also contains relict Kfs
178	Cassiterite	CC-1^2	no		
180	Spodumene	C-3-2	no	- altered (corroded) Spds with Lpd (Li) halos around them	aplitic material = Qtz 45%, Fsp 45%, Mica 10% ± others
180	Lepidolite	C-3-2	no	- coarse lepidolite assoc. w/ clevelandite; fine-grained lepidolite assoc. w/ saccharoidal Ab	aplitic material = Qtz 45%, Fsp 45%, Mica 10% ± others
180	Beryl	C-3-2	no	fluoresces bright greenish-white (beryl?) = Cs??	Lep(30%) + Ab(30%) + Qtz(25%) + Cass(5%) + alt Sp(10%)
180	Cassiterite	C-3-2	no	- as bands in massive Qtz assoc. w/ patchy Lep + saccharoidal Ab + beryl	Lep(30%) + Ab(30%) + Qtz(25%) + Cass(5%) + alt Sp(10%)
181	Cassiterite	C-3-3	no	- in massive Qtz	- garnet w/ (Ab 30%, Qtz 70%) at contact w/ schist
183	Lepidolite	C-3-2	no		- w/ Qtz + Fsp + alt'd Spd
186	K-feldspar	CC-1^2	no	- white-grey mottled, blocky	
188	Spodumene	C-3-?	no	- very pale pink, glassy crystals with some evidence of alteration (mica?) along fractures/cleavages	
189	Cassiterite	C-3-2	no	- same sample, same dike as 180(A)	
190	Spodumene	C-3-endA	no	1)- fluoresces ruby red; glassy splintery, anhedral (partially resorbed??) in aplitic matrix 2)- dark purple, splintery (illite?)	matrix = 45% Ab, 45% Qtz, 10% other (Ms, etc)

Appendix A: Sample list (continued).

Cat#	Species	Locality	Talus	Comments	Hand Specimen Petrology
191	Spodumene	C-4-1A	no	- up to 7 cm long, glassy crystals; prismatically euhedral but not well terminated; very outer rim fluoresces orange (core of 'clean' xl also fluoresces bright pink/purplish-white); irradiated samples (2.5 megarads using Co60 gamma source) turned green, are much more bright orange fluorescent and are phosphorescent, which unirradiated specimens are not; piece used for Mt 52 is deep pink and 'clean'	
192	Cassiterite	C-4-3	no	(A)- in massive quartz (+ Lpd); no F-spar	(A) Lpd(50%) + Qtz(45%) + Cass(5%)
193	Spodumene	C-4-1C	no	- same as 191, inlcuding irradiation and fluorescence; up to 15 cm long in massive Qtz + blocky, euhedral Kfs (up to 7 cm)	Sp 25%, Qtz 55%, Kfs 20%
195	Lithiophilite	LMM-5-8	no	- same dike/sample as Sample #278 and #230; intimately assoc. w/ Qtz	- in Qtz(60%) + Ab(35%) + Ms(5%)
196	Manganocolumbite	C-4-2A	no	(A)- in albitic unit; may be lithiophilite	white Ab(50%) + smoky Qtz(30%) + Ms(20%); grain size = 3-5 mm
196	Lithiophilite	C-4-2A	no	(B)- in alt'd blocky Kfs + blocky Qtz; definitely lithiophilite or some alteration product thereof	
197	Albite	LMM-10^11	yes	- montebrasite, apatite, manganocolumbite & cassiterite inclusions - (mostly) saccharoidal to cleavelanditic	- Ab 35%, massive Lpd 40%, Qtz 15%, Beryl 10%. -- - boundary between massive Lpd and sacch. Ab is somewhat diffuse, but commonly has Qtz grains concentrated at contact between Ab and Lpd-Qtz; black (oxide) grains peppered throughout Ab bands/pods (perhaps just see them better there)
197	Lepidolite	LMM-10^11	yes		- see Ab #197
197	Beryl	LMM-10^11	yes	- faint zoning in Mt #66; high Cs band (zoning) visible under UV light - fluoresces bright white	- see Ab #197
198	Cross-section	C-5-2	no	(A)- looks like plumose lepidolite; pink	
199	Lepidolite	LMM-5-8	no		- coarse grained books w/ cleavelanditic Ab + Qtz + alt'd Spd

Appendix A: Sample list (continued).

Cat#	Species	Locality	Talus	Comments	Hand Specimen Petrology
201	Contact	LMM-5-8	no		- Exocontact: dark, fine-grained (Tur + Biot?) - BZ: 1 mm; Qtz (50%) + Ab (50%) - INTZ: cleavelandite (bluish cast) + Qtz + Ms + alt'd Spd + Lit
203	Contact	LMM-5-8	no	- no tourmaline exocontact; host rock = schist	
207	Cassiterite	C-3	no	- in massive Qtz + heavily alt'd Spd + blotchy, aplitic-looking Fsp	
215	Manganocolumbite	LMM-2	yes		
218	K-feldspar	LLG-9^10-1	yes	- bright fluorescence (major portion = white, minor portion = green) with no difference in plane light between white-fluorescing areas and green-fluorescing areas.	blocky, white; assoc. w/ aplitic albite (dirty)
220	K-feldspar	LLG-9-2	no	- south half of cirque	blocky, white w/ bright fluorescent patches (white)
225	Garnet	C-5-5A	no	(B)- in dark gray, fine-grained Fsp near contact; contact between Fsp and garnet diffuse	
226	K-feldspar	C-5-5B	no	- blocky, blue-grey; fluoresces white; sample (A) there is a sharp boundary between white (Or) and red (Ab) fluorescence which corresponds to an equally sharp boundary between the blue-grey (Or) and white (Ab) in plane light, yet the sample seems to be crystallographically continuous (cleavage planes cut across this boundary = albitized?)	
227	Albite	C-5-6B	no	- "dirty" looking, platy	- w/ Qtz + alt'd Spd
227	Manganocolumbite	C-5-6B	no	- not 100% sure from this dike; in Qtz + Spd + Ab	
228	Manganocolumbite	C-5-6A	no	- speckles in aplitic stringer	
229	Cassiterite	C-4-1C	no	- in aplitiic, vuggy albite; originally thought to be titanite	

Appendix A: Sample list (continued).

Cat#	Species	Locality	Talus	Comments	Hand Specimen Petrology
230	Manganocolumbite	LMM-5-8	no	- LMM -5-8 = C5-7	
230	Spodumene	LMM-5-8	no	- pale pink to lilac w/ coarse Lpd (which may give a purplish appearance to Spd)	Spd 30%, Lpd 25%, Qtz 30%, Ap 15%
230	Lithiophilite	LMM-5-8	no	- intimately assoc. w/ Qtz, in white (not grey), salt&pepper aplitic material; LMM -5-8 = C5-7	
230	Lepidolite	LMM-5-8	no	- coarse-crained; purple	see Spd #230
230	Cassiterite	LMM-5-8	no	- in massive Qtz	Qtz(90+%) + Mica(5%)
233	Albite	LSE-10-1	no	- "morganite" dike	
233	Manganocolumbite	LSE-10-1	no	- in massive cleavelandite Ab + Qtz; "morganite" dike (also labelled as LBW-10)	massive cleavelandite + Qtz
234	Cassiterite	LMM-10	yes	- band of Cass xls divide fine and coarse grained Ab+Qtz+Lpd	- coarse: Ab (30%) + Qtz (40%) + Lpd (30%) - fine: Lpd (50%) + Qtz (45%) + [Fsp+oxides] (5%)
234	Lepidolite	LMM-10	yes		- see Cass #234
235	Garnet	C-6-2	no	(C) about 1 cm from contact in Ms-rich, Qtz-Ab OWZ; 3 mm crystal	(C) Qtz 50% + Ms 40% + Ab (5-10%) + oxides(<5%)
235	Muscovite	C-6-2	no	- coarse-grained in saccharoidal Ab + Qtz	- Qtz 50% + Ms 40% + Ab (5-10%) + oxides(<5%
235	Albite	C-6-2	no	(A)- cleavelanditic (B)- white (fluoresces red) and contains 'eyes' of orthoclase which is distinguishable by more prominent cleavage and greyer colour (also fluoresces white); appears to replace Or	(A) Ab(50%) + Qtz(35%) + Ms(15%)
235	Cassiterite	C-6-2	no	- in cleavelanditic Ab + Qtz + Mica + aplitic patches	(A) Ab(50%) + Qtz(35%) + Ms(15%)
240	Lepidolite	LMM-10	no	- purple; coarse	- in white, cleavelanditic Ab (60%) + Qtz (20%) + Lpd (20%)
242	Apatite	C-10	no	- bluish from vug: main dike	
244	Lithiophilite	LSE-2-7	no	- in aplitic material w/ Spd	
246	Zircon	LMM-5	yes	- under SEM: (in pegmatite) as inclusion in Ms+Kfs also as inclusions in Ab+Ms (this contained uraninite inclusion); contains minor Hf; 5 to 100 µm in size	

Appendix A: Sample list (continued).

Cat#	Species	Locality	Talus	Comments	Hand Specimen Petrology
246	Cross-section	LMM-5	yes	- cut section	- dike is about 7 cm wide; acentrically zoned - BZ: 0.5 mm on one side; Qtz + Ms + Ap - WZ: 3 mm; Kfs (85%) + Qtz (10%) + Ms (5%) - APL: 1.5 cm (WZ on this side is less than 0.5 cm, if at all); Ms(50%)+Ab(40%)+Qtz(10%); brownish coloured (Fe?) - INTZ: Kfs(60%)+Qtz(30%)+Ab(10%); Qtz (3 cm) rooted in WZ/APL, "fanning" inwards, smoky; Kfs (to 2 cm) over Qz, rimmed by milky white Ab? (alteration?)
246	Galena	LMM-5	yes	- inclusion in Kfs	
246	Albite	LMM-5	yes	- clevelanditic albite as well as albitized, white orthoclase (large, blocky)	- under SEM: Ab contains abundant inclusions of Ap, M-col/M-tan
246	Cookeite	LMM-5	yes	pale green/yellow vein perpendicular to contact	
247	Spodumene	LSE-2-5	no	- moderately altered, glassy in Qz rich matrix	
251	Manganocolumbite	LSE-2-1	no	- Probe (TSE) = all 4 columbite group mins	
251	K-feldspar	LSE-2-1	no	- blocky, greyish, fluoresces white	
251	Cassiterite	LSE-2-1	no	- assoc. w/ partially albitized Kfs; very similar to #122	
254	Apatite	LMM-5	yes	- similar to #246 in both ways (purple, non-fluorescent vug Ap + contact Ap); BZ Ap is about 1.5 cm thick!!; fluoresces orange (green & cll apatite - not purple apatite); not infilled by calcite ("true" vug)	
265	Spodumene	LRG-3-16	no	centre of dike; rich Spd with lepidolite veinlet perpendicular to the Spd xls	
277	Albite	LMM-1-1	no	- white, platy (cleavelanditic)	
281	Spodumene	LMM-6	yes	- green Spd in schist (at contact); from talus boulder	
282	Fluorite	LMM-5	yes	- purple, anhedral crystals in vug; appear etched; confirmed by SEM(EDS)	

Appendix A: Sample list (continued).

Cat#	Species	Locality	Talus	Comments	Hand Specimen Petrology
283	Albite	LSE-2-3	no	- albitization?; stringers and patchy appearance	
299	Garnet	LBW-9-top	no	- at contact between schist & dark gray Fsp + Ms; intimately assoc. w/ cassiterite	
301	Manganocolumbite	C-4-1C			
309	Beryl	LMM-6	yes	- gemmy, tabular; "goschenite"	- assoc. w/ Ms in Cc-filled vug
311	Manganocolumbite	NMM-1N-1	yes	- in coarse cleavelandite; mica along fracture	-cleavelanditic Ab(70%) + Qtz(25%) + Ms(5%); cleavelanditic Ab at contact with host rock (i.e. NO border unit)
311	Cassiterite	NMM-1N-1	yes	- in coarse cleavelandite; mica along fracture	- see M-col #311
313	Spodumene	NMM-1N-1	no	- heavily altered	- in "dirty" aplitic matrix mixed w/ alt'd peg (cleav. Ab + coarse Qtz)
314	Muscovite	NMM-1N-1	no	- v. coarse, fan-like aggregates w/ silky lustre	- in cleavelanditic Ab + Qtz
315	Contact	NMM-1N	no	small dike east of dike 4; same host rock as #318, except has no tourmaline exocontact; sample location not far from that of 317	
315	Cross-section	NMM-1N	no	small dike east of dike 4	- dike is 4.8 cm wide; shows concentric zoning - BZ: 0.5 mm; Qtz (80%) + Ms (20%) ± Ab - OWZ (WZ?): 3 mm; Kfs (50%) + Qtz (40%) ± Ms (10%); (grains <1 mm) - IWZ (INTZ?): 4 cm; Ab (35%) + Kfs (25%) + Qtz (25%) + Ms (15%); (grains >2 mm) - INTZ(?):
317	Cross-section	NMM-1N-5	no	(A)- tourmaline selvedge at contact (B)- hostrock 5 cm from contact (C)- hostrock about 1 m from contact A & B from same piece	
317	Tourmaline	NMM-1N-5	no	- exocontact	

Appendix A: Sample list (continued).

Cat#	Species	Locality	Talus	Comments	Hand Specimen Petrology
318	Cross-section	NMM-1N-7	yes	(A) white Fsp + coarse Ms cutting across dike banding; close to contact	- banded material is of two types: 1) 60% coarse white Fsp, 35% coarse smoky Qtz, 5% Ms, and 2) aplitic 60% Qtz, 35% Fsp, 5% Ms
318	Garnet	NMM-1N-7	yes	- grown over Tur, but overgrown by Ms; at contact associated with aplitic and coarse Ab/Ms pods cutting banding in dike	
318	Manganocolumbite	NMM-1N-7	yes	- in Ab+Qtz+Ms	Ab(40%) + smoky Qtz(50%) + Ms(10%)
318	Tourmaline	NMM-1N-7	yes	(A) overgrown by garnet (B) cluster of needles along fracture surface (⊥ to wallrock contact) (C) xl broken & curved (not all xls, just large one)	
319	Spodumene	NMM-1S-2s	yes	- pinkish grey, altered Spd; green material is alteration product	60% Ab, 20% Qtz, 15% Sp, 5% others (Mica, lithiophilite)
323	Albite	NMM-1S	yes	- Kaolinized? (clay smell when breathed upon)	
325	Muscovite	NMM-1S	yes	- same mineralogy, drastic increase in grain size about 4 cm from contact (2 mm to 2 cm)	- v. coarse books w/in 5 cm from contact - in granular, massive Qtz + Ab
326	Tourmaline	NMM-1S	yes	- intimately assoc. w/ Spd (intergrown); green	matrix = 25-30% Sp, 40% Fsp(blocky Kfs + finer, white Ab?), 30% Qtz, <5% Mica (Ms)
327	Manganocolumbite	NMM-1S	yes	- similar to #318	Ab(40%) + smoky Qtz(50%) + Ms(10%)
328	Cassiterite	NMM-1S	yes		
328	Manganocolumbite	NMM-1S	yes	- in saccharoidal albite	
329	Helvite	NMM-1N	yes	- gemmy, orange-yellow tetrahedral xls to 1.2 cm on edge (most less than 1.5 mm)	- in lammellar Cc-filled vug in INTZ (not cross-cutting fracture) intimately assoc/ w apatite, etched Kfs, cleavelandite
329	Galena	NMM-1N	yes		- intimately assoc. w/ apatite, chabazite, blocky Kfs, Ms
330	Beryl	NSE-1N-4	yes	- "aquamarine"	- in Cc-filled vug in INTZ (not cross-cutting fracture) intimately assoc/ w Ap, etched Kfs, cleavelandite, gemmy chabazite, stilbite, helvite, Ms
334	Tourmaline	NMM-1N-11A	no	- tourmalinized screen (planar feature) cross-cutting the dike	matrix = blocky, grey/white patchy (albitized?) Kfs 40%, Qtz 25%, Ab 30%

Appendix A: Sample list (continued).

Cat#	Species	Locality	Talus	Comments	Hand Specimen Petrology
336	Schist	NMM-1N	no	- in host rock between 1N-11c & 12	
339	Lithiophilite	NMM-1N^1S	yes	- few loose fragments	
340	Stellerite	NMM-1N-16	no	- confirmed by SEM(EDS)	- splintery/platy white sheets interlayered with calcite in apatite bearing fracture
340	K-feldspar	NMM-1N-16	no	- gemmy vug xl	
340	Apatite	NMM-1N-16	no	(A)- border zone fluoresces orange (= Ap)	
341	K-feldspar	NMM-1N-10	no	- gemmy xl in cross-cutting fracture; overgrowth on blocky Kfs cut by fracture	- assoc. w/ purple Ap + smoky Qtz + stilbite
341	Apatite	NMM-1N-10	no	- purple xl in vug w/ Qtz + Fsp	
344	Cross-section	NMM-1N-19	no	- contact has tour in schist	- dike 6 cm wide; somewhat concentrically zoned - BZ: Qtz (XX%) + Ab (XX%) - INTZ: Kfs (50%) + Ab (30%) + Qtz (20%); >cm-size, white, massive Ab; irregular (very patchy) white Kfs; irregular Qtz (no orientation)
344	K-feldspar	NMM-1N-19	no	- zoned -> outside rim not as cloudy	
345	Sphalerite	NMM-1N-7	yes	- near contact; in massive Qtz + Kfs	
346	Tourmaline	NMM-1N	yes	- small aplitic dikelet with Tur stringers leading away from it; in schistose host rock	
348	Cross-section	NMM-1N^1S-25	no	- fluoresces orange along border zone	- dike is 7.5 cm wide; appears more or less concentrically zoned - INTZ: Ab (75%) + Qtz (15%) + Ms (10%); large (2.5 cm) Ab grow right from contact; slight concentration of quartz near contact - APL: AB + Qz; occupies central portion of dike - WZ/INTZ: Ab (55%) + Qtz (15%) + Ms (5%) + aplitic material (25%); rusty, 'dirty' appearing mixture of aplitic and pegmatitic material - no Kfs at all in this dike
350	Tourmaline	NMM-1N	yes		- Tur veinlets perpendicular to peg contact, but parallel to bedding (foliation); denser closer to contact
354	Spodumene	NMM-1N-27	no	- partially altered	

Appendix A: Sample list (continued).

Cat#	Species	Locality	Talus	Comments	Hand Specimen Petrology
354	Albite	NMM-1N-27	no		- platy (clevelanditic); vuggy (plates like "house of cards) in some of the bladed aggregates
355	Lepidolite	NMM-1N	no	- cuts through Kfs crystal	
357	Kaolinite	NMM-1N-30A	no		- altered Spd; no cleavage, opaque; appears like #358, except red
357	Spodumene	NMM-1N-30A	no		- very pink (kunzite), glassy; some splintery (altered)
358	illite	NMM-1N-30A	no		- friable; dark purple-grey; "clay" smell after breathing on it
360	Banded	NMM-1N	yes	- from below LMM-0^1-1	- directional growth wrt to coarse Ab in Ab+Qtz layers, which alternet w/ fine, aplitic layers (crescumulate texture)
360	Muscovite	NMM-1N	yes	- from below LMM-0^1-1	- thick (1.5cm) 'vein' of pale green mica
363	illite	NMM-1N	yes	- near dike 27	- lilac, radiating, fibrous veinlets
363	Albite	NMM-1N	yes	- near dike 27	- large Ab plates (3-4 cm) interlocked; "vuggy" w/ euhedral LEP books partially filling "vugs"
363	Lepidolite	NMM-1N	yes		- "popcorn"-like; in open spaces between Ab blades
366	Albite	NSE-1N-3	no	- cleavelanditic; w/ open-space vugs containing Ab + Ms ± Ap	- Ab (55%) + Qtz (35%) + Ms (10%)
366	Manganocolumbite	NSE-IN-3	no	- up to 8 mm, blocky xls	- cleavelanditic Ab (55%) + Qtz (35%) + Ms (10%)
370	Manganocolumbite	NSE-1N-4	yes	- similar to #366	- massive, white cleavelanditic Ab(50%) + smoky Qtz(40%) + Ms(10%)
375	Manganocolumbite	NMM-1N-3	yes	- 1-3 mm xl	
377	Albite	NSE-1N-3^4	yes	- saccharoidal, white	
378	Manganocolumbite	NSE-1N-4	yes	- 1-2 mm xl	- white, grainy Ab + Qtz + alt'd Spd
380	Manganocolumbite	NSE-1N-1	no	- 1-2 mm xl	- in 12 cm grey, blocky Kfs (sgl xl!)
381	Manganocolumbite	NSE-1N-2	no	- 1-3 mm xls	- alt'd appearing Ab + Qtz
382	Cross-section	NMM-1S-2s	yes		- aplite with bits of alt'd Spd; no Kfs
384	Albite	NSE-1N-2	no	- radiating aggregate of cleavelanditic blades	- in Qtz + Ms =+ block Kfs
385	Manganocolumbite	NSE-1N-2	yes	- 1-3 mm xls	- in heavily alt'd peg; vuggy w/ Cc and heulandite
386	Cassiterite	NSE-1N-3^4	yes		- massive Cleavelanditic Ab + Ms + Qtz

Appendix A: Sample list (continued).

Cat#	Species	Locality	Talus	Comments	Hand Specimen Petrology
387	Cassiterite	NSE-1N-1	yes		
387	Lithiophilite	NSE-1N-1	yes	- small altered bits	
387	Manganocolumbite	NSE-1N-1	yes		
390	Beryl	LMM-5-8	no	- clear, colourless xls up to 1 cm	- in Lpd + Ab assoc. w/ cross-cutting Qtz vein
391	Apatite	LSE-8-2	no	- green	
394	Apatite	LMM-5	yes	- deep purple in vug w/ Ab+Ms+Stilbite+Qtz (Cc filled)	- paragenesis: Qtz/Ms -> Ap/Ab -> stilbite -> Cc
395	Spodumene	C-4	yes	- section broken perpendicular to Spd xls; parallel orientation wrt length of Spd xls, but random wrt cross-section; lithiophilite intergrown with Spd	30% Sp, 30% Ab, 40% Qtz
396	Cross-section		yes	- strongly banded lepidolite & feldspar	
397	Apatite	LRG-4	yes	- large (0.5 cm) xl; entire sample mounted	
398	Apatite	LMM-5	yes	- entire sample mounted	
399	Garnet	NMM-1S-2s		- entire sample mounted	
455	Banded	L-3	yes	- don't know original orientation to say "footwall" or "hanging wall", but this looks like miniature of classic zonation as seen in Foord (1976)	- shows colloform banding in aplitic material on one side, and large broadening (inward) white Fsp from opposite contact
455	Lepidolite	L-3	yes	- see "banded" #455	
458	K-feldspar	LSE-10-1	no	- "morganite" dike	

APPENDIX B

Electron probe microanalyses of feldspars, oxides, phosphates, spodumene, beryl, micas and tourmaline. The electron probe operating conditions are also included.

Table B-1: Electron probe operating conditions for feldspars, tourmaline, beryl, micas, apatite, garnet, spodumene and other phosphates.

Mineral Type	Element	Line	Standard Name	Crystal	Time (sec)
Feldspar	Na	Kα	Albite	TAP	25
	K	Kα	Sanidine	PET	25
Acc. Volt. (kV): 15	Rb	Lα	Microcline (Rb)	TAP	100
Beam Current (ηA): 20	Cs	Lα	Pollucite	PET	100
Beam Size (μm): 30	Mn	Kα	Tephroite	PET	100
	Ca	Kα	Diopside	PET	25
	Sr	Lα	Celestite	TAP	25
	Ba	Lα	Sanbornite	PET	100
	Pb	Mα	Crocoite	PET	100
	Al	Kα	Sanidine	TAP	25
	Fe	Kα	Almandine	PET	25
	Si	Kα	Sanidine	TAP	25
	P	Kα	Apatite	TAP	25
Tourmaline	Si	Kα	Bytownite	TAP	8
	Fe	Kα	Almandine	PET	25
Acc. Volt. (kV): 15	Ca	Kα	Gehlenite	PET	25
Beam Current (ηA): 20	Na	Kα	Na-amphibole	TAP	25
Beam Size (μm): 30	Mg	Kα	Enstatite	TAP	25
	Al	Kα	Bytownite	TAP	7
	Mn	Kα	Tephroite	PET	25
	K	Kα	Microcline (Rb)	PET	25
	Cr	Kα	Nichromite	PET	25
	Ti	Kα	Rutile	PET	25
	F	Kα	Phologopite	TAP	25
	V	Kα	VP_2O_7	PET	25
Beryl	Si	Kα	Albite	TAP	5
	Al	Kα	Albite	TAP	14
Acc. Volt. (kV): 15	Mg	Kα	Almandine	TAP	25
Beam Current (ηA): 20	Mn	Kα	Rhodochrosite	PET	200
Beam Size (μm): 30	Sc	Kα	REE Glass	PET	200
	V	Kα	VP_2O_7	PET	200
	Cr	Kα	Chromite	PET	200
	Fe	Kα	Almandine	PET	25
	Na	Kα	Albite	TAP	25
	K	Kα	Sanidine	PET	25
	Ca	Kα	Almandine	PET	25
	Cs	Kα	Pollucite	PET	200

Table B-1: (cont'd)

Mineral Type	Element	Line	Standard Name	Crystal	Time (sec)
Micas	Si	Kα	Phlogopite	TAP	5
(lepidolite, muscovite)	Al	Kα	Phlogopite	TAP	10
	K	Kα	Phlogopite	PET	25
Acc. Volt. (kV): 15	Mn	Kα	Tephroite	PET	25
Beam Current (ηA): 20	Na	Kα	Albite	TAP	25
Beam Size (μm): 30	Fe	Kα	Chlorite	PET	25
	Rb	Lα	Microcline (Rb)	TAP	50
	Ca	Kα	Gehlenite	PET	25
	Sr	Lα	Celestite	TAP	25
	F	Kα	Phlogopite	TAP	25
	Cs	Lα	Pollucite	PET	50
	Mg	Kα	Phlogopite	TAP	25
	Ba	Lα	Sanbornite	PET	25
Apatite	P	Kα	Apatite	PET	25
	Ca	Kα	Gehlenite	PET	25
Acc. Volt. (kV): 15	Si	Kα	Diopside	TAP	25
Beam Current (ηA): 20	Mn	Kα	Tephroite	PET	25
Beam Size (μm): 30	Na	Kα	Albite	TAP	25
	Ce	Lα	$CePO_4$	PET	25
	Fe	Kα	Almandine	PET	25
	Sr	Lα	Celestite	TAP	25
	V	Kα	VP_2O_7	PET	25
	Mg	Kα	Diopside	TAP	25
	F	Kα	Apatite	TAP	25
	Cl	Kα	Tugtupite	PET	25
	Nd	Lα	$NdPO_4$	LIF	25
Garnet	Si	Kα	Alm	TAP	25
	Ti	Kα	Rutile	PET	25
Acc. Volt. (kV): 15	Al	Kα	Alm	TAP	25
Beam Current (ηA): 20	Mg	Kα	Pyrope	TAP	25
Beam Size (μm): 10	Mn	Kα	Tephroite	LIF	25
	Fe	Kα	Alm	LIF	25
	Ca	Kα	Alm	PET	25
	Na	Kα	Albite	TAP	25
	Zr	Lα	Zircon	TAP	25
	Sn	Lα	Cassiterite	PET	25
	P	Kα	Apatite	TAP	25
	V	Kα	VP_2O_7	PET	25
	Cr	Kα	Chromite	LIF	25

Table B-1: (cont'd)

Mineral Type	Element	Line	Standard Name	Crystal	Time (sec)
Spodumene	Na	Kα	Albite	TAP	25
	K	Kα	Sanidine	PET	25
Acc. Volt. (kV): 15	Cs	Lα	Pollucite	PET	25
Beam Current (ηA): 20	Ca	Kα	Diopside	PET	25
Beam Size (μm): 30	Mg	Kα	Diopside	TAP	25
	Mn	Kα	Tephroite	PET	25
	Fe	Kα	Almandine	PET	25
	Al	Kα	Spodumene	TAP	25
	Cr	Kα	Chromite	PET	25
	Si	Kα	Spodumene	TAP	25
Phosphates	Fe	Kα	fayalite	LIF	20
	Mg	Kα	diopside	TAP	20
Acc. Volt. (kV): 15	Si	Kα	diopside	TAP	20
Beam Current (ηA): 20	Na	Kα	albite	TAP	20
Beam Size (μm): 10	P	Kα	apatite	PET	20
	Ca	Kα	apatite	PET	20
	F	Kα	apatite	TAP	40
	Mn	Kα	spessartine	LIF	20
	Ti	Kα	rutile	PET	20
	Al	Kα	albite	TAP	20

Appendix B-2: Electron probe microanalyses: list of files on diskette.

Files	Mineral	Sample #	Mount #	Points
apatite.oxi	apatite	391	150	1 - 8
		397	56	9 - 17
		98	83	18 - 26
		391	162 IV	27 - 29
		341	162 III	30 - 33
		340	162 II	34 - 41
		91	162 I	42 - 46
		394	162 V	47 - 50
		398	167	51 - 55
beryl-88.oxi	beryl	88	77	5-9
beryl-li.oxi ♠	beryl	330	178	1 - 4
		390	151	10 - 14
		309	179	15 - 18
		197	66	19 - 23
feld-1.oxi	feldspar	246	108	1 - 16
		197	102	17 - 27
		153	105	31 - 45
		167	104	46 - 56
		160	149	57 - 66
		113	71	67 - 70
		235	103	71 - 77
garnet.oxi	garnet	318	152	1 - 4
		84	84	5 - 11
		160	27	12 - 15
		399	148	16 - 25
		114	69	26 - 30
		225	153	31 - 39
lep-197.oxi ♠	lepidolite	197	102	28 - 30
lep2-197.oxi	lepidolite	197	102	28 - 30
lep-230.oxi ♠	lepidolite	199	65	17 - 21
lep2-230.oxi	lepidolite	199	65	17 - 21
lepid.oxi	lepidolite	114	75	1 - 8
		183	48	37 - 44
		9	9	45 - 57

Note: - Raw data stored on disk as text files.
- *.oxi = original probe data; *.tab = FORMULA results.
- ♠ = wet chemical data added to electron microprobe data.

Appendix B-2: Electron probe microanalyses: list of files on diskette (continued).

Files	Mineral	Sample #	Mount #	Points
mmfel1.oxi	feldspar	377	169	1 - 7
		341	170	8 - 27
		344	171	28 - 42
		363	172	43 - 56
		323	174	57 - 63
mmfel2.oxi	feldspar	340	175	1 - 17
		354	176	18 - 25
musc.oxi	muscovite	360	158	9 - 16
		314	156	22 - 30
		325	157	31 - 36
rg-feld1.oxi	feldspar	251	99	1 - 8
		167	97	9 - 17
		154	98	18 - 34
		226	101	35 - 51
		220	100	52 - 64
		186	106	65 - 76
		218	107	77 - 90
rg-feld2.oxi	feldspar	186	52	1 - 15
		161	6	16 - 28
rg-gar.oxi	garnet	225	153	1 - 26
		399	148	27 - 42
		299	42	43 - 47
		299	44	48 - 52
spod.oxi	spodumene	161	1	1 - 16
		230	46	17 - 31
		357	164	32 - 49
		281	161 II	50 - 58
		176	41	59 - 80
		191	57	81 - 91
		188	7	92 - 99
tour-318.oxi	tourmaline	318	177	9 - 18
tour-326.oxi	tourmaline	326	173	1 - 8

Note: - Raw data stored on disk as text files.
- *.oxi = original probe data; *.tab = FORMULA results.

APPENDIX C

Wet chemical procedures and results.

Appendix C.1: Wet chemical analytical procedures.

Element	Preparation	Analytical Method	Detection Limit (ppm)	Upper Limit (ppm)
Li	$HClO_4$-HNO_3-HF digestion	Atomic Absorption Spectroscopy	1	1000
B		Neutron Activation Analysis	5	10000
Sr	$HClO_4$-HNO_3-HF digestion	Atomic Absorption Spectroscopy	1	10000
Rb	$HClO_4$-HNO_3-HF digestion	Atomic Absorption Spectroscopy	1	10000
Ba	$HClO_4$-HNO_3-HF digestion	Atomic Absorption Spectroscopy	10	10000
Pb	HNO_3-aqua regia digestion	Atomic Absorption Spectroscopy - Bkgd. Corr.	1	10000
F	Carbonate-nitrate fusion	Specific Ion	20	10000
Mn	HNO_3-aqua regia digestion	Atomic Absorption Spectroscopy	5	10000
Cs	Trace rock, soil	Neutron Activation Analysis	0.5	10000

All wet chemical analyses performed by Chemex Labs, Ltd., North Vancouver, BC.

Notes:

For logistical purposes, lepidolite samples 197 and 230 were diluted and the results recalculated, to avoid results in excess of the upper limit of the analytical method.

Some differences exist between electron probe microanalyses and wet chemical analyses. These discrepancies can largely be attributed to inhomogeneities in material analyzed by wet chemical methods and/or different detection limits for each method. For example, no Pb was detected in K-feldspar using the electron microprobe, whereas AAS and Pb isotopic studies by mass spectrometry clearly show the presence of Pb. However, galena inclusions have been noted in some feldspar samples, though not in microprobe mounts made of the same samples from which the wet chemical analyses were made. A puzzling discrepancy is that shown by the Sr contents of albite versus those of K-feldspar. The wet chemical results are more typical in that Sr contents for albite are higher than in K-feldspar. The microprobe results, unexpectedly, do not show this trend. Other discrepancies have been mentioned in the mineralogy/geochemistry chapter.

Appendix C.2: Wet chemical analyses.

Species	#	Li	B	Sr	Rb	Ba	Pb	F	Mn	Cs
Albite	153	nd	30	17	nd	nd	nd	nd	nd	nd
	167	nd	20	42	nd	nd	nd	nd	nd	nd
	197	nd	20	1	nd	nd	nd	nd	nd	nd
	235	nd	25	25	nd	nd	nd	nd	nd	nd
	246	nd	20	37	nd	nd	nd	nd	nd	nd
	354	nd	45	nd	nd	nd	nd	nd	nd	nd
	363	nd	15	nd	nd	nd	nd	nd	nd	nd
	377	nd	5	nd	nd	nd	nd	nd	nd	nd
Orthoclase	154	240	nd	3	3500	<5	22	60	nd	nd
	167	172	nd	7	3700	10	53	40	nd	nd
	186	260	nd	6	3600	10	24	50	nd	nd
	218	280	nd	4	4700	5	22	100	nd	nd
	220	220	nd	4	3000	5	44	40	nd	nd
	226	76	nd	6	5500	20	112	50	nd	nd
	251	440	nd	4	4200	70	23	60	nd	nd
Micas	197	11000	110	nd	nd	nd	nd	nd	nd	nd
	230-1	16400	160	nd	nd	nd	nd	nd	nd	nd
	230-2	17800								
	103	16500								
	235	140	240	nd	nd	nd	nd	nd	nd	nd
Beryl	197	1500	nd	nd	nd	nd	nd	nd	100	2820
	309	3000	nd	nd	nd	nd	nd	nd	50	3090
	330	660	nd	nd	nd	nd	nd	nd	nd	nd
	390	1150	nd	nd	nd	nd	nd	nd	nd	nd
Tourmaline	326	1550	nd	nd	nd	nd	nd	nd	nd	nd
	334	275	nd	nd	nd	nd	nd	nd	nd	nd
Spodumene	92	nd	20	nd	nd	nd	nd	nd	nd	nd
	191	nd	20	nd	nd	nd	nd	nd	nd	nd
	230	nd	65	nd	nd	nd	nd	nd	nd	nd
	281	nd	20	nd	nd	nd	nd	nd	nd	nd
	313	nd	35	nd	nd	nd	nd	nd	nd	nd
Host Rock A	317	188	>10000	nd	nd	nd	nd	nd	nd	nd
Host Rock B	317	230	60	nd	nd	nd	nd	nd	nd	nd
Host Rock C	317	136	390	nd	nd	nd	nd	nd	nd	nd

Note:

- All wet chemical analyses performed by Chemex Labs, Ltd, North Vancouver, BC.
- Results are in ppm.

nd Not determined.

APPENDIX D

Petrographic Summaries.

Appendix D-2: Thin section descriptions.

TS#	CAT#	Main Feature	Petrology
1	348(a)	Cross-section	- Exocontact: Tur + Qtz - large Ab laths begin right at contact - no Kfs (staining)
2	348(b)	Cross-section	
3	336	Schist	- biotite and chloritoid porphyroblasts cut one major foliation; = 2 events (2nd event = 400 + [biotite]) - presence of Ctd incates more aluminous rock than average pelite - cordierite (Crd) w/ pleochroic haloes: timing equivocal (may be post-tectonic; lots of random Bt -> may be overgrowth); Ms, Chl & Tur around edges - not much retrogression
4	140(a)	Schist	- staurolite (St) porphyroblasts: curved intrusion trails (syndeformational); many Bt inclusions (staurolite is so skeletal that Bt could have formed w/in St during event 2) - Bt & Ctd overprinting major foliation (event 2) - subtle, late kinking visible - Ms present means rock probably not cooked higher than 700-750
5	140(b)	Schist	- similar to slide #4
6	382(a)	Cross-section	- APL: Qtz (45%) + Ab (40%) + Ms (12%) + Spd&oxides&other (3%) - Spd seems to have alteration rim (replacement by mica?) - 'fibrous, radiating' mineral grown into Spd (embayed); looks like plumose mica
7	382(b)	Cross-section	
8	346	Tourmaline group	
9	318(a)	Contact	
10	318(b)	Cross-section	- WZ: Qtz (50%) + Cc (30%) + Ab (15%) + Ms (5%) - INTZ: Qtz + Ab + Ms
11	318(c)	Cross-section	continuation of 318(b) [line up as read]
12	123(a)	K-feldspar	- alteration (?) along edge of crystal
13	123(b)	Spodumene	- not a good section
14	357	Spodumene	
15	203(a)	Quartz	- Qtz veinlet cutting dike
16	203(b)	Contact	- X-cutting Qtz veinlet meets contact - some Ab has strained appearance - Contact: Ab laths (somewhat poikiolitic at contact and less so away from contact) begin right at HR contact
17	226	K-feldspar	(albitization?) - large blocky Kfs w/ stringer perthite and yellow Ab patches (latter seem to be crystallographically continuous: all extinguish at same time when stage is rotated) - highly consertal contact between Ab and Kfs (replacement?)
18	317	Cross-section	- straight line contact between Kfs and Qtz (Kfs = euhedral) - some Kfs near contact (w/in 0.7 cm) shows tartan twinning (microcline)

Appendix D-2: Thin section descriptions (continued)

TS#	CAT#	Main Feature	Petrology
19	317	Contact	- HR: 1 cm from contact; Qtz (75%) + Bt (20%) + Tur (+ mins w/ radiation haloes) (<5%) - Exocontact: Tur (54%) + Qtz (45%) + Bt (1%) - BZ: Qtz (50%) + Ab (45%) + Tur (5%) - WZ: Ab (80%) + Kfs (10%) + Qtz (10%); Kfs along peg side of WZ; Qtz along HR side of WZ - INTZ: Ab (35%) + Qtz (3
20	355	Lepidolite	- Lpd band: Lpd (50%) + Qtz (50%) - consertal texture (between Lpd & Qtz and Lpd & Ab) - no Kfs in sample (offcut stained)
21	355(b)	Lepidolite	- Lpd-Fsp contact - relict spodumene; altered to ??
22	197(a)	Lepidolite	Qz-Lpd / Beryl contact - sharp and straight contact between beryl and Lpd-Qtz (beryl = euhedral) - paragenetic sequence: Brl -> Lpd -> Lpd-Qtz -> Qtz
23	197(b)	Albite	- Ab band: Ab (80%) + Qtz (15%) + Other (Lpd, oxides) (5%) - Lpd (dark) body: consertal Qtz (45%) + Lpd (45%) + Ab (10%) - sub to euhedral Qtz with concentric mica (Lpd) inclusions within Ab band - consertal texture between Lpd and Qtz in Lpd band
24	197(c)	Albite	- Qtz along boundary between Ab and Lpd-Qtz bands - Ab band has higher oxide content (3 - 5%) than Lpd-Qtz body
25	230	Spodumene	- symplectic Spd into Qtz and Ab - seems two be two bands of symplectite: a coarse-grained, inner band involving Spd and Qtz, and an outer, finer-grained band involving Spd and Ab (each band is 0.5 mm at its widest) - Kfs embayed by Ab - Qtz-Qtz and Q
26	175	Spodumene	- symplectic Spd and Qtz - Spd xl seems partially resorbed
27	234	Cassiterite	-
28	234	Lepidolite	- "Lpd patches" seen in hand sample: Lpd (55%) + Qtz (45%) + minor Ab (<1%); all consertal
29	201	Contact	- HR: Bt (70%) + Qtz (25%); 2 grain sizes of Bt oriented in 3 directions(// to contact, 45 to contact, 45 to contact [90 to 2)]) - BZ: consertal Qtz (35%) + Ab (50%) + Other (15%) - WZ: Kfs (60%) + Qtz (30%) + Ab (7%) + Ms (3%); Kfs = microcline (symplectic/tartan twinning); generally messed up appearance - INTZ: Ab (65%) + Qtz (25%) + Lpd & other (relict Spd) (10%); Ab laths pokiolitic/symplectic - microcline (tartan twinning) close to contact - relict Spd; replaced by Lpd+Ab+Qtz
30	366	Albite	Fsp-Qz contact
31	198	Contact	- HR: Qtz (50%) + Bt (15%) + other(35%): very fine-grained (?) - Exocontact: Qtz (80%) + Tur (18%) + Bt & other (2%); Qtz has sutured contacts (seems to be recrystallized within exocontact); Tur in bands // to original bedding (i.e. compositional) - BZ: about 0.7 to 1.0 cm wide; Qtz (50%) + Ms (49%) + Tour (1%) - WZ/(INTZ?): Ab (60%) + Qtz (25%) + Ms (15%)

Appendix D-2: Thin section descriptions (continued).

TS#	CAT#	Main Feature	Petrology
32	344	K-feldspar	- zoning in Kfs xl seen in hand sample not seen in thin section - Kfs - Qtz contact straight (Kfs = euhedral)
33	455	Banded	- Ab band: Ab (75%) + Qtz (18%) + Lpd (7%); some Ab = symplectic/poikiolitic - Lpd (dark) band: consertal Qtz (60%) + Lpd (25%) + Ab (15%) - generally, all sharp, clean grains (no signs of alteration)
34	455(a)	Banded	- colloform banding - dark band: Lpd (50%) + Qtz (48%) + Ab (2%) - light band: Ab (88%) + Qtz (10%) + Lpd (2%)
35	455(b)	Lepidolite	- Fsp-Lpd-Qz intergrowth
36	455(c)	Lepidolite	- Fsp-Lpd-Qz intergrowth
37	455	Lepidolite	- poikiolitic Ab - symplectic Lpd
38	360(a)	Banded	- APL band: Ab (85%) + Qtz (10%) + Mica+other (5%)
39	360(b)	Banded	- directional growth in bands, visible in hand sample; Ab-Qtz contact: Ab is subhedral in thin section; Qtz is consertal - Ab laths seem to grow out of aplitic 'substrate' and are surrounded by consertal Qtz
40	159	K-feldspar	- symplectic Spd between two blocky Kfs - APL: Qtz (40%) + Ab (30%) + Spd(relict-corroded) (15%) + Mica (10%) + <1% oxides - Kfs: perthitic; anhedral Ab inclusions // to Kfs outer face; Kfs heavily embayed by Qtz + Ab + Mica +Spd
41	354(a)	Albite	- very coarse-grained, bladed Ab (cleavelandite)-Lep-Qz
42	354(b)	Spodumene	- replaced Spd along edge of slide; symplectic growth into matrix - replacement mineral = Qtz + ? (mica?)
43	265(a)	Spodumene	- Spd cut by APL; Spd appears altered at contact with APL - APL: Qtz (45%) + Mica (25%) + Ab (25%) + oxides & relict Spd (5%)
44	265(b)	Spodumene	- Spd cut by APL
45	132(a)	Quartz	- Kfs-Qz contact straight & sharp - Qtz-Qtz contact consertal - Kfs appears heavily altered
46	132(b)	Contact	- Exocontact: Qtz (50%) + Tur (30%) + fine-grained unidentifiable (mica?) (20%) - Contact: Qtz - WZ: 0.5 to 1.0 cm; Qtz (60%) + Ms (40%); consertal - INTZ: Kfs[microcline] (80%) + Ms (12%) + Qtz (8%) - CORE: Qtz
47	458	K-feldspar	Kfs/Qtz contact
48	315(a)	Cross-section	
49	315(b)	Contact	- OWZ: Kfs (75%) + Qtz (20%) + Ms (5%) - directional growth in Ms

Appendix D-2: Thin section descriptions (continued).

TS#	CAT#	Main Feature	Petrology
50	246	Cross-section	This a polished block studied under SEM. - contact defined by band of apatite xls + Ms+Qtz. - WZ/APL only on one side of dike, INTZ directly at contact opposite - Pegmatite: Qtz-Ms BZ, followed by Ab-Ms-Qtz WZ/APL(?), then Ksp-Ab-Qtz INTZ. - BZ: fine-grained (<0.5mm), [75% Qtz, 20% Ms, 5% Ap] - WZ/APL: med-grained (0.5-3mm), [50% Ab, 35% Ms, 15% Qtz, minor Ap+oxides] - INTZ: coarse-grained (0.5cm-2cm), [60%Ksp, 30%Qtz, 10% Ab+Ap]; almost perthitic wrt Ap - many stringers and beads - accessory pegmatite mins: zircon(80µm) w/ uraninite inclusion(5µm) in WZ/APL; cassiterite in WZ & INTZ(Ta-cass); pyrite in WZ; col/tant in WZ - Ab seems to be replacing Ksp in some places (embayments w/ Ksp "islands just off coast") - Exocontact: -1st 3 mm: 50% Bt, 25% Tur, 20% Qtz, 5% other - accessory: allanite, monazite, titanite, zircon - tourmaline = Mg dominant over Fe (EDS peaks) w/ tiny Ca (dravite?)